A low–temperature thermochronologic insight into the thermal and exhumation history of the eastern Musgrave Province, South Australia

Thesis submitted in accordance with the requirements of the University of Adelaide for an Honours Degree in Geology

Kate Nicole Agostino

November 2015

THE UNIVERSITY of ADELAIDE

A LOW-TEMPERATURE THERMOCHRONOLOGIC INSIGHT INTO THE THERMAL AND EXHUMATION HISTORY OF THE EASTERN MUSGRAVE PROVINCE, SOUTH AUSTRALIA

EXHUMATION OF THE EASTERN MUSGRAVE PROVINCE

ABSTRACT

Multi–method thermochronological data are presented for 12 Mesoproterozoic granitoid samples collected from the eastern Musgrave Province within South Australia. Interpretation of these data with the aid of time–temperature modelling allows inference of multiphase cooling histories. Apatite fission track (AFT) results indicate four discrete exhumation events that induced cooling through AFT closure temperatures (~60–120°C), supported by additional apatite (AHe) and zircon (ZHe) (U-Th-Sm)/He data. Late Neoproterozoic cooling from deep crustal levels to temperatures <200°C was observed, which is thought to be related with the Petermann Orogeny. Subsequent cooling events at ~450–400 Ma (Silurian – Devonian) and ~310–290 Ma (Late Carboniferous) are thought to represent exhumation associated with the Alice Springs Orogeny. The latter event exhumed the sampled eastern Musgrave plutons at shallow crustal depths. An additional Triassic – early Jurassic thermal event was observed throughout the study area, thought to be related to elevated geothermal gradients at that time. The high sample density across the structural architecture of the study area furthermore reveals patterns of differential exhumation and preservation of the thermal record, indicating more shallow exhumation levels in the centre and deeper exhumation towards the margins of the sampled transect. The observed differential exhumation patterns match with a model of an inverted graben system, demonstrating how low temperature thermochronological techniques can reveal fault reactivation patterns. The results highlight that the eastern Musgraves record a complex Phanerozoic low-temperature thermal history revealing the poorly appreciated tectonic evolution of inland Australia.

KEYWORDS

Low–Temperature Thermochronology, Exhumation, Eastern Musgrave Province, Apatite Fission Track, South Australia, Apatite Helium, Zircon Helium.

TABLE OF CONTENTS

LIST OF FIGURES AND TABLES

INTRODUCTION

The Musgrave Province is a predominantly east-west trending basement inlier located in central Australia, bounded by Neoproterozoic to Palaeozoic sedimentary rocks of the Amadeus, Officer, and Eromanga Basins (Figures 1 and 2; Howard et al. 2015). The formation, architecture and high–temperature metamorphic history of the eastern portion of the Musgrave Province has been detailed (e.g. Camacho and Fanning 1995, Aitken and Betts 2009) however few comprehensive thermochronological studies have been conducted to investigate the timing of exhumation to shallow crustal levels. Reconnaissance regional Apatite Fission Track (AFT) studies, such as Gleadow et al. (2002b), suggest that exhumation to the subsurface throughout the Arunta (Northern Territory, Figure 2) and Musgrave Blocks largely occurred during the late Palaeozoic (~350–300 Ma). Tingate and Duddy (1996) investigated the thermal history of the western margin of the Eromanga Basin and Eringa Trough (Figure 1), with one sample within the eastern Musgraves, determined analogous Late Palaeozoic cooling (360–300 Ma). This result was attributed to uplift and erosion during the final stages of the Devonian to Carboniferous Alice Springs Orogeny (Tingate and Duddy 1996). Tingate and Duddy (2002) theorised exhumation in the Officer Basin to be mainly pre–Cretaceous (350–110 Ma), encompassing Late Palaeozoic episodes of cooling and Permian – Triassic reheating and subsequent cooling. In addition, a Late Cretaceous to Miocene (70–20 Ma) thermal episode suggests regional cooling correlating with results of nearby studies, including the Amadeus Basin, Arunta and Musgrave Blocks (Tingate 1990), the western margin of the Eromanga Basin (Figure 1; Tingate and Duddy 1996) and within the Adelaide Fold Belt (Figure 1; Foster et al. 1994). Pilot studies in the Gawler Craton and the Peake and Denison Ranges produce correlative AFT results (Figure 1; Hall 2014, Reddy et al. 2014). For the northern Gawler Craton, cooling ages

translate into four thermal events, ranging from the Neoproterozoic, Ordovician – Silurian, Devonian – Carboniferous, and Late Triassic – Jurassic, with one anomalous sample determining an Early Cretaceous thermal event (Reddy et al. 2014). For the Peake and Denison Ranges, three pulses of cooling and linked exhumation were documented throughout the Ordovician, Carboniferous and Early Jurassic (Hall 2014). Throughout most of these aforementioned regions of southern and central Australia, the occurrence of intracontinental deformation, crustal thickening and associated exhumation has been closely linked to large-scale compressional orogens, namely the Neoproterozoic Petermann Orogeny and the Palaeozoic Alice Springs Orogeny (Raimondo et al. 2014).

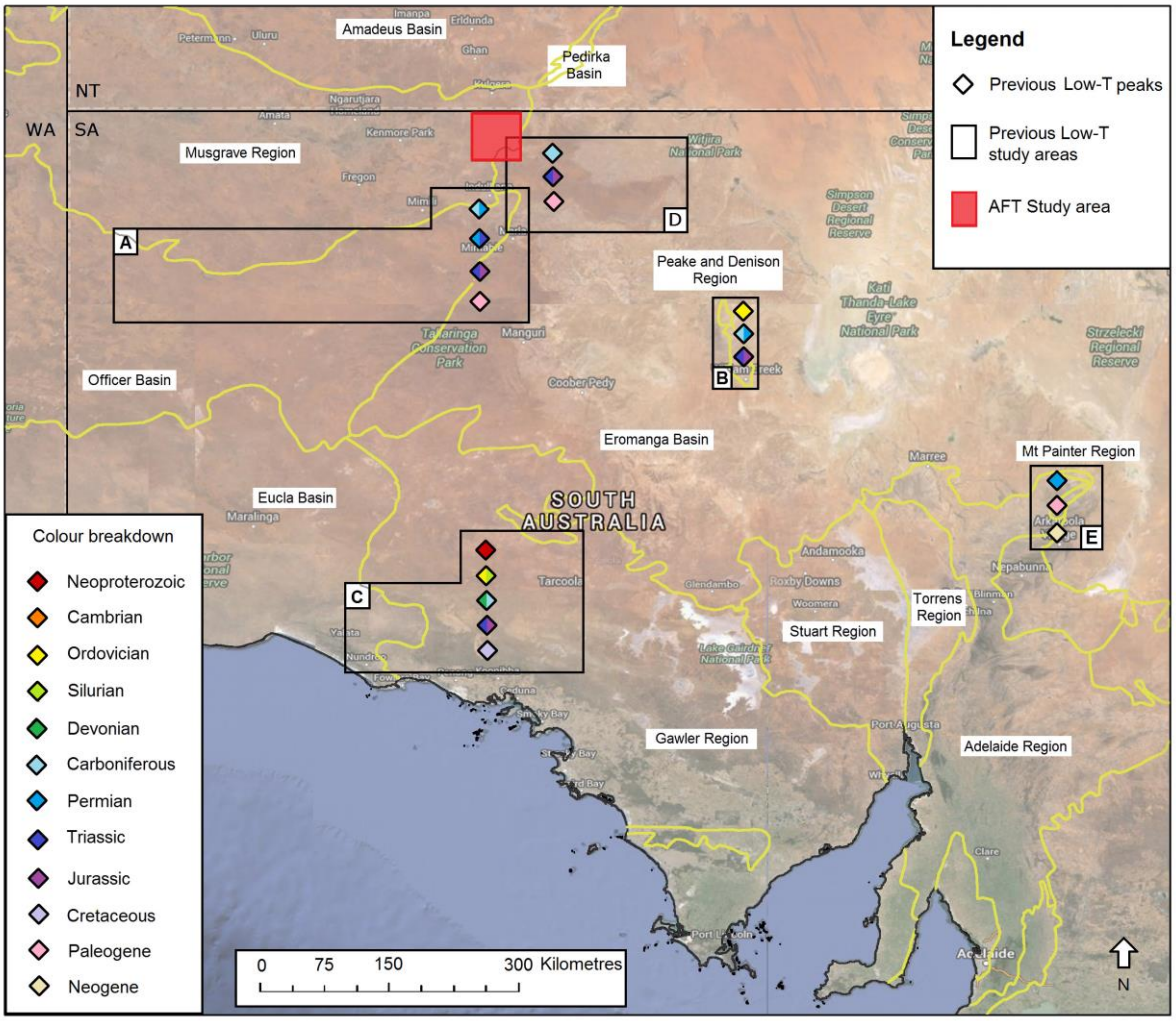

Figure 1: (previous page) Simplified map with *Google Earth* satellite image underlay indicating previous low–temperature thermochronological data obtained for the areas surrounding the Musgrave Province: studies include (a) Officer Basin, Tingate and Duddy (2002), (b) Peake and Denison Ranges (Northern Gawler Craton), Hall (2014), (c) Gawler Craton, Reddy (2014), (d) western Eromanga Basin and Eringa Trough, Tingate and Duddy (1996), (e) Adelaide Fold Belt (Mt. Painter Inlier), Foster et al. (1994). Entire previous study areas are represented by black boxes and coloured diamonds indicate the general periods of regional AFT age peaks obtained and discussed in the text. Diamonds with two colour divisions indicate AFT thermal events spanning across the two correlating time periods. The eastern Musgrave Province study area for this thesis is indicated by the red box.

This thesis aims to resolve the low–temperature exhumation history of the eastern Musgrave Province by applying thermochronometric methods on basement rock samples along a north–south transect across the main east–west trending structural architecture. Apatite Fission Track (AFT) thermochronology is conducted, using the laser–ablation inductively–coupled–plasma mass-spectrometry (LA-ICP-MS) method, as well as apatite (AHe) and zircon (ZHe) U-Th-Sm/He dating. The results obtained in this study will test the hypothesis that the Petermann and Alice Springs orogenies were the main causes for Phanerozoic exhumation in the region, and will determine if any later thermal events occurred. In addition, the sampling strategy across the main regional structures allows investigation of potential patterns of differential exhumation. This research forms part of a larger thermochronological project to constrain the low–temperature exhumation history of South Australia in collaboration with the Geological Survey of South Australia. This work aims to link the thermal history of the eastern Musgrave Province with recently obtained results for central and southern Australia, including the southern and eastern Gawler Craton (Reddy et al. 2014), the Peake and Denison Ranges, north–eastern Gawler Craton (Hall 2014), the Arunta Block and northern Musgrave region within the Northern Territory (Tingate 1990, Gleadow et al. 2002b), and the adjacent western Eromanga Basin and Eringa Trough (Tingate and Duddy 1996).

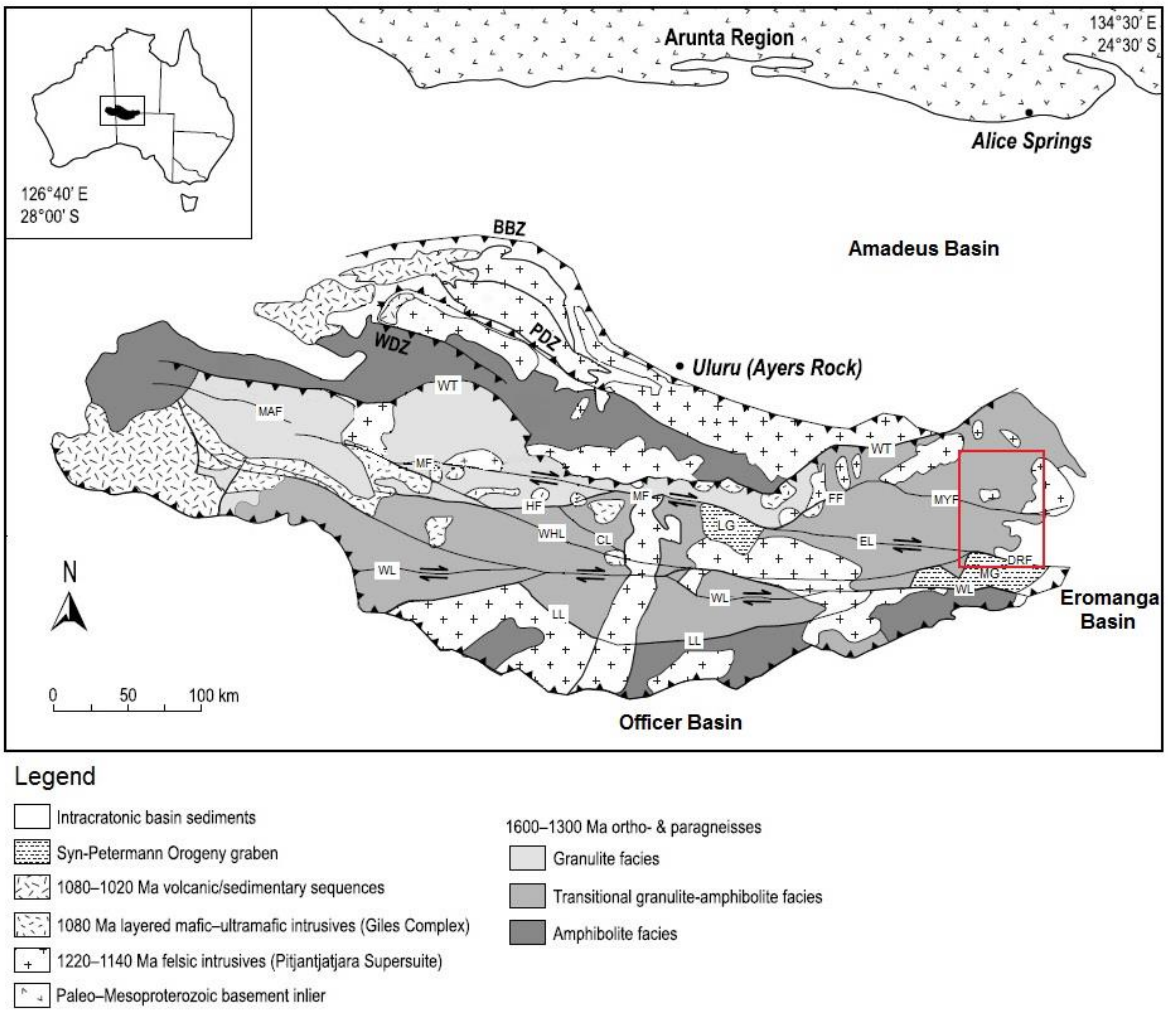

Figure 2: Regional geological map of the Musgrave Province, showing its position relative to the surrounding intracratonic sedimentary basins (Amadeus, Officer, and Eromanga). Also shown are the locations of key E–W trending fault structures. Boundaries of the study area discussed in this thesis are outlined in red. Modified from Raimondo et al. (2010). Abbreviations: BBZ – Bloods Backs Thrust Zone, CL – Caroline Lineament, DRF – De Rose Fault, EL – Echo Lineament, FF – Ferdinand Fault, HF – Hinckley Fault, LG – Levenger Graben, LL – Lindsay Lineament, MAF – Mount Aloysius Fault, MF – Mann Fault, MG – Moorilyanna Graben, MYF, Marryat Fault, PTZ – Piltardi Detachment Zone, WDZ – Wankari Detachment Zone, WHL – Wintiginna-Hinckley Lineament, WL – Wintiginna Lineament, WT – Woodroffe Thrust.

In this paper, newly obtained low-temperature thermochronological data from 12 granitoid rock samples within the eastern Musgrave Province are presented. Results were modelled to provide a detailed reconstruction of the low-temperature thermal history of the study region throughout the Phanerozoic. This thermal history model is linked with sedimentological records of adjacent basins, and important cooling phases and their tectonic significance are discussed.

GEOLOGICAL SETTING

The Musgrave Block covers roughly 120,000 km^2 and is bound to the east by the Eromanga Basin (Permian to Mesozoic), south and west by the Officer Basin, and north by the Amadeus Basin (both mid–Neoproterozoic to early–Palaeozoic; Edgoose et al. 2004, Wade et al. 2008). The dominant basement rock type in the eastern Musgrave Province is the felsic granulite to upper amphibolite facies Birksgate Complex. SHRIMP U–Pb zircon data from Edgoose et al. (2004) indicate protolith ages between ~1620–1550 Ma. They have been widely interpreted as volcanic–dominated supracrustal material (Major and Conor 1993, Howard et al. 2015). Myers et al. (1996) suggested the Musgrave Block accreted as new continental crust on the northern margin of the Gawler Craton.

The eastern Musgrave Province landscape has been subject to numerous orogenic events beginning with the widespread Musgravian Orogeny at 1200–1120 Ma (Camacho and Fanning 1995, Aitken et al. 2009, Dutch et al. 2013). The event involved amphibolite to granulite facies metamorphism and deformation, synchronous with the continental collision of the South Australian Craton to the Western and Northern Australian Cratons (Myers et al. 1996). This tectonic period also saw long–lived (~60 Ma) and voluminous felsic magmatism throughout the region, involving the emplacement of the porphyritic granites of the Pitjantjatjara Supersuite (Wade et al. 2008, Smithies et al. 2011). The extensional Giles Event (1080–1040 Ma) followed, emplacing the mafic–ultramafic sills and dykes of the Giles Complex as well as syntectonic gabbros and granites (Aitken et al. 2009, Raimondo et al. 2010). Deformation associated with this event has been recorded mainly in the western and central regions of the province (Glikson et al. 1996), with limited impact in the east

(Pawley et al. 2014). Related bimodal magmatism prevailed until ~1026 Ma which was followed by relative tectonic quiescence until the onset of the Petermann Orogeny (~600 Ma), punctuated only with the emplacement of two mafic dyke suites around 1000 Ma and 825 Ma (Raimondo et al. 2010, Dutch et al. 2013).

Significant influx of basement–derived sediments into the nearby Amadeus and Officer Basins at ~600 Ma signifies the beginning of the Petermann Orogeny (Sandiford and Hand 1998, Wade et al. 2005, Raimondo et al. 2010). The tectonic style of the intracratonic Neoproterozoic–Cambrian (600–530 Ma) Petermann Orogeny is best described as a high–strain, large crustal–scale transpressional event which exhumed the Musgrave Province to the subsurface from underneath the Centralian Superbasin via central uplift and associated thrust fault reactivations (e.g. Edgoose et al. 2004, Wade et al. 2005, Munson et al. 2013). The event induced major province–wide reworking resulting in the modern E–W trending architecture. High grade metamorphism is especially well preserved in the west of the orogen (Raimondo et al. 2009, 2010). Towards the east, the degree of strain and exhumation decrease to become largely confined to low–grade mylonitic shear zones and localized weak foliations with no clear evidence for pervasive high–temperature metamorphism (Camacho et al. 2002).

Phanerozoic deformation in the Musgrave Province is not well documented. Aitken et al. (2009) and Pawley et al. (2014) interpret the presence of epidote–quartz alteration in shear zones in the east as the reworking of the Musgraves during the Alice Springs Orogeny (ASO). The southern margin of the Musgrave Province and the adjacent Officer Basin are thought to have been more extensively affected by the ASO (Lindsay and Leven 1996, Pawley et al. 2014). In this regard, Tingate and Duddy (2002) suggest

that episodic uplift of the Officer Basin throughout the Phanerozoic might have also affected the Musgrave Province, leading to erosion, subsequent cooling and strengthening of the lithosphere. However, the crustal architecture of the Musgrave Province has been mainly preserved since the Late Palaeozoic – Early Cambrian succeeding the Petermann Orogeny (Aitken et al. 2009). Consequently, it is thought to be reasonably unaffected by later tectonic events despite multiple phases of Phanerozoic extension and shortening linked to the tectonic evolution of the Australian plate (Drexel and Preiss 1995).

Major tectonic events that induced exhumation of the Musgrave Province also had noteworthy effects on nearby sedimentary basins. Influx of Musgrave Block–derived sediments has been recorded syn– and post–Petermann Orogeny in the Officer Basin (Figure 2; Lake Maurice Group, Ungoolya Group, Marla Group; Wade et al. 2005) and the Amadeus Basin (Figure 2; Mt. Currie Conglomerate; Sandiford and Hand 1998, Camacho et al. 2002). Devonian sediment influx is also evident following the onset of the ASO (Lindsay and Leven 1996, Wade et al. 2005). Late ASO movements ultimately led to termination of sedimentation, with any further sedimentation surrounding the Musgrave Block deposited within the overlying Permian Arckaringa and Eromanga Basins, and only scattered deposits around the Amadeus Basin (Lindsay and Korsch 1991, Munson et al. 2013). Understanding the exhumation history of the eastern Musgrave Province will assist in constraining the landscape evolution in the far north of South Australia, and provide insights into the extent of Phanerozoic plate–margin stress propagation towards inland Australia.

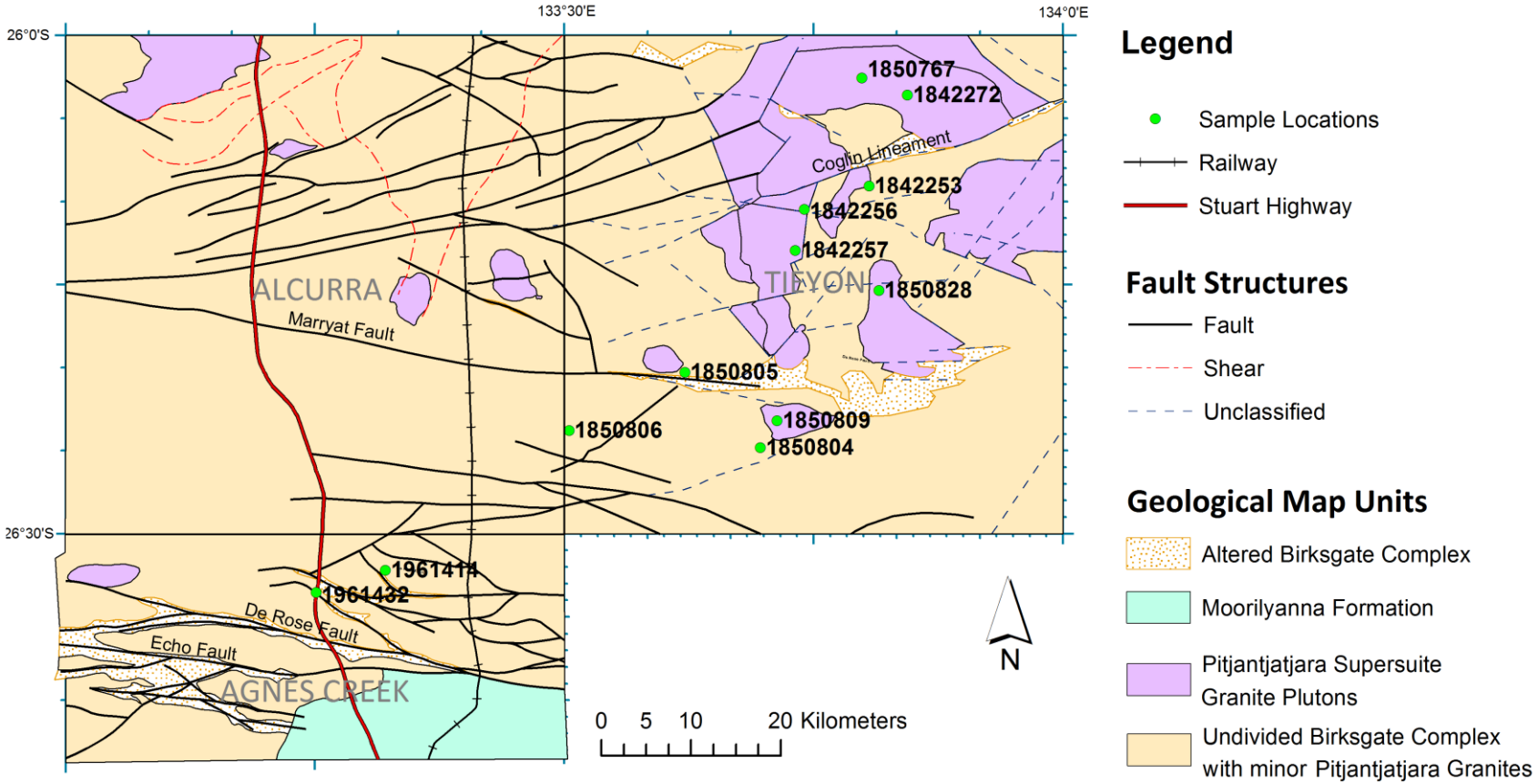

Figure 3: Simplified geological map of the eastern Musgrave Province study region, showing 1:500K geology and major fault structures throughout the study transect. Basic geology and fault structure map layers supplied by Mark Pawley, Geological Survey of South Australia (unpublished data). Sample locations for this study are indicated by green dots and their corresponding sample numbers. A northeast – southwest profile was sampled mainly targeting granitoids across several E–W trending fault structures.

METHODOLOGY

Multi–method (apatite fission track, apatite and zircon U-Th-Sm/He) thermochronology is a powerful tool to study the low–temperature thermal evolution and shallow crustal exhumation history of an intracontinental orogenic system, particularly when samples are taken along and across the main bounding structures of the region (Glorie and De Grave 2015). The following section summarises the methods applied in this thesis. For further detail, refer to Appendix A.

Apatite Fission Track Thermochronology

Apatite fission track (AFT) low-temperature thermochronology is based on the spontaneous fission decay of ^{238}Uranium (^{238}U) producing nuclear damage trails, or fission tracks, within the crystal lattice (Price and Walker 1962). Fission tracks are thermally unstable at elevated temperatures and are subject to progressive shortening (i.e. annealing) (Wagner and Van den haute 1992). AFT chronometry is able to date the time when fission tracks become thermally stable and remain preserved below a certain closure temperature. The AFT closure temperature is dependent on the cooling rate and chemical composition of the apatite, particularly the Chlorine/Fluorine ratio (Green et al. 1986). The fission tracks are only completely retained at temperatures ≤60°C. Between ~60°C and ~120°C, fission tracks shorten or anneal and above ~120°C the crystal lattice is able to completely repair itself from radiation damage thus no tracks are retained (Green et al. 1986). The range between these two temperatures is called the partial annealing zone (PAZ), and fission tracks anneal more the longer they remain within the PAZ. An AFT age can be calculated for a given sample by measuring both the density of spontaneous fission tracks and ^{238}U concentration. The AFT age generally represents the timing of cooling through the PAZ but can be largely meaningless when

this cooling occurred very slowly. The rate of cooling through the PAZ can be assessed by measuring the length of confined fission tracks (Green et al. 1986). AFT ages and length data can be modelled to construct a time–temperature representation of the thermal history of the study region (Tagami 2005). For a detailed insight of AFT thermochronology methods refer to Green et al. (1986), Wagner and Van den haute (1992) and Tagami and O'Sullivan (2005).

Apatite and Zircon (U-Th-Sm)/He Thermochronology

Apatite (AHe) and zircon (ZHe) (U-Th-Sm)/He low–temperature thermochronology is based on the diffusivity of radiogenic ^{4}He through a mineral crystal lattice during a particular temperature range. For apatite, this method records the timing of thermal events between ~45–75°C (Ehlers and Farley 2003). Zircon grains record much higher temperature thermal events: the ZHe method records ages of cooling between ~130–200°C (Wolfe and Stockli 2010).

Samples and Analytical Procedures

The following table outlines sample details including location, lithology and applied methodologies (Table 1).

Table 1: Sample location information, lithology, and applied methods. AFT = Apatite Fission Track, AHe = apatite U-Th-Sm/He, ZHe = zircon U-Th-Sm/He

Sample	Map Region (1:100K mapsheet)	Latitude	Longitude	Lithology	Stratigraphic Unit	Formation Age (Ma)	Methods Applied
1961432 (32)	Agnes Creek	-26.5588	133.2512	Monzogranite	Birksgate Formation	1600-1540	AFT AHe, ZHe
1961414 (14)	Agnes Creek	-26.5365	133.3208	Monzogranite	Birksgate Formation	1600-1540	AFT
1850806 (06)	Tieyon	-26.3964	133.5050	Monzogranite	Pitjantjatjara Granite	1190-1120	AFT AHe, ZHe
1850804 (04)	Tieyon	-26.4135	133.6968	Monzogranite	Pitjantjatjara Granite	1190-1120	AFT
1850809 (09)	Tieyon	-26.3865	133.7134	Monzogranite	Pitjantjatjara Granite	1190-1120	AFT
1850805 (05)	Tieyon	-26.3380	133.6209	Synogranite	Pitjantjatjara Granite	1190-1120	AFT
1850828 (28)	Tieyon	-26.2558	133.8155	Monzogranite	Pitjantjatjara Granite	1190-1120	AFT
1842257 (57)	Tieyon	-26.2157	133.7319	Monzodiorite	Pitjantjatjara Granite	1190-1120	AFT
1842256 (56)	Tieyon	-26.1744	133.7408	Monzodiorite	Pitjantjatjara Granite	1190-1120	AFT AHe, ZHe
1842253 (53)	Tieyon	-26.1513	133.8058	Monzogranite	Pitjantjatjara Granite	1190-1120	AFT
1842272 (72)	Tieyon	-26.0597	133.8442	Monzogranite	Pitjantjatjara Granite	1190-1120	AFT
1850767 (67)	Tieyon	-26.0429	133.7986	Monzogranite	Pitjantjatjara Granite	1190-1120	AFT

Granitoid rock samples were collected from outcrop locations throughout the Eastern Musgrave Province by researchers of the Geological Survey of South Australia (Figure 3). Twelve samples were selected according to apatite abundance and crushed to obtain the intermediate (79–425 μm) grain size for mineral separation. Each sample was panned, magnetically separated and treated through heavy liquid to extract the apatite and zircon–rich portion. Suitable apatite grains were picked and mounted, set in epoxy resin on a slide, and ground and polished to expose the top surface of each grain. Samples were then exposed to 5M HNO_3 at 20°C for 20 seconds to etch out fission tracks, widening tracks so they can be observed under an Olympus BX51 Microscope at 1000x magnification (Wagner and Van den haute 1992). Fission tracks were counted using an eyepiece grid raster as a reference area and all results recorded. To better constrain the rate of cooling through AFT closure temperatures, the lengths of

completely horizontal confined tracks were measured. The lengths (μm) of confined tracks, fission track etch pits (D_{par}) and the angles between the confined tracks and the c-axis of the grains were measured and recorded using the Olympus DP21 camera and computer attachment.

Laser-Ablation Inductively-Induced-Plasma Mass-Spectrometry (LA-ICP-MS) using a New Wave UP213 laser attached to an Agilent 7500CX Quadrupole ICP-MS at Adelaide Microscopy was used to precisely measure the concentrations of ^{238}U, ^{235}Uranium and ^{43}Calcium, required to calculate the AFT age of each counted apatite grain. These concentrations were derived from the exact spot where the fission tracks were counted due to the varied nature of U and Ca concentrations throughout an apatite grain (Hasebe et al. 2004). Calibration of the LA-ICP-MS was performed against a suite of NIST glass standards as primary standards (Pearce et al. 1997) and two apatite secondary standards with known AFT ages (Durango and Arkaroola) were used to check data accuracy. For a detailed description of the calibration procedures used in this thesis refer to Appendix B. For each laser run, the ^{238}U signal intensity was calibrated against ^{43}Ca (internal standard), which is present in both the standards and the apatite unknowns within the grain matrix (De Grave et al. 2012).

Data reduction was applied to LA-ICP-MS results using in–house *Excel*® spreadsheets. A minimal amount of data (<10%) with unreliable U–concentrations due to apparent uranium zoning were excluded from AFT age calculations.

Select apatite and zircon separates were sent to the John De Laeter Centre for Isotope Research at Curtin University for (U-Th-Sm)/He analysis. Three samples were chosen

across the study region, with 10-15 grains of both minerals selected based on quality (e.g. grain shape, inclusion free). ^{4}He gas was thermally extracted from the grains using a 1064 nm Nd-YAG laser before they were dissolved in acid. ^{4}He abundance as well as U, Th and Sm concentrations were determined using isotope dilution inductively-coupled mass spectrometry via the Agilent 7500CS mass spectrometer. For further details on this process, see Appendix A or refer to Danišík et al. (2012).

Modelling and Data Representation

AFT thermochronometry uses radial plots (Galbraith plots) to graphically display the spread in age data with their uncertainties and to determine potential multiple age peaks (Galbraith and Green 1990). For each sample, AFT age peaks were statistically identified using the automatic mixture model in the *RadialPlotter* software (Vermeesch 2015). Where complimentary thermochronometric data was present, the AFT age peaks were assessed against apatite and zircon U-Th-Sm/He data. Overlapping AFT and AHe/ZHe age peaks reveal periods of fast cooling and therefore preservation of a low–temperature thermal events in the data. The different age components were colour coded and pooled according to location to identify regional trends in the dataset. AFT age calculations, length distributions and (U-Th-Sm)/He age results were then modelled using the *HeFTy* software (Ketcham 2005) to constrain the thermal evolution history of the study region between ~200°C and surface outcrop temperatures. All data and modelling results are discussed further below.

OBSERVATIONS AND RESULTS

Apatite Fission Track Results

Fission track analysis was carried out on 12 samples from the eastern Musgrave Province. For all LA-ICP-MS data (after data reduction) obtained for this study the reader is referred to Appendix C. All results from AFT dating and length measurements are summarised in Table 2. All samples except 1850828 show a large enough dispersion of AFT ages to determine multiple age components, and age population peaks were calculated using the automatic mixture model in *RadialPlotter* (Vermeesch 2015). ^{238}U concentration was plotted as a yellow–red colour gradient. The uranium concentration is used as an indicator for radiation damage that may result in differential fission track annealing rates throughout the sample and is therefore used as an aid to validate age discriminations. Patterns between ^{238}U measurements and the single grain ages are generally weak throughout most samples, thus the decomposition of the data–sets into multiple age components is generally unsupported by this factor. Additional AHe and/or ZHe ages are indicated on the plots as well and further support the AFT age–discrimination process.

Radial plots for all samples are shown in Figure 4. In the southwest corner of the study region, sample 32 yields 27% dispersion of grain ages. Using the automatic mixture model in *RadialPlotter* (Vermeesch 2015), three age-components were differentiated at 183±16 Ma (Early Jurassic), 311±16 Ma (Carboniferous), and 457±37 Ma (Late Ordovician). The length histogram is a broad unimodal distribution with an average confined track length of 12.96μm and a standard deviation of 1.29 μm. For sample 14 sampled in the southwest, two AFT age populations were obtained, a Carboniferous (322±12 Ma) age and a Late Ordovician (450±47 Ma) age. Track length data produces a

broad unimodal distribution with an average length of 12.27 μm and standard deviation of 1.54 μm.

In the middle of the study region, sample 06 yields two main age populations peaking during the Late Permian (254±16 Ma) and during the Devonian (396±47 Ma), with the majority of the sample grains contributing towards the Permian peak (73%) while the older, Devonian peak is less well preserved (27%). Confined track lengths produce a mean track length of 13.24 μm and a standard deviation of 1.44 μm, with a bimodal distribution reflecting multiple cooling episodes. Sample 04 records two AFT age populations during the Late Carboniferous – Early Permian (299±12 Ma) and the Ordovician (448±73 Ma). The Carboniferous age is the dominant result with 90% of grains contributing to this age peak, with only 10% constraining the Ordovician peak. Confined track measurements produce a unimodal length distribution with a mean of 12.67 μm and standard deviation of 1.14 μm. Sample 09 yields 25% dispersion, differentiating two age-components at 115±21 Ma (Cretaceous) and 290±13 Ma (Early Permian). The youngest Cretaceous age peak is constrained by two single grains only and caution is required to not interpret this age in too much detail at the individual sample level. Confined track lengths produce a unimodal distribution with an average confined track length of 12.08 μm and standard deviation of 1.2 μm. Sample 05 yields 19% dispersion between individual grains, decomposing the age data into two AFT peaks: a Triassic age (240±28 Ma) and a Silurian – Devonian age (416±18 Ma). The length histogram suggests a bimodal distribution with mean length of 12.99 μm however with only 17 confined tracks measured this result may not be thoroughly conclusive.

In the mid–north section of the study region, sample 28 presents only 8.5% dispersion amongst the spread of individual ages and therefore records one single AFT population peak during the Late Permian (252.4±8.1 Ma). Fission track length data could not be obtained due to insufficient confined fission tracks in the apatite grains. For sample 57, two AFT age populations have been chosen to best fit the spread despite dispersion being relatively low at 11%. This can be accounted for with the clear difference in ^{238}U concentration between both age clusters, which may be indicative for differential annealing rates and AFT age preservation potential. Age populations peak at 267 ± 25 Ma (Permian) and 342 ± 43 Ma (Carboniferous). The length histogram is bimodal with mean track length 11.72 μm and a large standard deviation of 2.03 μm, reflecting a complex thermal history as observed by the multiple AFT age peaks. Sample 56 yields 31% dispersion and this constrained three AFT age peaks at 291±15 Ma (early Permian), 485±50 Ma (Early Ordovician), and 625±83 Ma (Neoproterozoic – Cambrian). Confined track lengths show a moderately bimodal distribution with a mean length of 11.11μm and standard deviation of 1.49 μm. This sample records the oldest preserved AFT ages of the study area. Sample 53 yields two AFT age peaks, an early Triassic (249±18 Ma) age and a Late Devonian (364±29 Ma) age. Minor scatter of individual ages between populations is present, but statistically half the grains contribute to each peak. The length histogram produces a unimodal spread with an average length of 12.72 μm with a standard deviation of 1.17 μm.

In the northwest of the study area, sample 72 shows two distinctive AFT age populations at 197±15 Ma (Early Jurassic) and 328±13 Ma (Carboniferous). The majority of the grain ages contribute to the Carboniferous peak (79%) with 4 grains constraining the Jurassic peak. Confined track lengths reflect the two ages with a spread

of both longer and shorter lengths preserved, an average length of 11.85 μm and a standard deviation of 1.63 μm. Sample 67 yields one single AFT age peak which is Carboniferous (301.8±8.5 Ma) in age. Track length data produced a mean track length of 10.93 μm with a standard deviation of 1.75 μm. However only 13 confined track lengths were measured so caution is required to not interpret this distribution in too much detail.

When all samples are pooled on the same radial plot, four main age populations can be distinguished: 589±79 Ma (Neoproterozoic – Cambrian), 423±44 Ma (Ordovician – Devonian), 305±13 Ma (Carboniferous – Early Permian), and 218±14 Ma (Late Triassic – Jurassic) (Figure 5). All AFT age peaks are supported by AHe or ZHe data that fall within the grey shaded areas. These age populations are interpreted to represent the timing of significant cooling episodes through the AFT closure temperatures ~120–60°C as response to regional tectonic events.

Figure 4: (pages 23, 24, 25). Radial Plots of Apatite Fission Track (AFT) ages from all samples in this study displaying all low-T data obtained. Central value indicates the central age of the sample, n=number of grains measured, dispersion indicates percentage of age dispersion within the sample data. Each analysed age is plotted corresponding to its precision, which is used to determine multiple age-components (peaks). Individual AFT ages are determined by running a straight line from the 0 point on the left of the plot, through the grain (coloured dot) to the curved scale on the right side which reveals age (in Ma). Grey shaded areas highlight the AFT peak population zones taking into account the age standard deviation. The standard deviation (σ/t) is measured along the x-axis, decreasing from left to right; therefore the age of the grains are more precise if they plot closer to the right side of the plot. The error bar is shown as ± 2 σ on the left which is constant for all grains. The yellow-red colour scale bar indicates concentration of ^{238}Uranium (ppm). Radial plot was constructed using *Radial Plotter* (Vermeesch 2015). Where more than one age population is present, the central age is spit into age peaks using the automatic mixture model within *RadialPlotter* (Vermeesch 2015). All ages obtained from all radial plots are presented in Table 2. To the right of each radial plot (except sample 28) is an AFT length distribution histogram, which is used to assess the cooling rate (see text). AFT length is in μm, n indicates the number of confined tracks measured, l_m is the average track length, and σ is the standard deviation of the sample lengths.

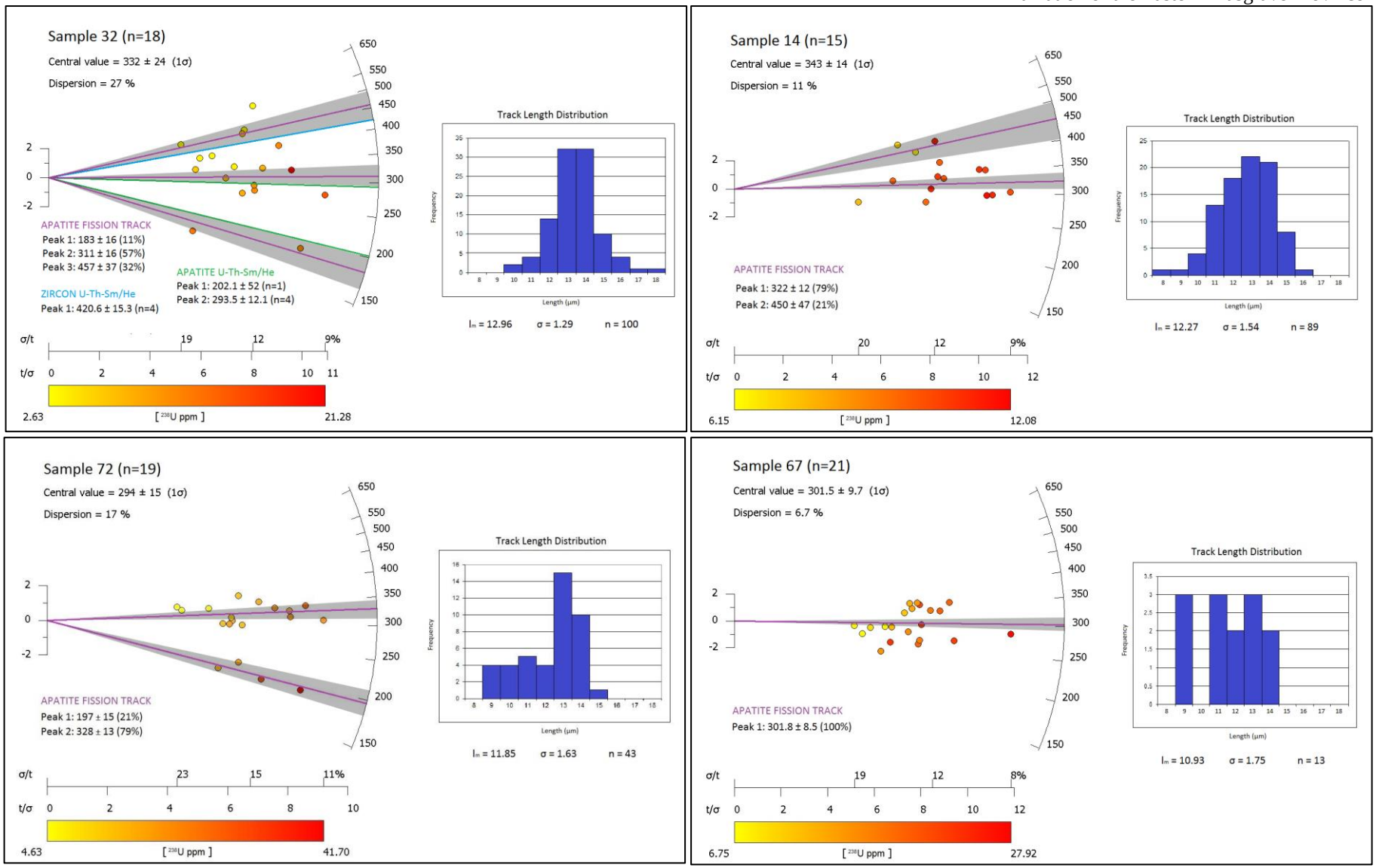

Figure 4: For full description see above. Margin samples, southwest (32 and 14) and northeast (72 and 67).

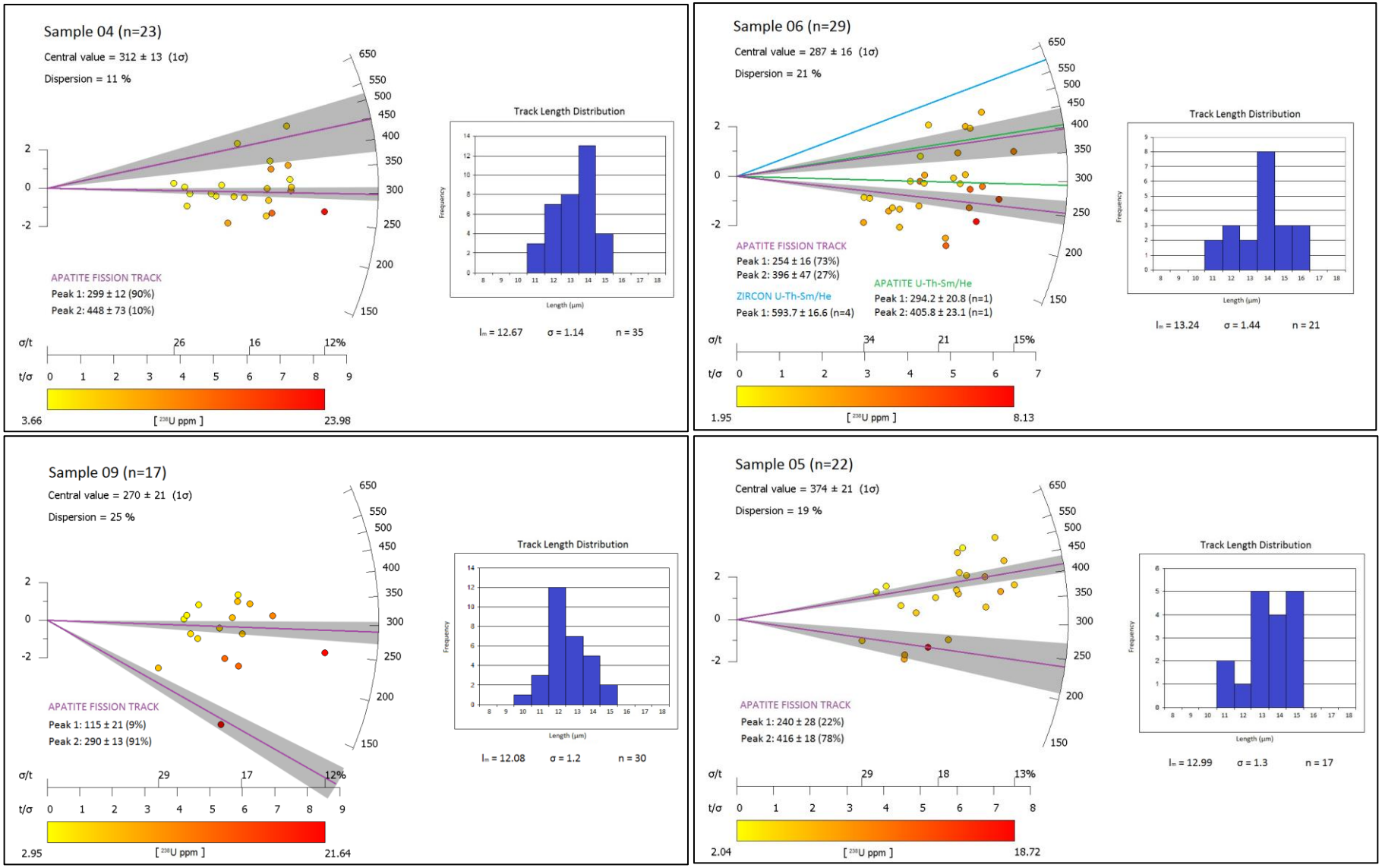

Figure 4: (continued). Samples 04, 06, 09 and 05 from the middle of the study region.

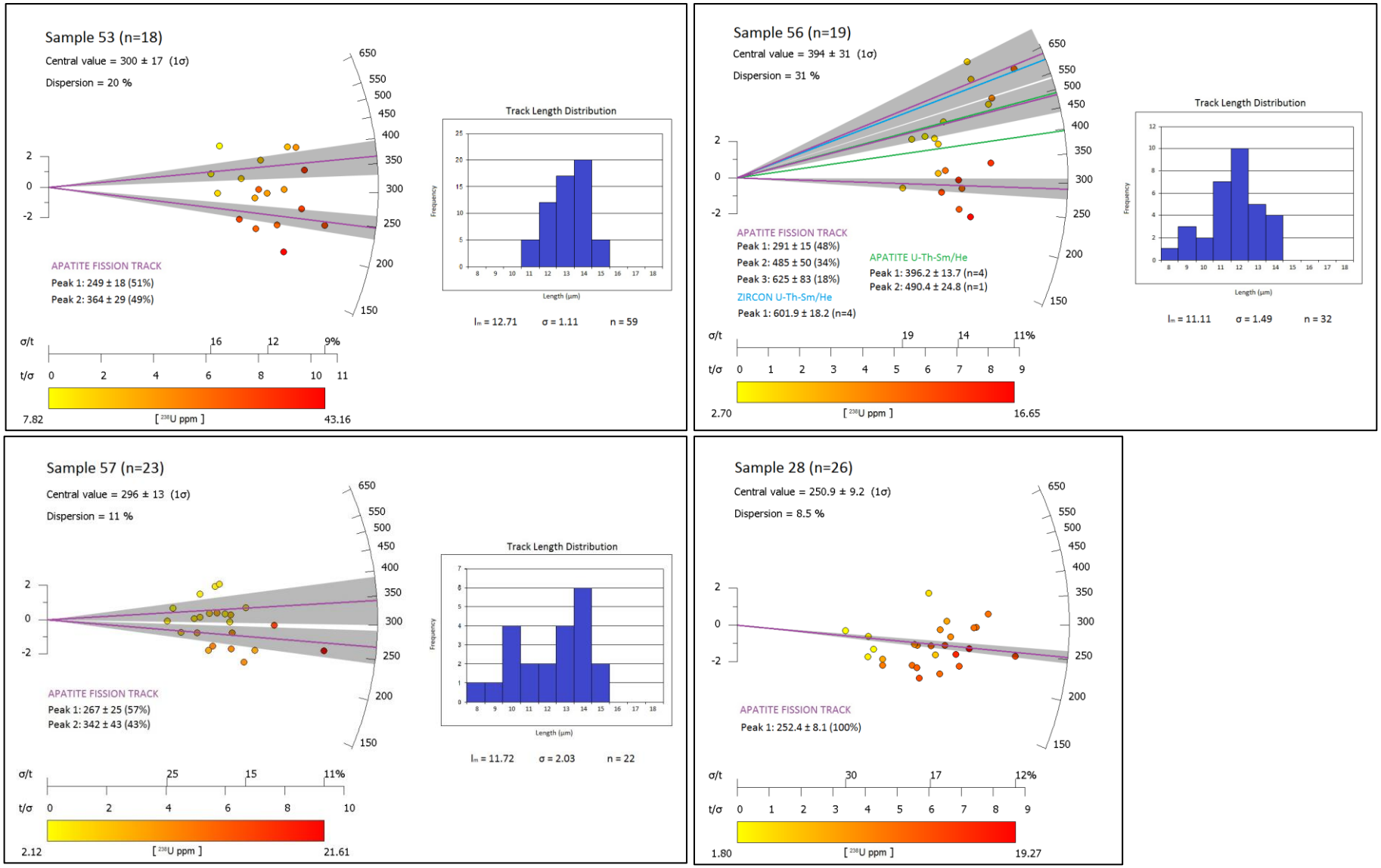

Figure 4: (continued). Samples 53, 56, 57 and 28 from the mid-north of the study region.

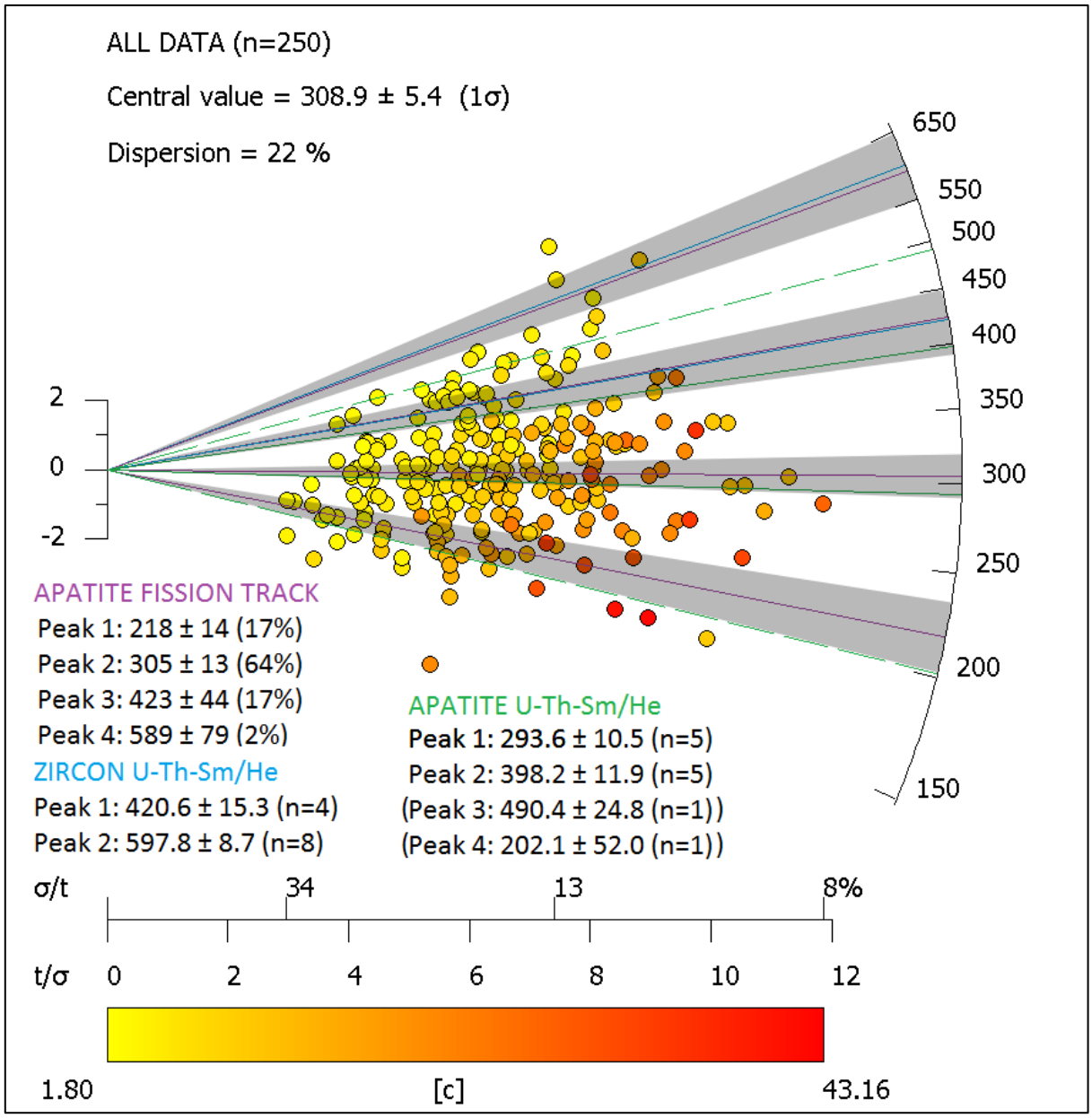

Figure 5: Cumulative radial plot of all the AFT ages obtained in this study, illustrating the main AFT age peaks. Plot was constructed using the *RadialPlotter* software program (Vermeesch 2015). For a detailed description on radial plots see Figure 4. AFT, AHe and ZHe age peaks are defined. Grey zones highlight the four cumulative age peaks of this study based on all low-T chronometers applied.

Sample	Lithology	ρs	N_s	N	^{238}U σ	AFT age (σ)	AFT Peak 1	AFT Peak 2	AFT Peak 3	l_m	n	σc
32	Monzogranite	14.28	86	18	8.415 0.522	332 (24)	183 (16)	311 (16)	457 (37)	12.96	100	1.29
14	Monzogranite	18.87	82	15	10.077 0.328	343 (14)	322 (12)	450 (47)		12.27	89	1.54
06	Monzogranite	63.41	24	29	4.162 0.188	287 (16)	254 (16)	396 (47)		-	-	-
04	Monzogranite	12.75	44	23	7.774 0.438	312 (13)	299 (12)	448 (73)		12.67	35	1.14
09	Monzogranite	12.34	34	17	9.124 0.397	270 (21)	115 (21)	290 (13)		12.08	30	1.20
05	Syenogranite	11.12	37	22	5.862 0.271	374 (21)	240 (28)	416 (18)		12.99	17	1.30
28	Monzogranite	13.49	43	26	10.253 0.555	250.9 (9.2)	252.4 (8.1)			-	-	-
57	Monzodiorite	11.76	44	23	7.677 0.517	296 (13)	267 (25)	342 (43)		11.72	22	2.03
56	Monzodiorite	17.20	57	19	8.420 0.420	394 (31)	291 (15)	485 (50)	625 (83)	-	-	-
53	Monzogranite	37.62	92	18	24.208 1.354	300 (17)	249 (18)	364 (29)		12.72	60	1.17
72	Monzogranite	26.26	62	19	17.090 1.147	294 (15)	197 (15)	328 (13)		11.85	43	1.63
67	Monzogranite	26.99	70	21	16.637 0.767	301.5 (9.7)	301.8 (8.5)			10.93	13	1.75

Table 2: Sample details, AFT results, and confined track length data for all samples. Averages of measured data are shown, where ρs is the surface density of spontaneous fission tracks (in 10^5 tracks/cm^2). N_s is the number of counted spontaneous tracks, N is the number of successful grains analysed. ^{238}U is the average ^{238}U concentration, measured by LA-ICP-MS (in µg/g). AFT age is the central age statistically generated for each sample (in Ma). Per sample, results of individual age peaks are labelled AFT Peak 1, 2, 3 (in Ma). σ is the standard deviation (units dependent on result). For length data, l_m is the average confined track length, n is the number of confined tracks measured, and σc is the standard deviation of confined track measurements.

(U-Th-Sm)/He Thermochronology

AHe and ZHe analysis was carried out on three samples in this study: 06, 56 and 32. Results from AHe and ZHe dating are summarised in Tables 3 and 4, and peaks are illustrated on radial plots in Figure 4.

For sample 56, two AHe age peaks are distinguished, a Devonian age (396.2±13.7 Ma) and a Cambrian age (490.4±24.8 Ma). The Cambrian age is based on a single grain aliquot, and the Devonian age encompasses the average of four single grain aliquots ranging from 383–413 Ma. The Cambrian age mimics the middle AFT age peak (485±50 Ma). The Devonian age plots in between the two youngest AFT age populations (291±15 and 485±50 Ma), and could either represent a mixing age between the two AFT results or excess helium accumulation in the apatite crystals (Flowers et al. 2009, Chew and Spikings 2015). Two AHe age peaks are identified for sample 32, a Late Triassic (202.1±52 Ma) and an Early Permian (293.5±12.1 Ma) age. The Triassic age is based on one apatite grain however it corresponds well with the youngest AFT age cluster for this sample (183±16 Ma). The Permian age is an average based on four grain analyses and corresponds well with the middle AFT age (311±16 Ma). For sample 06, two apatite grains were analysed, yielding a Permian age (294±20.8 Ma) and a Devonian age (405.8±23.1 Ma). Both ages correspond well with the obtained AFT age clusters of 254±16 and 396±47 respectively.

ZHe ages were obtained for the same three samples. Each sample analysed four single zircon grains and produced an average ZHe single age, assuring the results are reliable. For sample 06 a Neoproterozoic age was identified (593.7±16.6 Ma) which is much

older than all AFT and AHe data. This is interpreted to date cooling of the rock through the ZHe closure temperatures (~200–130°C) during the late Neoproterozoic. Sample 56 yields a ZHe age of 601.9±18.2 Ma, which is comparable with, and within error of the oldest AFT age mean (625±83 Ma). Sample 32 yields are younger Silurian (420.6±15.3 Ma) ZHe age, correlating well to the oldest AFT age of 457±37 Ma.

Table 3: Apatite (U-Th-Sm)/He dating results. Concentrations for U, Th and Sm are in ng. Concentrations for ^{4}He are in ncc/µg. Ft is the α-ejection correction factor (Farley 2002). He Age is given in Ma. AFT Age peaks (in Ma) for each sample are also indicated if they correlate well with He ages. N is the number of grains analysed that contributed to each He age peak.

AHe Sample	^{238}U σ	^{232}Th σ	^{147}Sm σ	^{232}Th/^{238}U	^{4}He σ	Ft	He Age	N	AFT Age
06	0.0085.9	0.1005.7	0.0070.4	11.77	0.8072.2	0.70	294 ± 20.8	1	254 ± 16
	0.0075.9	0.0735.7	0.0080.5	10.79	0.6802.2	0.57	405.8 ± 23.1	1	396 ± 47
56	0.0264.6	0.1944.5	0.0260.3	7.42	2.1334.6	0.59	396.2 ± 13.7	4	-
	0.0185.9	0.0985.7	0.0170.4	5.28	1.3182.1	0.52	490.4 ± 24.8	1	485 ± 50
32	0.1714.2	0.0001143.6	0.0260.4	0.0004	3.14323.6	0.74	202.1 ± 52	1	183 ± 16
	0.1215.0	0.0115.0	0.0270.4	0.10	3.3972.7	0.75	293.5 ± 12.1	4	311 ± 16

Table 4: Zircon (U-Th-Sm)/He dating results. Concentrations for U, Th and Sm are in ng. Concentrations for ^{4}He are in ncc/µg. Ft is the α-ejection correction factor (Farley 2002). He Age is given in Ma. AFT Age peaks (in Ma) for each sample are also indicated if they correlate well with He ages. N is the number of grains analysed that contributed to each He age peak.

ZHe Sample	^{238}U σ	^{232}Th σ	^{147}Sm σ	^{232}Th/^{238}U	^{4}He σ	Ft	He Age	N	AFT Age
06	0.3471.9	0.7021.4	0.0021.7	1.97	26.22.3	0.68	593.7 ± 16.6	4	-
56	0.4171.9	0.3751.4	0.00123.0	0.87	26.63.0	0.69	601.9 ± 18.2	4	625 ± 83
32	1.4981.9	0.6621.4	0.00224.1	0.44	65.02.2	0.74	420.6 ± 15.3	4	457 ± 37

HeFTy Time-Temperature Models

Representative *HeFTy* time–temperature models are presented in Figure 6. The *HeFTy* software models the path the rocks travelled in time-temperature space from a chosen time to the present using combinations of AFT ages, length data, and AHe/ZHe ages if available. To produce a statistically acceptable model, AFT ages and length data are the minimum input required. High and low time/temperature endpoints were set at near the oldest obtained data (800–600 Ma, ~600°C), and present-day outcrop temperature (~20°C). This modelling is primarily designed to model low–temperature cooling (below ~200°C) therefore the exact timing and extent of the thermal history above this temperature cannot be estimated with precision. It is assumed all samples started at significant depth and high temperatures prior to the Ediacaran–aged Petermann Orogeny.

The models for samples for which only AFT ages and length data were available (samples 14, 04, 09, 05, 57, 53, 72 and 67) are not well constrained. These models show a general trend of unconstrained cooling from before the Petermann Orogeny (~650 Ma) to their first AFT age constraint. The samples then exhibit a period of thermal quiescence, remaining near AFT PAZ temperatures (~120–60°C) until a second AFT age constraint (ranging anywhere between 350–200 Ma) is reached. The exception is sample 67 with only one constraining AFT peak, yet this sample still shows a protracted crustal history within these temperatures. From then on all samples follow a gradual cooling path through shallow near–surface conditions towards exposure. Overall, the models suggest all samples were cooled to temperatures below ~120°C at some stage between the Neoproterozoic and the Carboniferous, but clear evidence for thermal

events or any cooling rate estimates within this period are not constrainable by AFT data only in these samples, and these models are therefore not discussed further (refer to Appendix D).

Samples 32, 06 and 56 for which additional AHe and ZHe data were obtained, exhibit a complex and better constrained thermal history, producing more reliable thermal history paths. Cooling pulses during the Neoproterozoic are constrainable in samples 06 and 56 from the middle region of the study area, utilising a combination of AFT and ZHe age data. Both samples show rapid cooling to ZHe or lower AFT closure temperatures during the late Neoproterozoic (~600Ma), followed by slow cooling or thermal quiescence to subsurface temperatures at ~450 Ma. Sample 06 shows an increased cooling rate at ~440 Ma reach to surface temperatures at ~430 Ma. The model for sample 56 shows little thermal perturbations since the Ordovician besides a gentle thermal pulse at ~300 Ma and an apparent increase in cooling rate since the Late Cretaceous. The model for sample 06 yields a similar although better defined thermal event at ~300 Ma and little thermal perturbations since the end of the Palaeozoic. Sample 32 from the southwest records no constrained path through the Neoproterozoic, instead ZHe data suggest a model where rocks reach ~200–100°C during the Silurian, then remain around these temperatures until a pronounced cooling pulse brought the sample to near surface temperatures in the Carboniferous (~350–320 Ma). The model further suggests that the sample may have undergone shallow reheating towards the end of the Triassic followed by slow cooling towards present day exposure.

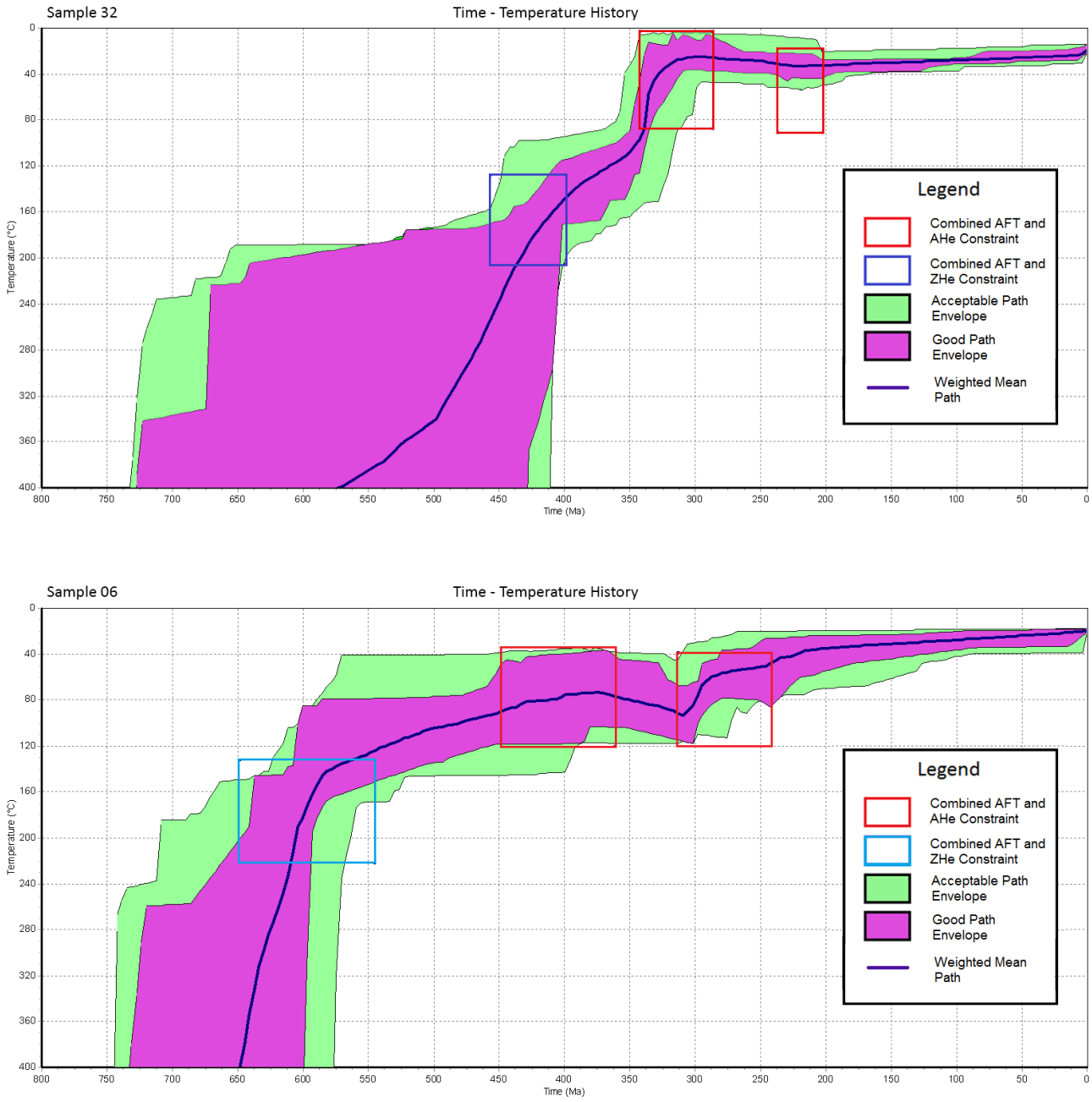

Figure 6: Time-Temperature models for representative samples across the study region (samples 32, 06 and 56). Models were constructed using the modelling software *HeFTy* (Ketcham 2005). Low–T thermochronological constraints are shown as boxes with different colours representing different low–T methods used in this study. Acceptable cooling path envelopes are shown in green, statistically good fit path envelopes are shown in purple. For all samples the default merit value for good paths of 0.5 and merit value for acceptable paths of 0.05 were used. Models for these samples exhibit more complex thermal histories with constraints based on AHe and ZHe data as well as AFT ages.

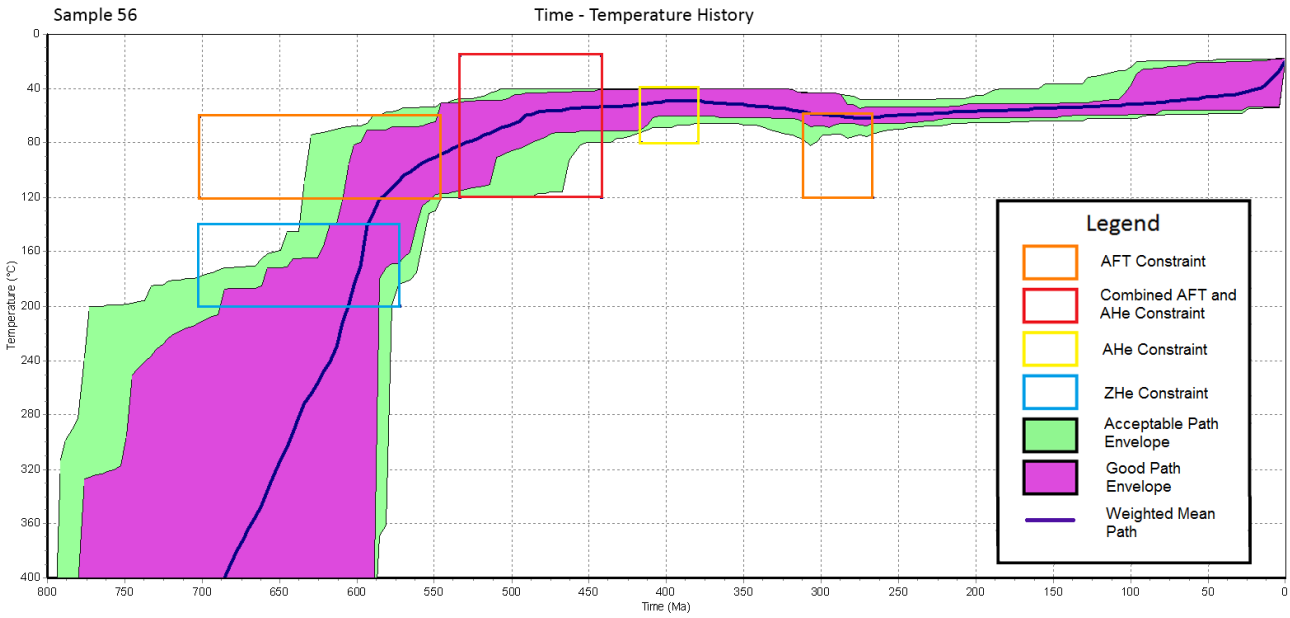

Figure 6: Continued.

DISCUSSION

Regional thermal history interpretation

For the pooled sample radial plot, four main age populations can be distinguished at: 589±79 Ma, 423±44 Ma, 305±13 Ma, and 218±14 Ma (Figure 5). This plot is based on 250 individual AFT ages and is representative for the low temperature thermal history of the entire study area. The four defined age populations are mimicked with two ZHe and four AHe analyses and are interpreted to represent the timing of significant tectonothermal episodes during the Neoproterozoic – Cambrian, Silurian – Early Devonian, Carboniferous – Early Permian, and Late Triassic – Jurassic.

NEOPROTEROZOIC – CAMBRIAN

The oldest AFT and ZHe cooling ages collected in this study (~590 Ma) are synchronous with the Petermann Orogeny (~600–530 Ma). The Petermann Orogeny has been widely interpreted in literature as being driven by N–S compression of the Australian plate during the amalgamation of Gondwana in the Neoproterozoic (e.g. Hand and Sandiford 1999, Raimondo et al. 2010). Edgoose et al. (2004) describes the tectonic style of the Petermann Orogeny as a large–scale transpressional event and most literature confirms that the Musgrave Block was largely exhumed to the subsurface during this event (e.g. Cawood and Korsch 2008, Raimondo et al. 2010). In the western Musgraves, Raimondo et al. (2010) found peak metamorphic conditions ~570 Ma with rocks cooling to 660 – 600°C by 540 Ma. Data from this study suggests that in the east of the orogen, cooling may have progressed to much lower temperatures earlier than this, however due to the large AFT age error this remains speculation. Nevertheless, the observation of Petermann–aged exhumation in this study is concordant with known exhumation of the entire Musgrave Province during this time.

SILURIAN – EARLY DEVONIAN

The late Silurian – Early Devonian thermal event, evidenced by multiple thermochronological data from this study (423±44 Ma) can be linked with an early pulse of the Alice Springs Orogeny (ASO; Mawby et al. 1999, McLaren et al. 2009). The ASO caused significant crustal thickening and exhumation throughout central parts of Australia, especially to the north of the Amadeus Basin in the Arunta Block (Ballèvre et al. 2000, McLaren et al. 2009). The ASO is classically linked to exhumation in central Australia, mainly within the Northern Territory (Wells et al. 1970, Kohn et al. 2002) but is now increasingly recognised as affecting regions in southern Australia (e.g.

Mitchell et al. 1998, Gibson and Stüwe 2000, Hall 2014). AFT ages from the central Gawler Craton suggest prolonged cooling and exhumation spanning most of the Palaeozoic (Gleadow et al. 2002b, Kohn et al. 2002, Boone 2013). Reddy et al. (2014) attributes Gawler Craton Palaeozoic cooling to the Delamerian Orogeny (514–490 Ma) which was further enhanced during the onset of the ASO since ~450 Ma (Raimondo et al. 2014). Results from this thesis suggest that the eastern Musgrave Province was distally affected during the early stages of the ASO resulting in a pulse of exhumation. The data presented here furthermore shows no clear signs for Delamerian induced cooling and exhumation, suggesting that the Delamerian Orogeny did not affect the eastern Musgraves.

CARBONIFEROUS – PERMIAN

The Carboniferous – Permian thermal event in the data presented in this study (peaking at 305±13 Ma) correlates well with the final stages of the ASO (McLaren et al. 2009). Regional AFT studies (Gleadow et al. 2002b, Kohn et al. 2002) propose that Carboniferous exhumation occurred throughout most of South Australia. Tingate and Duddy (2002) record evidence for Carboniferous – Permian cooling (~350–250 Ma) in the Officer Basin and correlate this cooling with uplift and erosion in the Amadeus Basin to the north during the ASO (Wells et al. 1970, Tingate 1990). Carboniferous exhumation has been observed by several studies throughout the Gawler Craton (Boone 2013, Hall 2014, Reddy 2014) and Carboniferous – Permian exhumation is also documented for the Adelaide Fold Belt in South Australia (Gibson and Stüwe 2000). Results from this study further confirm a Carboniferous pulse of the Alice Springs Orogeny affected central and southern Australia on a regional scale.

TRIASSIC – JURASSIC

The youngest Triassic – Jurassic event is evident to varying degrees across the study area. Southern Australia was landlocked and largely tectonically stable during the Triassic (Drexel and Preiss 1995). Towards the Middle Jurassic a new tectonic regime initiated, reflecting global changes with the onset of the break–up of Gondwana and consequent plate–motion induced crustal instability (Drexel and Preiss 1995). The youngest AFT age peak produced in this study is predominately Triassic and therefore more likely reflects an event that pre–dates the beginning of Gondwana rifting. Early Mesozoic events have been documented for the Officer and Cooper Basins, the Gawler Craton, and the northern Flinders Ranges (Mavromatidis 2007, Hall 2014, Reddy et al. 2014, Weisheit et al. 2014). In the central Gawler Craton, Reddy et al. (2014) interpret this event to local exhumation in response to distal southern Australian margin rifting, whereas Hall (2014) and Weisheit et al. (2014) relate early Mesozoic ages to hydrothermal activity within the Peake and Denison Ranges and the northern Flinders Ranges, respectively. Within the Officer Basin, Permian – Triassic AFT ages are assumed to be related with heating by sedimentary burial. The thermal history models for this study suggest that Triassic – Jurassic reheating occurred within the eastern Musgraves as well. During this period sedimentary deposition in inland Australia was dominated by low–energy fine clastics now preserved in northeastern South Australia in the Cooper and Simpson Basins (Drexel and Preiss 1995). Sedimentary units in the Simpson Basin and the overlying Eromanga Basin to the east of the Musgraves may be suggestive of erosion and deposition, possibly in response to far–field stress from the onset of Gondwana rifting (Drexel and Preiss 1995). In this study we suggest an elevated thermal gradient at that time as the most plausible model for this thermal event.

More data are needed to understand this thermal event in more detail, however the results for this study suggest that the early Mesozoic thermal event affected inland Australia on a more regional scale than previously anticipated.

Differential exhumation across the Eastern Musgrave Province

The four thermal events are displayed in variable extent on the radial plots and the regional representative *HeFTy* models. The model for sample 32 shows little evidence for Neoproterozoic cooling (Petermann Orogeny) and a more extensive record of Alice Springs orogenic cooling (~423 and ~305 Ma; Figure 6). The model for sample 06 exhibits thermal events during both the Petermann and Alice Springs orogenies and sample 56 shows only clear evidence for Neoproterozoic cooling and little evidence for subsequent events (Figure 6). Given that all these samples were taken from a confined study area, it is unlikely that the ASO only affected part of the study area while other segments were unaffected. The differences in thermal histories are therefore interpreted as representing different preservation of thermal pulses in the upper crust as a result of differential exhumation along the main bounding structures of the study area. Given that only few reliable *HeFTy* models were obtained, individual and pooled radial plots are used to discuss this differential exhumation and preservation of the thermal history record across the study area. In order to provide more details on this differential exhumation model, data were pooled according to sample locations, taking into account their relation to major E–W–trending fault systems. Four fault–bounded blocks are discussed separately below.

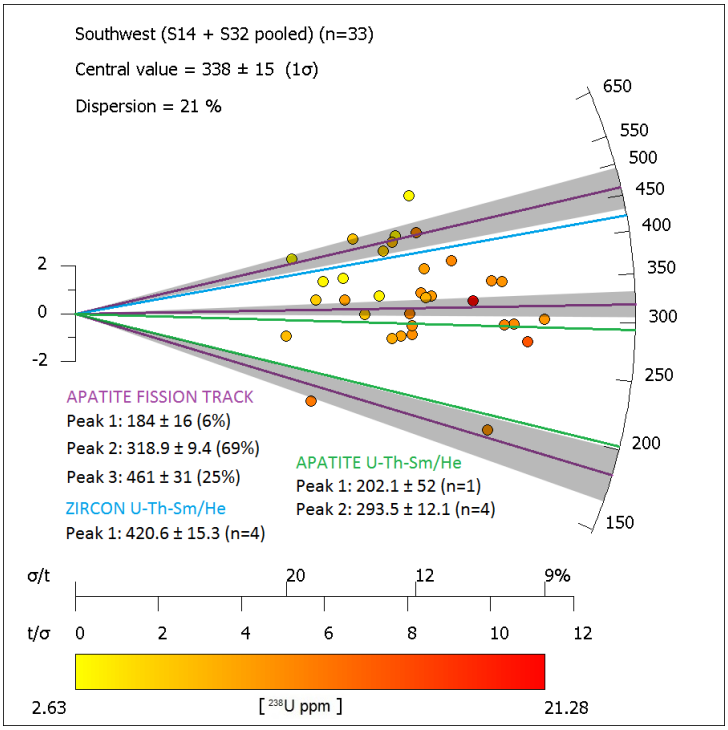

Figure 7: Pooled radial plot of AFT ages for samples 32 and 14 in the southwest of the study region. AFT age peaks were constructed using the software program *RadialPlotter* (Vermeesch 2015). For a detailed description of radial plots see Figure 4. Here, three AFT age peaks are defined, as well as AHe and ZHe age peaks. Grey zones highlight the cumulative AFT age peaks taking into account the age standard deviation.

Figure 7 illustrates a pooled radial plot of data obtained for the southern–most samples, 32 and 14, located just north of the De Rose and Echo fault systems. Silurian (~450–420 Ma, early ASO), Carboniferous (~320–290 Ma, late ASO) and late Triassic – Jurassic (~200–180 Ma) thermal events are observed. All three thermal events are constrained by multiple thermochrometric methods. The Silurian data are constrained with ZHe and AFT methods suggesting that the samples cooled quickly from higher temperatures (~200-120°C) and deeper crustal levels during this time. The Carboniferous and late Triassic – Jurassic data are constrained by the AFT and AHe methods, indicating more shallow thermal perturbations. This is modelled as two cooling steps and a subtle reheating step in the representative thermal history model for sample 32 (Figure 6). The two samples are thus interpreted to have undergone two pulses of cooling during the

ASO (at ~420 Ma and ~300 Ma), followed by a reheating episode during early Mesozoic. The latter pulse is attributed to a regional elevated geothermal gradient at that time. Overall, the south–western region of the study area accumulatively preserves three of the four thermal events recorded within the study area. Neoproterozoic ages were not preserved, suggesting that the south–western segment of the study area preserves a relatively deep level of exhumation.

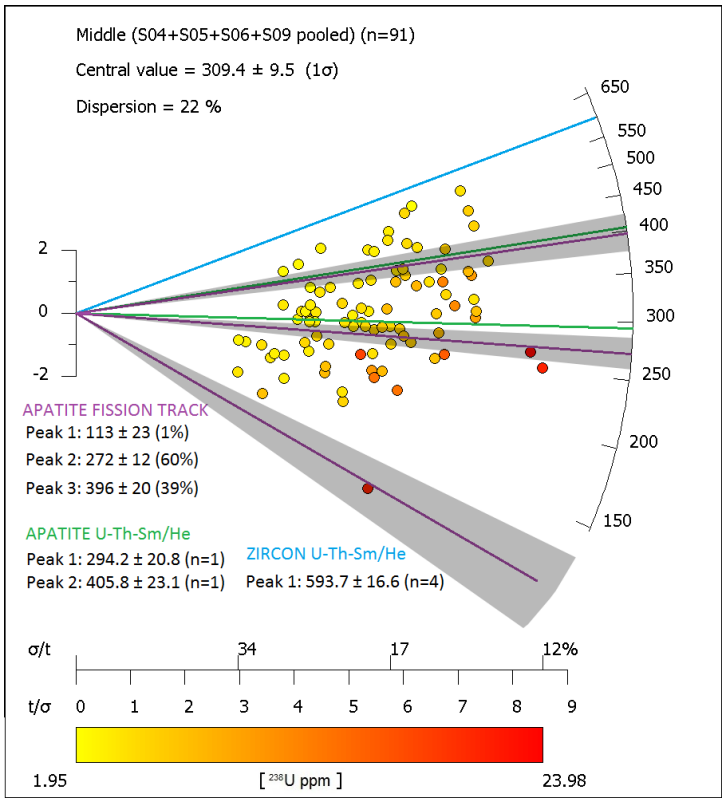

Figure 8: Pooled radial plot of AFT ages for samples 04, 05, 06 and 09 in the middle of the study region. AFT age peaks were constructed using the software program *RadialPlotter* (Vermeesch 2015). For a detailed description of radial plots see Figure 4. Here, three AFT age peaks are defined, as well as AHe and ZHe age peaks. Grey zones highlight the cumulative AFT age peaks taking into account the age standard deviation.

All data for the middle section of the study region (samples 04, 05, 06 and 09) are pooled together in Figure 8. This region preserves all four thermal events to varying degrees. In contrast to the southwest, here Neoproterozoic cooling is preserved in the

ZHe data and indicates a slightly lower exhumation level. This cooling is however not observed in AFT data, suggesting that it is not preserved at shallow crustal levels. Abundant AFT results constrain at least two later events (~400 Ma, early ASO; ~280–290 Ma, late ASO). The pooled plot furthermore shows a diffuse trend of younger (Mesozoic) AFT data towards an anomalously young Cretaceous AFT age (constrained by only 1% of the total AFT data). This plotted trend suggests that Mesozoic reheating affected this study area as discussed above but no clear conclusions can be made on the precise timing of this event. The Cretaceous peak is not well constrained and therefore not discussed further.

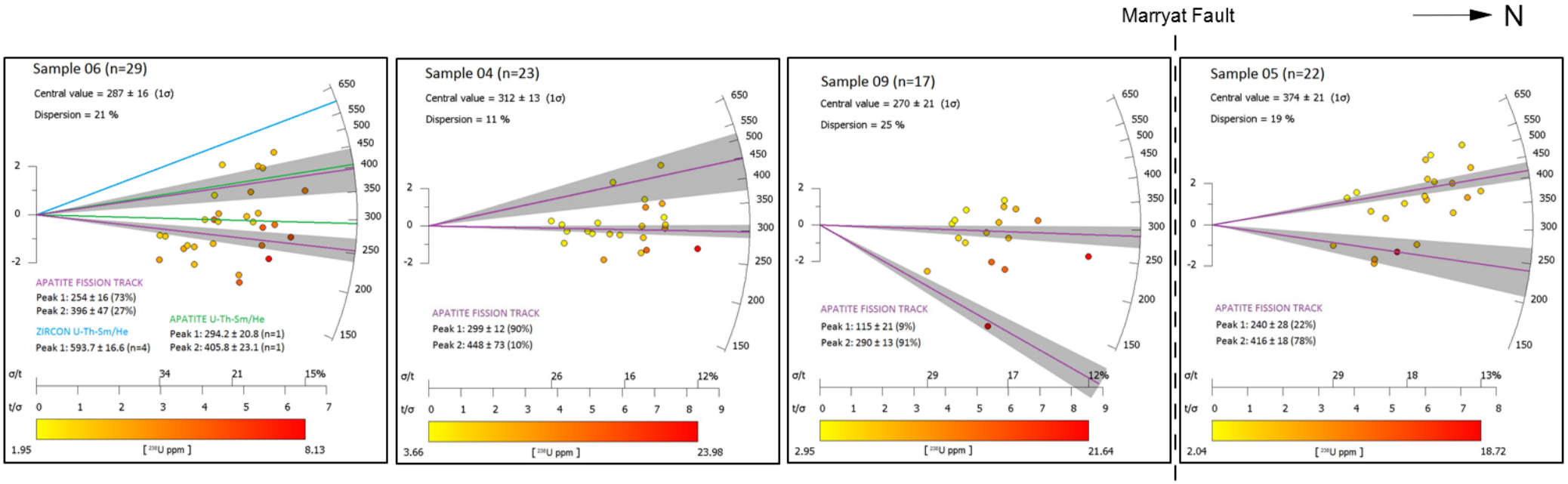

Figure 9: Radial Plots for the middle region of the study area (samples 04, 06, 09 and 05). AFT age peaks were statistically constructed using the software program *RadialPlotter* (Vermeesch 2015). For a detailed description of radial plots see Figure 4. AFT age peaks are defined in purple, AHe age peaks in green and ZHe age peaks in blue. Percentage of total grains (for AFT) and number of grain aliquots (for AHe/ZHe) contributing towards each population peak are indicated. Grey zones highlight the cumulative AFT age peaks taking into account the age standard deviations.

Comparing samples from the middle of the sample transect reveals a clear pattern of increasing exhumation northwards towards the Marryat Fault. Figure 9 illustrates this model by lining up the radial plots for samples 06, 04, and 09 south of the Marryat Fault, and 05 located just north of the fault (Figure 3). Starting furthest from the fault, sample 06 shows two thermal events peaking during the Devonian (~400 Ma, early ASO) and Late Permian (~250 Ma, late ASO). These results are modelled as two cooling steps and a distinct reheating step in the thermal history model for sample 06 (Figure 6). Similar to the southwest, the two AFT peaks can be attributed to exhumation during the early and later stages of the ASO, with the late pulse being more pronounced. In sample 04 closer towards the fault, early ASO ages (~450 Ma) are noticeably less preserved compared to sample 06 and the younger late ASO (~300 Ma) peak becomes more defined. Closer to the fault again, sample 09 shows no preservation of an early ASO thermal event, but exhibits a strong Carboniferous – Permian age (~290 Ma). This sample also preserves the youngest AFT age obtained in this study (~115 Ma) but as it is only constrained by 2 single grain ages more data are required to validate this result. Importantly, these three samples preserve increasingly deeper levels of exhumation towards the major E–W–trending Marryat Fault. To the north of the fault, sample 05 shows the largest cluster of Silurian – Devonian AFT ages (peaking at ~420 Ma, early ASO) indicating a shift back to a shallower level of exhumation. This transition provides strong evidence for differential exhumation on either side of the Marryat Fault and therefore suggests that Phanerozoic (post–300 Ma) fault reactivation affected the study area (Figure 13).

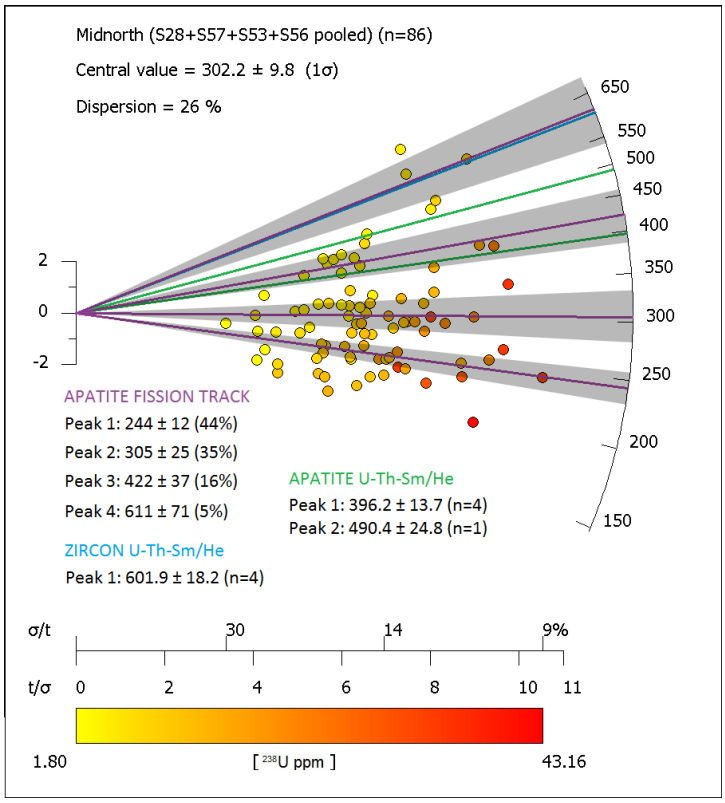

Figure 10: Pooled radial plot of AFT ages for samples 28, 57, 53 and 56 in the mid-north of the study region. AFT age peaks were constructed using the software program *RadialPlotter* (Vermeesch 2015). For a detailed description of radial plots see Figure 4. Here, four AFT age peaks are defined, as well as AHe and ZHe age peaks. Grey zones highlight the cumulative AFT age peaks taking into account the age standard deviation.

Figure 10 depicts a pooled plot of AFT data for samples 28, 57, 53 and 56 from the mid–north sampling region. Neoproterozoic (~610–600 Ma, Petermann Orogeny), Silurian (~420–400 Ma, early ASO), Late Carboniferous – Permian (~300 Ma, late ASO) and Triassic (~240 Ma) thermal events are preserved to varying degrees. Out of the four main study regions, Neoproterozoic cooling is most extensively preserved here with both AFT and ZHe data recording fast cooling to temperatures below ~200°C during the onset of the Petermann Orogeny. The Silurian data is constrained by both AFT and AHe methods, indicating a cooling step to shallower crustal levels coinciding with the start of the ASO. Shallow thermal perturbation during the later stages of the ASO (~300 Ma) and during the Triassic – Early Jurassic are observed, similar to the

aforementioned southwest and middle regions. Given that these samples from the mid–north preserve all four thermal events, particularly the Neoproterozoic event, this region records the lowest level of exhumation in the study area.

In the same way as discussed for the middle region, Figure 11 aligns the individual mid–north radial plots to illustrate trends in exhumation level with respect to the main structural architecture. Sample 56 is located in close proximity to the Coglin fault zone and exhibits the oldest AFT age data for this study. These Petermann Orogeny–aged AFT data are supported by concordant ZHe data, indicating preservation of fast Neoproterozoic cooling at shallow crustal levels just south of the Coglin fault. The Cambrian – Early Ordovician data shows a rather diffuse trend and is thought to represent a mixing age between the Petermann Orogeny and ASO cooling pulses. Samples 53, 57 and 28 do not preserve signs of Neoproterozoic cooling and exhibit a clear pattern of deeper exhumation further south of the Coglin fault zone. While sample 53 still preserves minor signs for early ASO peak cooling, this signal is completely erased in samples 57 and 28. The latter sample only preserves a diffuse cluster of late ASO (~300 Ma) and Triassic –Jurassic age data and therefore records the deepest level of exhumation within the mid–north sampled section.

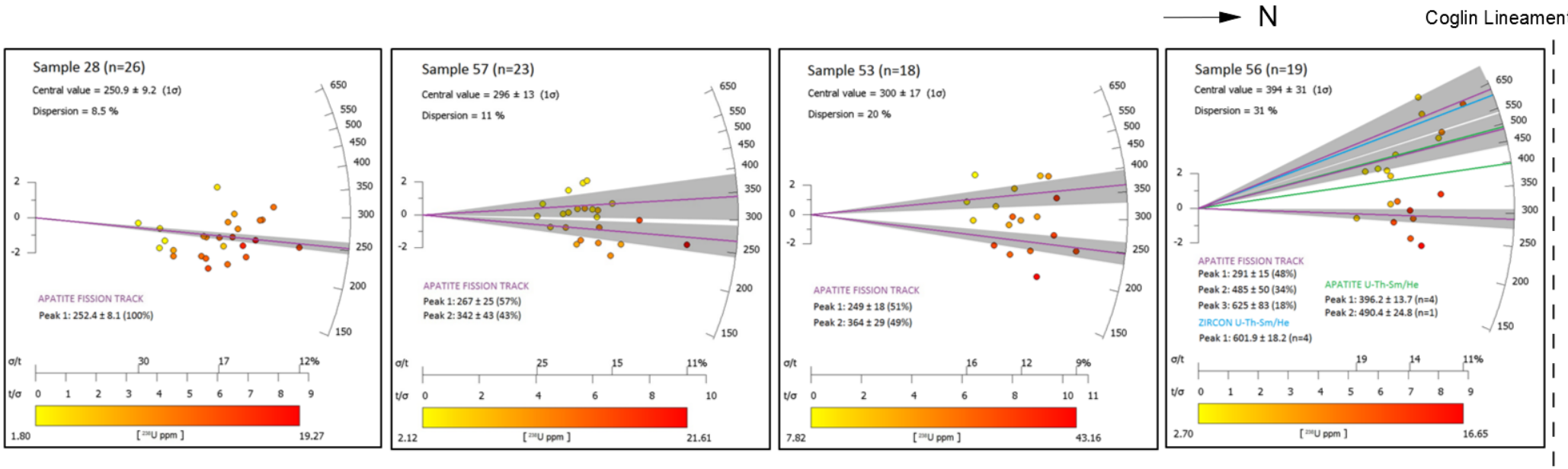

Figure 11: Radial Plots for the mid–north region of the study area (samples 53, 56, 57 and 28). AFT age peaks were statistically constructed using the software program *RadialPlotter* (Vermeesch 2015). For a detailed description of radial plots see Figure 4. AFT age peaks are defined in purple, AHe age peaks in green and ZHe age peaks in blue. Percentage of total grains (for AFT) and number of grain aliquots (for AHe/ZHe) contributing towards each population peak are indicated. Grey zones highlight the cumulative AFT age peaks taking into account the age standard deviations.

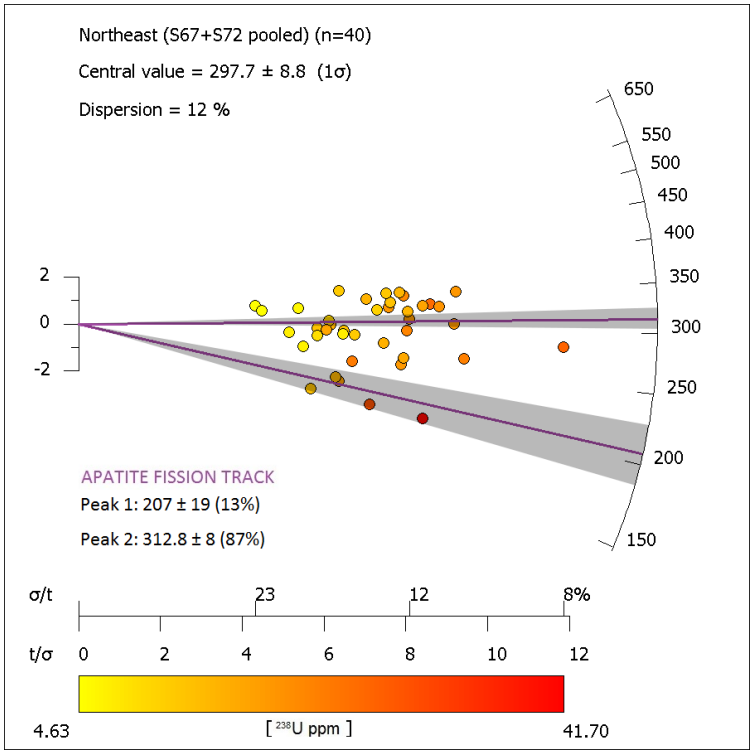

Figure 12: Pooled radial plot of AFT ages for samples 67 and 72 in the northeast corner of the study region. AFT age peaks were constructed using the software program RadialPlotter (Vermeesch 2015). For a detailed description of radial plots see Figure 4. In this region only AFT data was obtained, and two age population peaks are defined. Grey zones highlight the cumulative AFT age peaks taking into account errors.

Figure 12 shows the pooled radial plot for samples 67 and 72 from the northeast. Like the southern margin samples (14 and 32) these AFT results indicate the deepest level of exhumation across the study transect and only record clear signs for late ASO and Triassic – Jurassic thermal events. However, due to the lack of ZHe data we must exercise a degree of caution around this interpretation. Without this data we are unable to conclusively infer that no Petermann Orogeny–aged or early ASO events were preserved for these samples. However, given that the AFT data only records the youngest thermal events of the study area, it is anticipated that the ZHe system will record a maximum age corresponding to the early ASO data as observed for the southernmost section.

To illustrate the overall regional upper–crustal thermochronological interpretations outlined above, a simplified digital visualisation of the inferred low–temperature exhumation profile from this study is presented in Figure 13. The thermochronological data presented in this thesis suggest different levels of exhumation across the NE–SW transect, which can be explained by differential movement across the major E–W faults (outlined in Figure 3). The data fits an inverted graben structural model, with coloured sections used as indicators of AFT age "isochrons". Neglecting associated denudation, the generalised exhumation profile suggests fault reactivation of Normal faults in a roughly N–S compressional regime (Figure 13b) at some stage after the Neoproterozoic. After denudation, the current exposure of the exhumation level of the sampled rocks is inferred (Figure 13c). The deepest exhumation levels are recorded to the south of the Marryat Fault and to the north of the Coglin Lineament, reflecting deformed horst margin uplifts.

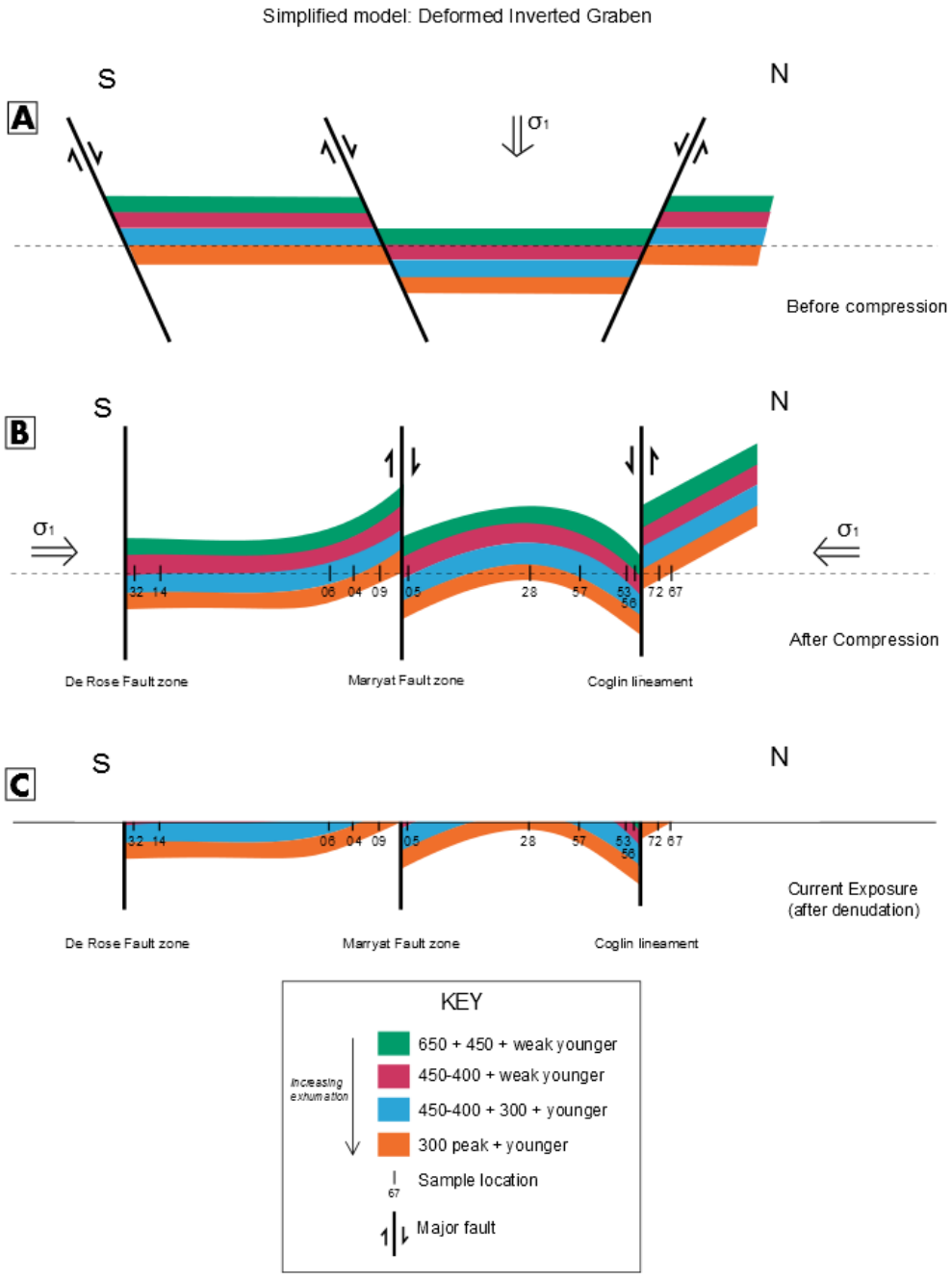

Figure 13: Simplified cartoon model of a deformed inverted graben profile based on thermochronometric data for the eastern Musgrave Province. Low–T thermochronological results have been summarised into main age isochrons (coloured layers) indicating the distribution of AFT age peaks obtained for each sample. AFT ages are in Ma. Sample locations are placed roughly in relation to their proximity to major bounding faults along a N–S transect (not to scale). Major faults are indicated in black along with kinematic indications of movement interpreted for this model. Principle stress σ_1 is indicated with directional arrows. (a) – Simple inverted graben profile before compression; (b) – Inverted and deformed model after N–S compression; (c) – Current exhumation profile exposure after denudation.

Summarised thermal history model for the Eastern Musgrave Province

The thermal history model presented in Figure 14 was fitted relative to all data points and correlated with the sedimentary data presented by Wells et al. (1970), Morton and Drexel (1997) and Munson (2014). Stratigraphic continuity between Amadeus and Officer Basins suggests that they comprised part of a larger intracratonic sedimentary basin (Centralian Superbasin) formed after the amalgamation of the Australian craton during the assembly of Rodinia (Myers et al. 1996, Wade et al. 2008, Raimondo et al. 2010). It is inferred that some sediment sequences sourced from the Musgrave Province between the two sedimentary basins are analogous (Morton and Drexel 1997). Three differential pathways through the upper crust are outlined, the first two (yellow path – mid–north region, blue path – middle region) encompassing fast cooling and exhumation during the Neoproterozoic. These models are supported by ZHe data and indicate that the central regions of the eastern Musgrave Block exhumed rapidly to temperatures ~200–130°C in response to the onset of the Petermann Orogeny (~600 Ma to 530 Ma). Syn– and post–orogen denudation and sedimentation into the surrounding basins is evidenced by the clastic influx of the Lake Maurice, Ungoolya, Marla and Munda Groups in the Officer Basin (Wade et al. 2005) and detrital–zircon ages specific to the Musgrave Complex basement contributing to the sediment supply of the Amadeus Basin (Mount Currie Conglomerate; Sandiford and Hand 1998, Camacho et al. 2002). For the southern margin of the study region, the pink path represents the thermal history of rocks exhumed at deeper levels of the crust. Neoproterozoic cooling was not evidenced from AFT data and this is interpreted to mean the samples south of the Marryat Fault record a deeper level of exhumation with overlying rocks preserving exhumation events >450 Ma eroded away (Figure 13). An early pulse of the Alice

Springs Orogeny ~420 Ma brought the central samples into AHe closure temperatures (75–45°C), and the southernmost samples to temperatures <200°C (~420 Ma ZHe age). This was followed by a period of slow thermal cooling or near quiescence where we see sediments of the Mimili Formation shed into the Officer Basin, thought to correlate with the Pertnjara Group from the Amadeus Basin (Morton and Drexel 1997). Late in the Alice Springs Orogeny (~300) another thermal episode indicates slight shallow reheating of the central regions to temperatures >60°C, whereas the southern region experiences significant pulse of cooling to shallow crustal temperatures <80°C. Permian sediments in surrounding basins were deposited during and shortly after this event. During the Triassic – Jurassic all aforementioned sample regions experience slight reheating resultant of an elevated geotherm widespread throughout the sample transect. Some sedimentary influx was observed in the Simpson and Eromanga Basins to the east however more data are needed to interpret this thermal event with confidence. Due to the lack of ZHe data for the northernmost sample region (above the Coglin Lineament) we use the exhumation profile in Figure 13 to infer a similar exhumation path to the southernmost region, however more data is required to confirm this conclusion.

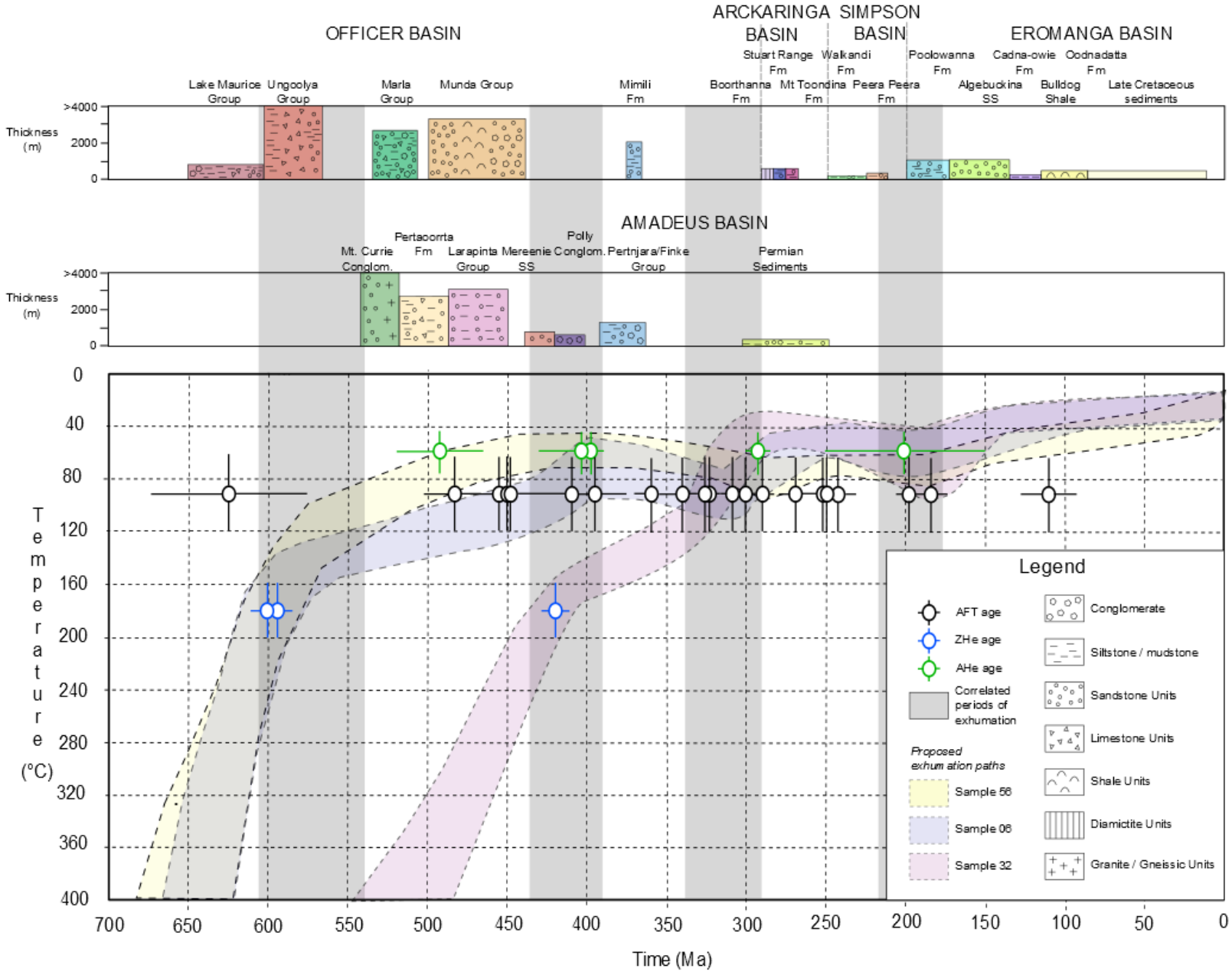
OFFICER BASIN
ARCKARINGA BASIN
SIMPSON BASIN
EROMANGA BASIN
Lake Maurice Group
Ungoolya Group
Marla Group
Munda Group
Mimili Fm
Boorthanna Fm
Stuart Range Fm
Mt Toondina Fm
Walkandi Fm
Peera Peera Fm
Poolowanna Fm
Cadna-owie Fm
Algebuckina SS
Oodnadatta Fm
Bulldog Shale
Late Cretaceous sediments
Thickness (m)
>4000
2000
0
AMADEUS BASIN
Mt. Currie Conglom.
Pertacorrta Fm
Larapinta Group
Mereenie SS
Polly Conglom.
Pertnjara/Finke Group
Permian Sediments
Temperature (°C)
0
40
80
120
160
200
240
280
320
360
400
700
650
600
550
500
450
400
350
300
250
200
150
100
50
0
Time (Ma)
Legend
AFT age
ZHe age
AHe age
Correlated periods of exhumation
Proposed exhumation paths
Sample 56
Sample 06
Sample 32
Conglomerate
Siltstone / mudstone
Sandstone Units
Limestone Units
Shale Units
Diamictite Units
Granite / Gneissic Units

Figure 14: Summarised time-temperature history model with proposed exhumation paths of three main study regions in the eastern Musgrave Province (sample 32 – southwest, sample 06 – middle, sample 56 – mid–north). Simplified stratigraphic columns of adjacent sedimentary basins adapted from Wells et al. (1970), Morton and Drexel (1997), and Munson (2014). Apatite helium (AHe) ages are indicated by green dots, zircon helium (ZHe) ages by blue dots, and apatite fission track (AFT) age populations are indicated by black dots. All age data include horizontal lines indicating age standard error, and vertical lines indicating each thermochronological method closure temperature range. For each region–representative sample, a best–fit exhumation model was constructed to match corresponding low–T data, estimated cooling rates from the *HeFTy* models, and the sedimentological record of adjacent basins. Proposed periods of regional exhumation are shaded grey indicating correlation with unconformities in basin sedimentary records.

CONCLUSIONS

Low–temperature thermochronology of the eastern Musgrave Province reveals a complex and structurally–influenced Phanerozoic upper crustal thermal history. Four main thermal events were identified across the study transect. Neoproterozoic – Cambrian AFT ages evidenced in the central study regions are interpreted as exhumation triggered by the widespread Petermann Orogeny, cooling the basement from temperatures in excess of 400°C to <200°C by ~600 Ma. Slightly younger Silurian – Devonian and Carboniferous – Early Permian AFT age clusters indicate the eastern Musgrave Province was affected by two distinct episodic pulses during the early and late stages of the Palaeozoic Alice Springs Orogeny. The earlier pulse induced exhumation to AFT and AHe temperatures across the entire study transect, and the latter saw shallow reheating in the middle regions yet cooling along the marginal regions. A subsequent Triassic – Jurassic shallow perturbation seen across all regions suggests an elevated geothermal gradient may have affected central and southern Australia extensively at this time. Differential AFT age preservation and exhumation patterns are revealed across the sampled transect relative to the major E–W structural architecture, proposing shallow exhumation levels in the centre and deeper exhumation towards the margins. The sampled exhumation profile best fits a model of an inverted graben system, demonstrating how low–temperature thermochronological techniques can reveal

important structural reactivation trends. The eastern Musgrave Province experienced several shared exhumation events with proximal areas such as the western Eromanga Basin, Officer Basin and the Gawler Craton, which is suggestive of widespread tectonic regimes throughout central and southern Australia in the Phanerozoic.

ACKNOWLEDGMENTS

This thesis was conducted thanks to the financial support of the Geological Survey of South Australia and the University of Adelaide. A sincerely huge thankyou to Dr. Stijn Glorie (The University of Adelaide) for outstanding supervision and patience, Rian Dutch (GSSA) for the sample donations, Prof. Alan Collins (The University of Adelaide) for his supervision, and Mark Pawley (GSSA) for numerous contributions to this research. Thanks are warmly extended to James Hall and Gilby Jepson for their support and guidance, Dr. Katherine Howard and Dr. Rosaling King for honours and thesis support, Renee Tamblyn for being a GIS mastermind, and Tavis Callaghan for keeping me sane. Special thanks to The John De Laeter Center at Curtin University for collecting the He data, and Adelaide Microscopy for the use of the LA-ICP-MS.

REFERENCES

AITKEN A. R. A. & BETTS P. G. 2009. Multi-scale integrated structural and aeromagnetic analysis to guide tectonic models: An example from the eastern Musgrave Province, Central Australia. *Tectonophysics* **476**, 418-435.

AITKEN A. R. A., BETTS P. G., WEINBERG R. F. & GRAY D. 2009. Constrained potential field modeling of the crustal architecture of the Musgrave Province in central Australia: Evidence for lithospheric strengthening due to crust-mantle boundary uplift. *Journal of Geophysical Research: Solid Earth* **114**, n/a-n/a.

BALLÈVRE M., MÖLLER A. & HENSEN B. J. 2000. Exhumation of the lower crust during crustal shortening: an Alice Springs (380 Ma) age for a prograde amphibolite facies shear zone in the Strangways Metamorphic Complex (central Australia). *Journal of Metamorphic Geology* **18**, 737-747.

BOONE S. C. 2013. Apatite Fission Track Anomaly within the Archean-Proterozoic Gawler Craton: The Thermal Record of a Paleoaquifer System. Masters Thesis. (unpubl.).

CAMACHO A. & FANNING C. M. 1995. Some isotopic constraints on the evolution of the granulite and upper amphibolite facies terranes in the eastern Musgrave Block, central Australia. *Precambrian Research* **71**, 155-181.

CAMACHO A., HENSEN B. J. & ARMSTRONG R. 2002. Isotopic test of a thermally driven intraplate orogenic model, Australia. *Geology* **30**, 887-890.

CAWOOD P. A. & KORSCH R. J. 2008. Assembling Australia: Proterozoic building of a continent. *Precambrian Research* **166**, 1-35.

CHEW D. M. & SPIKINGS R. A. 2015. Geochronology and Thermochronology Using Apatite: Time and Temperature, Lower Crust to Surface. *Elements* **11**, 189-194.

DANIŠÍK M., ŠTĚPANČÍKOVÁ P. & EVANS N. J. 2012. Constraining long-term denudation and faulting history in intraplate regions by multisystem thermochronology: An example of the Sudetic Marginal Fault (Bohemian Massif, central Europe). *Tectonics* **31**, n/a-n/a.

DE GRAVE J., GLORIE S., RYABININ A., ZHIMULEV F., BUSLOV M. M., IZMER A., ELBURG M., VANHAECKE F. & VAN DEN HAUTE P. 2012. Late Palaeozoic and Meso-Cenozoic tectonic evolution of the southern Kyrgyz Tien Shan: Constraints from multi-method thermochronology in the Trans-Alai, Turkestan-Alai segment and the southeastern Ferghana Basin. *Journal of Asian Earth Sciences* **44**, 149-168.

DREXEL J. F. & PREISS W. V. 1995. The Geology of South Australia. Geological Survey, South Australia.

DUTCH R. A., WERNER M., KRAPF C. B. E. & RUSAK T. 2013. Geology of the Tieyon 1:100 000 map sheet (5645), Report Book 2013/00011. *Geological Survey of South Australia. Department for Manufacturing, Innovation, Trade, Resources and Energy, South Australia Report* 1-75.

EDGOOSE C. J., SCRIMGEOUR I. R. & CLOSE D. F. 2004. Geology of the Musgrave Block, Northern Territory. *Northern Territory Geological Survey Report* **15**, 1-44.

EHLERS T. A. & FARLEY K. A. 2003. Apatite (U–Th)/He thermochronometry: methods and applications to problems in tectonic and surface processes. *Earth and Planetary Science Letters* **206**, 1-14.

FARLEY K. A., WOLF R. A. & SILVER L. T. 1996. The effects of long alpha-stopping distances on (U・Th)/He ages. *Geochimica et Cosmochimica Acta* **60**, 4223-4229.

FARLEY K. A. 2002. (U-Th)/He Dating: Techniques, Calibrations, and Applications. *Reviews in Mineralogy and Geochemistry* **47**, 819-844.

FARLEY K. A. & STOCKLI D. F. 2002. (U-Th)/He Dating of Phosphates: Apatite, Monazite, and Xenotime. *Reviews in Mineralogy and Geochemistry* **48**, 559-577.

FLOWERS R. M., KETCHAM R. A., SHUSTER D. L. & FARLEY K. A. 2009. Apatite (U–Th)/He thermochronometry using a radiation damage accumulation and annealing model. *Geochimica et Cosmochimica Acta* **73**, 2347-2365.

FOSTER D. A., MURPHY J. M. & GLEADOW A. J. W. 1994. Middle tertiary hydrothermal activity and uplift of the northern flinders ranges, South Australia: Insights from apatite fission-track thermochronology. *Australian Journal of Earth Sciences* **41**, 11-17.

GALBRAITH R. F. & GREEN P. F. 1990. Estimating the component ages in a finite mixture. *International Journal of Radiation Applications and Instrumentation. Part D. Nuclear Tracks and Radiation Measurements* **17**, 197-206.

GIBSON H. J. & STÜWE K. 2000. Multiphase cooling and exhumation of the southern Adelaide Fold Belt: constraints from apatite fission track data. *Basin Research* **12**, 31-45.

GLEADOW A. J. W., BELTON D. X., KOHN B. P. & BROWN R. W. 2002a. Fission Track Dating of Phosphate Minerals and the Thermochronology of Apatite. *Reviews in Mineralogy and Geochemistry* **48**, 579-630.

GLEADOW A. J. W., KOHN B. P., BROWN R. W., O'SULLIVAN P. B. & RAZA A. 2002b. Fission track thermotectonic imaging of the Australian continent. *Tectonophysics* **349**, 5-21.

GLIKSON A. Y., STEWART A. J., BALLHAUS C. G., CLARKE G. L., FEEKEN E. H. J., LEVEN J. H., SHERATON J. W. & SUN S. S. 1996. Geology of the Western Musgrave Block, Central Australia, with particular reference to the mafic-ultramafic Giles Complex. *Australian Geological Survey Organisation, Canberra Bulletin* **239**, 1-177.

GLORIE S. & DE GRAVE J. 2015. Exhuming the Meso–Cenozoic Kyrgyz Tianshan and Siberian Altai-Sayan: A review based on low-temperature thermochronology. *Geoscience Frontiers*.

GREEN P. F., DUDDY I. R., GLEADOW A. J. W., TINGATE P. R. & LASLETT G. M. 1986. Thermal annealing of fission tracks in apatite: 1. A qualitative description. *Chemical Geology: Isotope Geoscience section* **59**, 237-253.

HALL J. 2014. Exhumation of the Peake and Denison Ranges; insights from low-temperature thermochronology. Honours Thesis. University of Adelaide, Adelaide (unpubl.).

HAND M. & SANDIFORD M. 1999. Intraplate deformation in central Australia, the link between subsidence and fault reactivation. *Tectonophysics* **305**, 121-140.

HASEBE N., BARBARAND J., JARVIS K., CARTER A. & HURFORD A. J. 2004. Apatite fission-track chronometry using laser ablation ICP-MS. *Chemical Geology* **207**, 135-145.

HOWARD H. M., SMITHIES R. H., KIRKLAND C. L., KELSEY D. E., AITKEN A., WINGATE M. T. D., QUENTIN DE GROMARD R., SPAGGIARI C. V. & MAIER W. D. 2015. The burning heart — The Proterozoic geology and geological evolution of the west Musgrave Region, central Australia. *Gondwana Research* **27**, 64-94.

KETCHAM R. A. 2005. Forward and Inverse Modeling of Low-Temperature Thermochronometry Data. *Reviews in Mineralogy and Geochemistry* **58**, 275-314.

KOHN B. P., GLEADOW A. J. W., BROWN R. W., GALLAGHER K., O'SULLIVAN P. B. & FOSTER D. A. 2002. Shaping the Australian crust over the last 300 million years: insights from fission track thermotectonic imaging and denudation studies of key terranes. *Australian Journal of Earth Sciences* **49**, 697-717.

LINDSAY J. F. & KORSCH R. J. 1991. The evolution of the Amadeus Basin, central Australia. *Bureau of Mineral Resources Bulletin* **236**, 7-32.

LINDSAY J. F. & LEVEN J. H. 1996. Evolution of a Neoproterozoic to Palaeozoic intracratonic setting, Officer Basin, South Australia. *Basin Research* **8**, 403-424.

MAJOR R. B. & CONOR C. H. H. 1993. The Musgrave Block. *In* DREXEL J. F., PRIESS W. P. & PARKER A. J. eds. *The Geology of South Australia, Vol 1 The Precambrian.* pp. 156-167. Geological Survey of South Australia Bulletin **54**.

MAVROMATIDIS A. 2007. Exhumation Study in the Cooper-Eromanga Basins, Australia and the Implications for Hydrocarbon Exploration. *Energy Sources, Part A: Recovery, Utilization, and Environmental Effects* **29**, 631-648.

MAWBY J., HAND M. & FODEN J. 1999. Sm–Nd evidence for high-grade Ordovician metamorphism in the Arunta Block, central Australia. *Journal of Metamorphic Geology* **17**, 653-668.

MCDOWELL F. W., MCINTOSH W. C. & FARLEY K. A. 2005. A precise 40Ar–39Ar reference age for the Durango apatite (U–Th)/He and fission-track dating standard. *Chemical Geology* **214**, 249-263.

MCLAREN S., SANDIFORD M., DUNLAP W. J., SCRIMGEOUR I., CLOSE D. & EDGOOSE C. J. 2009. Distribution of Palaeozoic reworking in the Western Arunta Region and northwestern Amadeus Basin from 40Ar/39Ar thermochronology: implications for the evolution of intracratonic basins. *Basin Research* **21**, 315-334.

MITCHELL M. M., KOHN B. P. & FOSTER D. A. 1998. Post-Orogenic Cooling History of Eastern South Australia from Apatite FT Thermochronology. *In* VAN DEN HAUTE P. & DE CORTE F. eds. *Advances in Fission-Track Geochronology.* pp. 207-224. Springer Netherlands

MORTON J. G. G. & DREXEL J. F. 1997. The Petroleum Geology of South Australia. Vol 3: Officer Basin. *Department of Mines and Energy, South Australia Report Book* **97/19**, pp. 47-86.

MUNSON T. J., KRUSE P. D. & AHMAD M. 2013. Chapter 22: Centralian Superbasin. *In* AHMAD M. & MUNSON T. J. eds. *Geology and mineral resources of the Northern Territory.* Northern Territory Geological Survey Special Publication **5**.

MUNSON T. J. 2014. Petroleum geology and potential of the onshore Northern Territory, 2014. *Northern Territory Geological Survey Report* **22**, 1-238.

MYERS J. S., SHAW R. D. & TYLER I. M. 1996. Tectonic evolution of Proterozoic Australia. *Tectonics* **15**, 1431-1446.

PAWLEY M. J., DUTCH R. A., WERNER M. & KRAPF C. B. E. 2014. Repeated failure: long lived faults in the Eastern Musgrave Province. *MESA Journal* **75**, 45-55.

PEARCE N. J. G., PERKINS W. T., WESTGATE J. A., GORTON M. P., JACKSON S. E., NEAL C. R. & CHENERY S. P. 1997. A Compilation of New and Published Major and Trace Element Data for NIST SRM 610 and NIST SRM 612 Glass Reference Materials. *Geostandards Newsletter* **21**, 115-144.

PRICE P. B. & WALKER R. M. 1962. Chemical Etching of Charged-Particle Tracks in Solids. *Journal of Applied Physics* **33**, 3407-3412.

RAIMONDO T., COLLINS A. S., HAND M., WALKER-HALLAM A., SMITHIES R. H., EVINS P. M. & HOWARD H. M. 2009. Ediacaran intracontinental channel flow. *Geology* **37**, 291-294.

RAIMONDO T., COLLINS A. S., HAND M., WALKER-HALLAM A., SMITHIES R. H., EVINS P. M. & HOWARD H. M. 2010. The anatomy of a deep intracontinental orogen. *Tectonics* **29**, n/a-n/a.

RAIMONDO T., HAND M. & COLLINS W. J. 2014. Compressional intracontinental orogens: Ancient and modern perspectives. *Earth-Science Reviews* **130**, 128-153.

REDDY M. 2014. Low-temperature thermochronologic insights into the exhumation of the northern Gawler Craton (South Australia). Honours Thesis. University of Adelaide, Adelaide (unpubl.).

REDDY M., GLORIE S., REID A. J. & COLLINS A. S. 2014. Phanerozoic cooling history of the central Gawler Craton: implications of new low-temperature thermochronological data. *MESA Journal* **75**, 56-60.

SANDIFORD M. & HAND M. 1998. Controls on the locus of intraplate deformation in central Australia. *Earth and Planetary Science Letters* **162**, 97-110.

SMITHIES R. H., HOWARD H. M., EVINS P. M., KIRKLAND C. L., KELSEY D. E., HAND M., WINGATE M. T. D., COLLINS A. S. & BELOUSOVA E. 2011. High-Temperature Granite Magmatism, Crust–Mantle Interaction and the Mesoproterozoic Intracontinental Evolution of the Musgrave Province, Central Australia. *Journal of Petrology* **52**, 931-958.

TAGAMI T. & O'SULLIVAN P. B. 2005. Fundamentals of Fission-Track Thermochronology. *Reviews in Mineralogy and Geochemistry* **58**, 19-47.

TAGAMI T., O'SULLIVAN, P. B. 2005. Fundamentals of Fission-Track Thermochronology. *Reviews in Mineralogy and Geochemistry* **58**, 19-47.

TINGATE P. R. 1990. Apatite fission track studies from the Amadeus Basin, central Australia. PhD Thesis. University of Melbourne, Melbourne (unpubl.).

TINGATE P. R. & DUDDY I. R. 1996. The thermal history of the Eringa Trough and western Eromanga Basin. *In* ALEXANDER E. & HIBBURT J. eds. *The Petroleum Geology of South Australia, vol. 2. Eromanga Basin.* pp. 111-123. South Australian Department of Mines and Energy Resources

TINGATE P. R. & DUDDY I. R. 2002. The thermal history of the eastern Officer Basin (South Australia): evidence from apatite fission track analysis and organic maturity data. *Tectonophysics* **349**, 251-275.

VERMEESCH P. 2015. RadialPlotter: a Java application for fission track, luminescence and other radial plots. *Radiation Measurements* **44**, 409-410.

WADE B. P., HAND M. & BAROVICH K. M. 2005. Nd isotopic and geochemical constraints on provenance of sedimentary rocks in the eastern Officer Basin, Australia: implications for the duration of the intracratonic Petermann Orogeny. *Journal of the Geological Society* **162**, 513-530.

WADE B. P., KELSEY D. E., HAND M. & BAROVICH K. M. 2008. The Musgrave Province: Stitching north, west and south Australia. *Precambrian Research* **166**, 370-386.

WAGNER G. A. & VAN DEN HAUTE P. 1992. Fission Track-Dating. *Kluwer Academic Publishers, Dordrecht, the Netherlands*.

WEISHEIT A., BONS P. D., DANIŠÍK M. & ELBURG M. A. 2014. Crustal-scale folding: Palaeozoic deformation of the Mt Painter Inlier, South Australia. *Geological Society, London, Special Publications* **394**, 53-77.

WELLS A. T., FORMAN D. J., RANFORD L. C. & COOK P. J. 1970. Geology of the Amadeus Basin, central Australia. *Bureau of Mineral Resources Bulletin* **100**.

WOLFE M. R. & STOCKLI D. F. 2010. Zircon (U–Th)/He thermochronometry in the KTB drill hole, Germany, and its implications for bulk He diffusion kinetics in zircon. *Earth and Planetary Science Letters* **295**, 69-82.

APPENDIX A: EXTENDED METHODOLOGY

Sample Acquisition

Apatite Fission Track analysis was carried out on 12 samples from the eastern Musgrave Province. The samples were collected in the field by researchers of the Geological Survey of South Australia. Ten of the samples: 1850806 (shortened to 06), 1850804 (04), 1850809 (09) & 1850767 (67) – biotite monzogranite; 1850828 (28) – biotite micro-monzogranite; 1850805 (05) – biotite synogranite; 1842257 (57) & 1842256 (56) – hornblende-biotite meta-quartz monzodiorite; 1842253 (53) & 1842272 (72) – biotite monzogranite; were collected from the Tieyon map region, and two of the samples: 1961432 (32) – hornblende-biotite monzogranite; & 1961414 (14) – biotite monzogranite; were from the Agnes Creek map region (Figure 2). All samples were received for this project in partially crushed form, to be separated for further analysis.

Sample Preparation

The crushed samples required further crushing before mineral separation that would produce suitable apatite grain sizes for analysis. Crushing and mineral separation was conducted in the basement laboratories within The University of Adelaide's Mawson Building. Samples were crushed using conventional crushing machinery and equipment, and separated via magnetic and heavy liquid techniques.

Initial lab training was conducted by Dr Katherine Howard (The University of Adelaide) with all procedures and safety requirements outlined clearly as followed. Cleaning procedures were explained in training sessions and outlined on posters in each of the three laboratories. Cleaning of the labs was essential to minimising bias and contamination of samples, and procedures were adhered to before and after each sample was processed. Appropriate safety gear was worn including safety glasses, ear plugs and a lab coat.

Crushing

Crushing of samples was undertaken in the Crushing Room. The Crushing Room was cleaned thoroughly before and after each day session, as per the posters and prior training instructions. Crushed samples were transferred between the Pulverisette Disc Mill and Sieve Shaker using A3 sheets of butcher's paper. Initial crushing of samples had already been undertaken prior to my receiving the samples, therefore only the disc mill was required to further crush the samples to smaller grain sizes. The Disc Mill was cleaned before and after each sample by blowing high pressured air using the air gun, wiping with paper towel and ethanol before using the air gun to clean once again. The two discs within the Disc Mill were set approximately 2 mm apart initially using the lever. To start the machine the on/off knob was used. Partially crushed samples were fed into the machine from the butcher's paper with the help of a paintbrush. Once the sample had run through the Disc Mill the machine was turned off by the same on/off

knob or by using the red stop button. The milled sample was collected from the tray at the bottom of the Disc Mill and transferred to the Sieve that sat within the Sieve Shaker.

The Sieve Shaker and the items used in constructing the Sieve were cleaned by following the same steps as with the Disc Mill before and after their use. The Sieve was constructed for each separate sample by placing the blue base plate on a piece of clean butcher's paper the bench. The Sieve was then constructed in the following order: lower plate, fine sieve mesh (79 μm), upper plate, another lower plate, coarse sieve mesh (425 μm), upper plate, sieve lid. The Sieve was then placed in the Sieve Shaker and secured in place by tightening the clamps on either side. The Sieve Shaker was turned on using the on–switch at the front of the machine. The machine was run until a significant portion of the sample had penetrated both the coarse and fine mesh. The entire Disc Mill and Sieve processes were repeated, each time decreasing the disc separation within the Disc Mill in slight increments until approximately 0.7 mm apart. After final sieving, the various particle sizes within the Sieve were placed into separate sealable sample bags and labelled accordingly. The grains within the 79–425 μm size range were used in mineral separation.

Mineral Separation

Mineral separation took place in the Mineral Separation Room in the basement of the Mawson Building. Cleaning procedures as outlined in training as well as listed on a poster within the room were followed before and after each day session. Separation required three main steps: panning, running the sample through a Frantz Isodynamic Separator and treating the sample with heavy liquids. Apatite has a specific gravity of 3.16 – 3.22 which is greater than most minerals such as quartz and feldspars. Panning can therefore help separate out apatite from these minerals. Each sample was panned by placing it in the small black panning bowl found below the sink. Water was then added to the bowl and carefully tipped down the sink to remove only rock dust from the sample. Once this had been achieved the sample was panned over the top of the larger green bowl found below the sink. This ensured that panned light minerals would be captured in the green bowl. Once panning removed most (approximately 90%) of the sample into the green bowl, these panned lights could be placed to dry in a funnel set up on the sink, lined with filter paper from the top drawer closest to the door. All of the panned light minerals were then moved to and dried in a low temperature oven (<50°C) and kept in a sealed sample bag for possible future use. The panned heavy minerals which contained most of any apatite present in the sample were also placed into a funnel containing filter paper to initially dry before being placed on a hotplate to dry further before the next step. It was critical that the hotplate did not exceed 60°C as this is the temperature at which apatite can begin to partially anneal (Wagner and Van den haute 1992). Once the panned heavy minerals from the sample had dried, a magnet was used to remove any highly magnetic minerals. Three kimwipes were wrapped around the magnet so those magnetic minerals could be quickly removed and sealed in a labelled sample bag for possible use later.

The remaining part of the sample was put through the Frantz Isodynamic Separator (Frantz) to remove the residual magnetic minerals. Prior to use, the Frantz was cleaned using the airgun. To ensure all components of the Franz were cleaned, the Frantz track

was removed by undoing the four bolts located on each side of the track. Once clean and reassembled, the Franz was turned on using the on switch at the front of the machine, and the magnet was switched on using the switch on the adjacent control box. The remaining sample was run through the Franz at 0.5 Amperes and then again at 1.4 Amperes. Both the magnetic minerals and the non-magnetic minerals (to be used in the next step) were collected at the base of the Frantz track in two separate beakers, both cleaned with ethanol and the air gun prior to use. The magnetic minerals were added to the labelled magnetic sample bag for potential future use.

Heavy liquid (Methylene Iodide, density 3.3 g mL^{-1}, diluted with acetone to a density of ~3g mL^{-1}) was then used to further separate out apatite grains, based on density, from other minerals such as quartz and feldspars. This step was carried out within the fume cupboard at the back of the room. James Hall (hons. BSc) oversaw this step the first time it was carried out to ensure that all steps outlined in the lab training were adhered to. The non-magnetic fraction of minerals which passed through the Frantz were poured into the top of the heavy liquid separation apparatus and the grains that sank to the bottom in the heavy liquid were collected in filter paper and rinsed with acetone to remove all traces of heavy liquid. Once this process was complete, the apatite fraction was dried on a hotplate and placed into a labelled vile using a paintbrush. The paintbrush and vial were placed in a small sealable sample bag that was also labelled accordingly. The light minerals and any magnetic minerals that did not sink and were left after the heavy liquid separation were also collected in filter paper, rinsed with acetone, and placed in a labelled vile and sample bag for potential future use.

Picking and Mounting Apatite Grains

Mounting of apatite grains on to a glass slide was carried out in the University of Adelaide's Mawson Building Microscope Room (G36). Two Olympus SZ61 picking microscopes were used, set up side-by-side. Picking apparatus including two petri dishes and a needle pick were cleaned using ethanol and kimwipes followed by a visual check under the microscope. This was crucial to avoid contamination of the samples. Glass slides were prepared by cleaning with ethanol and kimwipes. One glass slide with two small crosses (+) drawn on, in line with each other ~15 mm from one end and ~7.5 mm from each side, was taped to the underside of a second mounting glass slide. Double-sided sticky tape was applied over the crosses and adhered firmly to remove air bubbles. The slide with the crosses acts as a guide for the location where the apatite grains will be placed on the double-sided tape when the two slides are lined up correctly. The slides were then placed in one clean petri dish under one microscope. A small portion of a sample was placed onto the other petri dish. Inclusion-free apatite grains were selected based on their clear looking appearance and hexagonal or euhedral – subhedral grain shape. Selected apatite grains were placed on to the double-sided tape using a pick (using the natural oils from the skin as an adhesive) and arranged into a raster. Each sample raster was constructed on top of and within one cross to ensure grains could be reached by the LA-ICP-MS. Sample numbers were recorded on the slides using fine permanent marker and covered with clear tape. Approximately 100–120 apatite grains were picked for each sample, thus rasters of at least 10 x 11 grains were preferable, however, in cases where apatite was not as abundant smaller square rasters were used. When mounting was finished the remaining sample in the petri dish

was returned to the vial using clean paper and a paintbrush. Between each sample all apparatus were cleaned thoroughly again with ethanol and kimwipes, and the mounted raster covered by a clean glass slide to ensure no contamination while another sample was being picked. A total of six glass slides were used with two samples on each slide mounted over the crosses.

Epoxy Resin

Epoxy Resin was placed on top of the completed apatite rasters. This was conducted in the University of Adelaide's Mawson Building lapidary. Lab coat, safety glasses and gloves were worn at all times. The resin was prepared by mixing EpoxiCure™ Epoxy Resin (20-8130-032) and EpoxiCure™ Epoxy Hardener (20-8132-008) together in a plastic cup stirring with a popstick for 20 minutes to ensure it could be considered homogenously mixed. A ratio of 5:1 Resin:Hardener was achieved using scales. The popstick was then used to place 1-2 small drops of the resin mixture onto the apatite rasters. Additional clean glass slides were arranged around the mounted raster glass slide at both ends perpendicular to the raster slide to then allow a final clean glass slide to be placed on top of that arrangement, meaning the resin would set exactly 1 slide-width thick. The resin needed to be big enough to completely cover each raster of grains and high enough to stick to the top glass slide. The resin was left to dry for 5 days before the two perpendicular end slides were removed and the two slides attached to the resin were separated using a razor blade. To do this, the razor blade was slid between the double-sided tape and the slide that the tape was attached to, and once separated any residual tape on the resin was peeled off. This left the apatite grains now exposed at the top of the resin and the other surface of the resin attached to the top slide. If the resin detached itself from the top slide in the slide separation process, it could be reattached using another piece of double-sided tape. If this occurred the sample numbers could also be permanently scratched onto the underside of the resin before reattaching.

Grinding

Samples were ground in the Mawson Building lapidary. Grinding reveals an internal surface within the apatite grains. Before samples were ground, the sharp edges of the glass slides were rounded off using the Zinc Lapping Disc. This was to reduce wear and tear on the polishing cloths once polishing was commenced. Samples were then washed with water and dried with paper towel. Samples were ground by running the slides resin-side down in a figure eight motion applying minimal pressure so as not to scratch the resin or compromise any loose apatite grains. This was done initially on Waterproof Silicon Carbide Paper FEPA P# 1000 followed by FEPA P# 2000, applying a few drops of water to the surface of each before grinding. Samples were intermittently checked every 5–10 figure eight cycles under the microscope to ensure that only the tape, top layer of resin and the top of the apatite grains were ground off. Any large visible signs of tape were removed from the sample by wiping with ethanol and paper towel or kimwipes to dissolve the remaining tape. If needed, the sample could be washed with water at any stage to help clean the resin or any residue. Samples were checked under the microscope with the aid of a clean pick, and if any apatite grains were felt sitting above the level of the resin more grinding was required. Once apatite grains were

ground to the level of the resin (but not past the middle of the grains) samples were ready for polishing.

Polishing

A Struers™ DP-U4 Cloth Lap was used to polish samples, located in the Mawson Building lapidary. A 3µm Struers MD Dac™ polishing cloth and 1µm Struers MD Nap™ polishing cloth were placed onto the magnetic plate of the polishing apparatus and used to polish the samples. 3-4 sprays of 3µm and 1µm Diamond Suspension Polishing Lubricant was applied to the 3µm and 1µm polishing cloths before use respectively. The machine was set to 100 RPM and the sample glass slides were secured in a slide holder and held gently on the polishing cloths. While polishing, the samples were held horizontal and were constantly rotated to apply an even polish on the sample. Polishing was completed in five minute blocks to monitor the removal of scratches upon apatite grains, first on the 3µm cloth and later on the 1µm cloth for finer polishing. Samples were checked using an Olympus BX51 microscope at 1000x magnification within the Mawson Building's Microscope Room (G36).

Etching

Etching of samples was undertaken within the Mawson Building B13 laboratory. Access to the room was acquired through contacting David Bruce (email: david.bruce@adelaide.edu.au). Etching of samples is required to enable fission tracks to be seen in the apatite grains under the microscope via dissolving the surface of the grain, therefore increasing the size of the fission tracks. Samples were cleaned gently with ethanol and kimwipes. Safety equipment including lab coat, shoe covers, safety glasses and gloves were worn at all times and safety rules listed on the laboratory door were adhered to.

In preparation for etching, a large bottle containing 5 mol/L Nitric acid (HNO_3), a 50ml clear plastic vile and two large beakers (~1L) filled with distilled water were placed within the fume cupboard. Following this approximately 40ml of nitric acid was poured carefully into the 50ml plastic vile from the large bottle which was then recapped and returned to the plastic tub it was stored in. A thermometer was used to ensure that the temperature of the plastic vile containing nitric acid was between 19.5°C and 20.5°C. Once this was achieved by either heating using body heat from hands or cooling under the fume cupboard, the thermometer tip was rinsed using distilled water. Slides were then chemically etched in pairs by holding the slides back to back and submerging the slides halfway into the nitric acid for 20 seconds, swirling around gently. After 20 seconds the slides were then immediately dipped and swirled into the first beaker of water for approximately 10 seconds to wash off the acid and then placed into the second beaker of water to dilute any remaining acid on the samples. After etching 3 slides worth of samples the nitric acid was poured out carefully and the vile rinsed with distilled water into the liquid waste bottle using a funnel, then the vile was refilled with 40ml of new nitric acid. After all samples were etched the nitric acid was poured carefully into the liquid waste bottle and the vile was disposed of in the bin. The first beaker of distilled water was also poured into the liquid waste bottle and rinsed, and the

second beaker of distilled water was poured into the sink. The slides were then removed from the second beaker and dried using paper towel, the second beaker was rinsed and all apparatus returned to the fume cupboard.

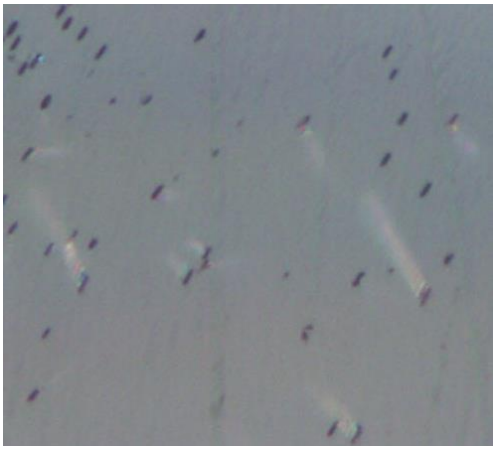

Figure 1: An example of an etched apatite grain surface. The black marks are the etch pits (Dpar) of the fission tracks that intersect the surface. The photo was taken in reflected light using an Olympus BX51 Microscope, with an Olympus DP21 camera and computer attachment on 1000x magnification.

Counting and Measuring

Apatite crystals contain trace amounts of Uranium. When a Uranium atom undergoes spontaneous nuclear fission within a mineral, the products of decay leave a damage trail in the crystal lattice. This trail is called a 'fission track' (Figure 2) and each single fission track is the remanent of a single event of radioactive decay (Gleadow et al. 2002a). For apatite, temperature plays an important role in the annealing (healing) properties of the crystal lattice. Above 60°C fission tracks can start to anneal, and above 120°C the crystal lattice may completely repair itself. Below 60°C fission tracks are preserved in the mineral crystal lattice (Wagner and Van den haute 1992) and this is referred to as the closure temperature. The zone between 60°C – 120°C is known as the partial annealing zone (PAZ) and it is within this temperature zone fission tracks are likely to start annealing but not completely repair the damaged lattice. The longer time period spent within the PAZ the more a fission track will anneal and thus shortening their overall length. Fission track lengths can give an indication therefore of the rate of cooling the apatite grain experienced by indicating whether the grain remained in the PAZ for a long or short period. The PAZ is the temperature range essentially preserved when we count etched fission tracks, and these counts combined with the Uranium concentration of the grain reveal an AFT age (or multiple ages) of when the rock was within this temperature zone.

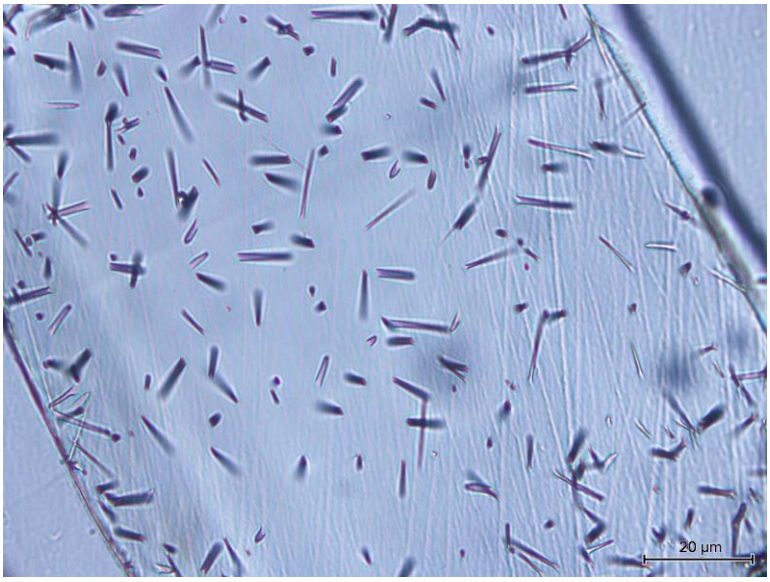

Figure 2: An example of an etched apatite grain with spontaneous fission tracks (dark lines within the crystal). The photo was taken using transmitted light on an Olympus BX51 Microscope, with an Olympus DP21 camera and computer attachment, on 1000x magnification.

All track counting and length measurements were conducted on an Olympus BX51 Microscope with an Olympus DP21 camera and computer attachment. All samples were observed under 100x zoom using both transmitted and reflected light. Counting was undertaken with the intention of counting at least 1000 fission tracks in total over all samples, using 20–30 grains per sample.

Grains selected for counting required:

1. Large enough polished grain surface to fit at least 3 x 3 micron raster within
2. Random spread of fission tracks, and all varied lengths
3. Reasonable amount of tracks
4. Tracks needed both an etch pit and a tail to be counted
5. Tracks must be completely straight
6. Tracks must be parallel to the c-axis of the grain (i.e. no hexagonal etch pits)
7. Raster was positioned at least 10 microns away from the edges of the grain
8. Area to be counted must not be zoned. Homogenous density of tracks was desired.

Once a grain was selected for counting, the raster eye-piece was positioned over the desired region of the grain and the chosen dimensions of the counted area were recorded. All identifiable fission tracks were counted within this raster and the total recorded. A photograph was taken in both transmitted and reflected light in case of verification of track counts later. This process was repeated on each desirable grain possible until at least 20 grains/1000 tracks were recorded.

Tracks used for length measurements must be horizontal and completely confined within the crystal lattice, as well as etched through due to being intersected either by another track (Figure 3; TINT) or a crack/cleavage (Figure 3; TINCLE). Measuring was undertaken with the intention of recording at least 30 confined tracks per sample, 100 confined tracks maximum if possible. Length of track was determined using the

Olympus DP21 camera and computer attachment software, by selecting each end of the confined track and recording the distance shown on the screen (Figure 3). The angle to the c-axis and 5 etch pit (Dpar) length measurements (Figure 4) were also recorded per chosen grain. The type of track-intersection (TINT or TINCLE) was noted, and again, photographs in both transmitted and reflected light were taken for later reference. This process was repeated for as many grains as possible, until 20–100 confined tracks were measured per sample.

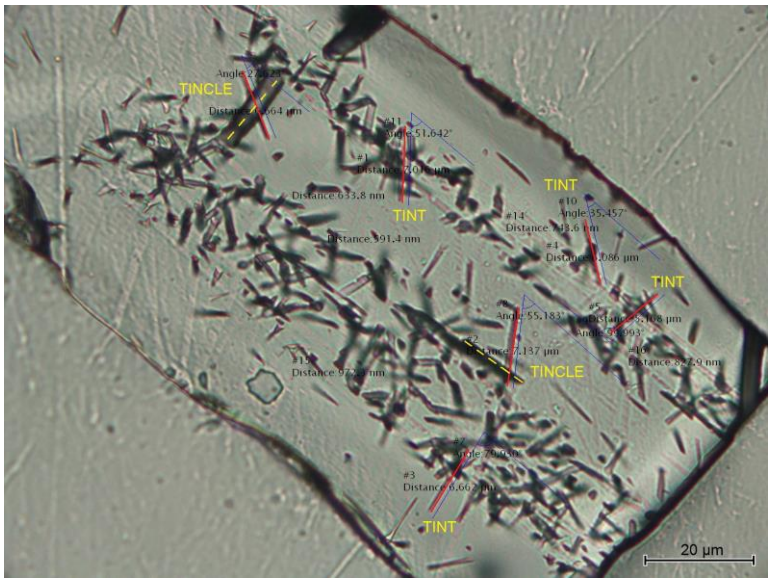

Figure 3: An example of confined tracks (both TINT and TINCLE) within an apatite grain. Red lines indicate the entire track length measured out, blue angle measurements indicate the angle of the track to the C-axis of the grain, and the yellow dotted lines mark out the crack/cleavage intersecting the TINCLE confined tracks. The photo was taken using transmitted light on an Olympus BX51 Microscope, with an Olympus DP21 camera and computer attachment, on 1000x magnification.

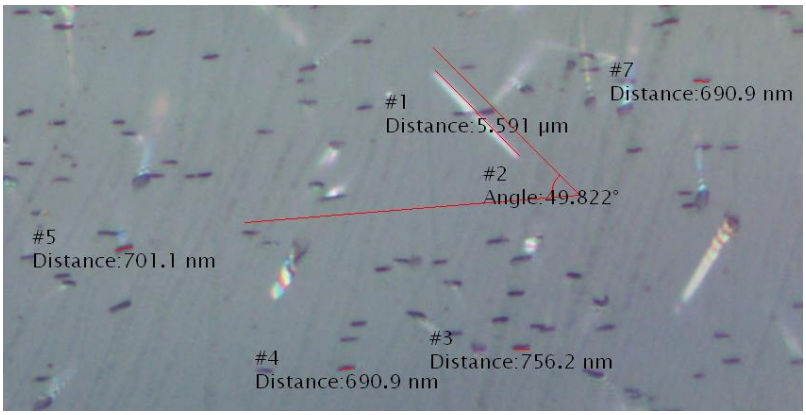

Figure 4: An example of a TINT confined track measurement, with the angle to the C-axis also shown. The other measurements indicated the length of etch pits within the grain (Dpar). The photo was taken using reflected light on an Olympus BX51 Microscope, with an Olympus DP21 camera and computer attachment, on 1000x magnification.

LA-ICP-MS

The Laser-Ablation Inductively-Coupled-Plasma Mass-Spectrometer was used to determine the concentrations of desired elements and isotopes (U^{238}, U^{235}, and Ca^{43} in particular) for each counted apatite grain. Additional isotopes were also measured as directed by liaison with Stijn Glorie (supervisor) and Ben Wade (Adelaide Microscopy trained expert). All required information was gathered via ablating the selected apatite crystals within the chosen counted raster area to achieve consistency between the two methods of data collection. In most cases, the laser ablation spot size was smaller than the counted region and therefore was placed in the exact centre of the region provided the region chosen appeared homogenous in track density. These details are important as the concentrations of Uranium and Calcium can change over a single apatite grain (Hasebe et al. 2004). The Mass-Spectrometer then calculates the concentrations and all data obtained is recorded on a computer. All parameters and setup information for the LA-ICP-MS are outlined in Table 1 below.

In total, 290 apatite grains were sampled on the laser, along with two sets of apatite standards (with known ages) and 3 types of glass standards (with known element concentrations). The exact order in which the laser spots were set was recorded as a sequence for ease in the data reduction process. The first 3 sequences consisted of 70 unknown apatite grains plus standards, and the 4th sequence contained 80 unknowns plus standards. The sequence outline was as follows:

- 3 glass standards (NIST610, NIST612 and NIST614), each measured twice
- 1 Durango apatite standard
- 1 Alternate apatite standard
- 10 unknowns from Eastern Musgrave samples

This sequence order was repeated for each laser run until 70 (or 80) unknowns were measured, making sure the known glass standards were measured at the end of each sequence to conclude.

Table 1: Parameters for LA-ICP-MS instrumental setup, data acquisition and data reduction

LA- ICP-MS	
Brand and model	Agilent 7500CX Quadrupole
Forward power	1300 W
Gas Flows (L/min)	
Cool (Ar)	15.00
Auxiliary (Ar)	0.89
Carrier (He)	0.70
Sample (Ar)	0.93
Laser	
Type of Laser	New Wave UP213 laser
Pulse duration	30 s
Spot size	30 µm

Repetition rate	5 Hz
Energy attenuation	50%
Laser fluency	~6 J/cm^{-2}
Laser warm up (background collection)	30 s
Data acquisition parameters	
Data acquisition protocol	Time-resolved analysis
Scanned masses	235, 238, 43
Samples per peak	1
Number of scans per peak	1
Detector mode	Pulse counting
Detector deadtime	35 ns
Background collection	30 s
Ablation for age calculation	30 s
Washout	10 s
Standardisation and data reduction	
Primary standard used	NIST 610, NIST 612, NIST 614 calibration line
Secondary standard used	Durango apatite (McDowell et al. 2005)
Data reduction software used	In-house *Excel*® spreadsheet

(U-Th-Sm)/He Dating

Helium (^{4}He) diffusion through the radiogenic decay of Uranium and Thorium can be a useful tool in calculating the age at which a grain passed through a certain temperature (dependent on grain type). Above this closure temperature zone, Helium can freely diffuse out of the mineral, but below this temperature zone ^{4}He is trapped within the grain. By determining how much ^{4}He has been retained in a grain, versus the amount of U and Th remaining, this ratio can help constrain the age at which the grain cooled past the lower temperature boundary of this closure zone. For apatite, this is 45°C and for zircon ~130°C (Ehlers and Farley 2003, Wolfe and Stockli 2010).

In this study, both apatite and zircon grains were selected for (U-Th-Sm)/He analysis, to help provide two separate time/temperature constrains for the same samples. Three samples were selected across the sampling area, chosen based on their proximity to major fault structures. Separates for each of the 3 samples were analysed for perfect apatite and zircon grains under two Olympus SZ61 picking microscopes. Grains with the best grain shape, over 70 micrometres in diameter and free of inclusions or zonation were picked. The grains were then sent to the John De Laeter Centre at Curtin University in Perth for (U-Th-Sm)/He analysis. For a more detailed description of this dating method, refer to Li et al. (2014) and Farley and Stockli (2002).
Upon receiving the samples in Perth, grains which best suited the criteria for analysis were measured for the calculation of an alpha-ejection correction factor (Farley et al. 1996).

Apatite:
^{4}He was extracted from the chosen grains by loading the grains into a platinum micro-crucibles and heating using a 1064nm Nd-YAG laser. The U and Th concentrations were concluded using isotope dilution. The apatite was dissolved in 7M HNO_3 over 12 hours and the resulting concentrations of U and Th were recorded and calibrated against a standard using a mass spectrometer.

Zircon:
The chosen zircon grains were loaded into Niobium microvials and ^{4}He extracted by heating the crystals to >1200°C using a 1064 nm Nd-YAG laser. Isotope dilution inductively coupled mass spectrometry was again used to determine the concentrations of U and Th. The zircons were dissolved in 350µl of HF for 40 hours at 240°C, then 300µl of HCl was applied to the grains at 200°C for 24 hours to dissolve any remaining fluoride salts. Following this, the U and Th concentrations were measured with a mass spectrometer.

APPENDIX B: CALIBRATION PROCEDURES (DURANGO APATITE STANDARD)

Fission track analysis in apatite was the primary method applied in this thesis to investigate the low–temperature thermal history of the eastern Musgrave Province. Two standards were used for calibration purposes to check the accuracy of the obtained results. These are the international standard apatite (Durango apatite) and an in–house apatite standard (ARK – from Arkaroola). The results from the Durango apatite standard are presented in Figure 5. Durango apatite is a commonly used standard for fission track research and has been precisely dated using the ^{40}Ar–^{39}Ar method at 31.44 ± 0.18 Ma (McDowell et al. 2005).

In this study, 30 Durango analyses were performed and resulted in an overall mean AFT age of 34.5 ± 1.7 (1σ) Ma. The standardised ^{40}Ar–^{39}Ar age of 31.44 ± 0.18 Ma falls within two standard deviations of this result, and the difference is translated into a calibration factor used to correct all unknown sample ages against.

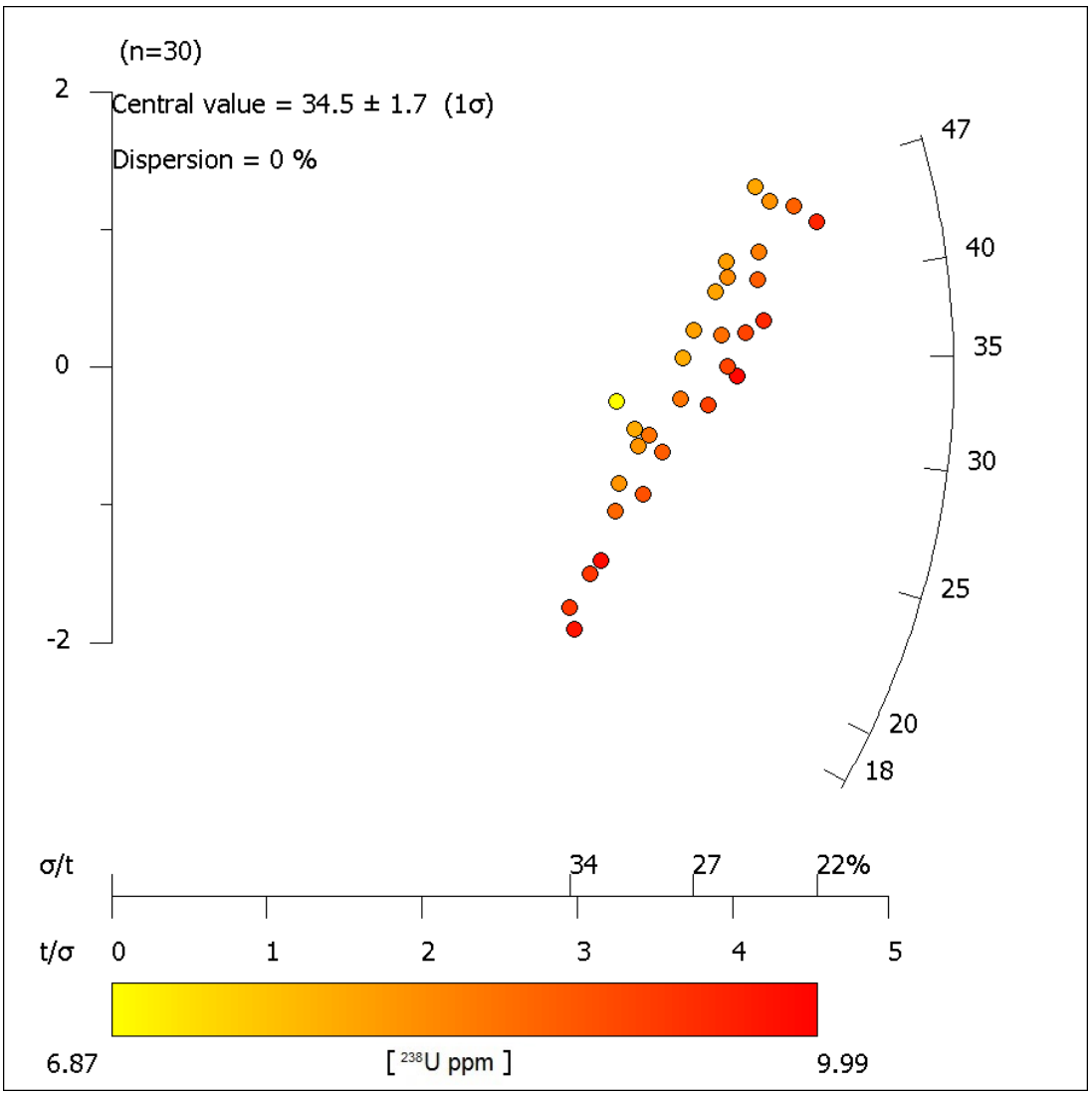

Figure 5: Radial plot of Apatite Fission Track (AFT) ages of the Durango international standard, using the laser-ablation inductively-coupled-plasma mass-spectrometer (LA-ICP-MS) method. Plots indicate the degree of dispersion (%), central age, and number (n) of grain areas analysed. Each analysed age is plotted corresponding to its precision, which is used to determine multiple age-components (peaks). Individual AFT ages are determined by running a straight line from the 0 point on the left of the plot, through the grain (coloured dot) to the curved scale on the right side which reveals age (in Ma). The standard deviation (σ/t) is measured along the x-axis, decreasing from left to right; therefore the age of the grains are more precise if they plot closer to the right side of the plot. The error bar is shown as ± 2 σ on the left which is constant for all grains. The yellow-red colour scale bar indicates concentration of ^{238}Uranium (ppm). Radial plot was constructed using *Radial Plotter* (Vermeesch 2015).

APPENDIX C: EXTENDED DATA SPREADSHEETS

Appendix C shows the input for all samples that was used in the data reduction process. Data reduction procedures and AFT age calculations were carried out using an in–house MS Excel® spreadsheet provided by Dr. Stijn Glorie (The University of Adelaide), based on the protocols outlined in Hasebe et al. (2004). ‘SEQ’ refers to each run sequence carried out on the LA-ICP-MS. Data reduction was carried out separately for each sequence.

Secondary Standard (Durango)

	Name	Drift Corr. Slope	meas 238	SD %	meas 43	SD %	meas 238/43	SD %	238U Dur	RF	SD	Ns	A	rho s	t (Ma)	SD t	AVG t(Ma)	AVG SD	SE of mean	AVG COUNT	AVG U	rho
SEQ1	dus3_2	5.5538941	8985.198	4.561676	99132.738	4.537361	0.091467	2.544359	8.857	4.149260	0.367490	20	10000	200000	45.04	10.24						
	dus3_3	5.335832	8823.349	5.453638	100110.435	4.918977	0.088539	2.626362	8.924	4.515297	0.402927	18	10000	180000	40.25	9.66						
	dus3_4	5.11777	10341.248	5.026748	125200.970	5.047360	0.082902	1.878118	8.711	4.619903	0.402458	16	10000	160000	36.66	9.32						
	dus3_5	4.8997079	13028.570	2.928616	143854.364	3.029539	0.090984	1.944965	9.986	5.282220	0.527492	17	10000	170000	33.98	8.44						
	dus3_6	4.6816458	11882.949	3.376173	145918.536	3.269856	0.081771	2.089760	9.393	6.105291	0.573477	9	10000	90000	19.15	6.49						
	dus3_7	4.4635838	11408.641	2.751678	146628.388	2.664731	0.078124	2.094941	9.413	7.016173	0.660402	10	10000	100000	21.23	6.88	32.72	8.50	3.472	15	9.214	1.628
SEQ2	dus3_8	5.9265108	6982.941	1.958400	69428.146	2.888339	0.101854	2.529129	9.242	3.141379	0.290340	16	10000	160000	34.56	8.71						
	dus3_9	6.1189364	7572.812	1.952460	72286.387	2.731685	0.105913	2.399362	9.309	3.111074	0.289596	15	10000	150000	32.17	8.37						
	dus3_10	6.3113621	6497.351	2.265621	58243.410	2.756079	0.112714	2.555660	9.604	3.414397	0.327926	18	10000	180000	37.40	8.91						
	dus3_11	6.5037878	11772.365	3.253954	101005.460	2.751063	0.116376	1.281136	9.623	2.931434	0.282088	21	10000	210000	43.53	9.58						
	dus3_12	6.6962135	11171.486	3.300861	97407.847	3.510064	0.115165	1.597103	9.249	3.440500	0.318215	17	10000	170000	36.68	8.99						
	dus3_13	6.8886392	11536.229	3.054341	91922.554	3.320136	0.126225	1.775315	9.854	3.897268	0.384041	9	10000	90000	18.25	6.13						
	dus3_14	7.0810649	8047.633	3.266937	71964.837	2.716085	0.112066	2.198081	8.511	4.467462	0.380226	18	10000	180000	42.19	10.12						
	dus3_15	7.0938933	7852.658	3.978718	65550.206	3.462345	0.119665	1.908982	9.072	4.357436	0.395294	12	10000	120000	26.42	7.71	33.90	8.56	3.028	15.75	9.308	1.692
SEQ3	dus3_17	107.2444	3376.997	2.097830	2189.539	3.278027	1.584835	3.985460	7.947	4.944948	0.392986	14	10000	140000	35.16	9.56						
	dus3_18	110.69365	3117.863	2.602380	1993.893	5.070892	1.662224	5.845250	8.076	6.664409	0.538189	15	10000	150000	37.07	9.89						
	dus3_20	117.59214	2901.143	1.566769	1998.055	3.761648	1.502107	4.324993	6.870	5.916913	0.406466	11	10000	110000	31.97	9.82						
	dus3_21	121.04139	2792.863	1.927236	1563.960	4.554308	1.875366	4.996078	8.332	6.732275	0.560945	17	10000	170000	40.71	10.25						
	dus3_22	124.49063	2911.641	2.579525	1614.840	3.632921	1.873501	5.014560	8.093	7.077072	0.572766	17	10000	170000	41.91	10.59	37.36	10.02	4.481	14.8	7.864	1.882
SEQ4	dus3_23	212.227	2868.254	2.287678	936.406	4.408571	3.241759	5.776428	8.215	5.796496	0.476159	12	10000	120000	29.17	8.59						
	dus3_24	214.0213	2910.889	2.333558	970.408	5.088174	3.200142	5.771226	8.041	5.831116	0.468889	16	10000	160000	39.70	10.19						
	dus3_25	215.8156	3105.150	2.524189	996.911	5.524447	3.299060	4.906456	8.221	5.080733	0.417677	11	10000	110000	26.73	8.17						
	dus3_26	217.6099	3035.144	2.886677	908.780	4.514944	3.489044	5.047614	8.623	5.368309	0.462884	14	10000	140000	32.42	8.84						
	dus3_27	219.4042	3048.260	1.813991	870.862	4.128132	3.645478	4.461481	8.935	5.037021	0.450080	13	10000	130000	29.05	8.19	31.17	8.77	2.774	13.2	8.534	1.547

	dus3_28	221.1985	2930.318	2.439590	961.490	5.256643	3.263987	6.078252	7.935	6.711097	0.532557	12	10000	120000	30.20	8.95					
	dus3_29	222.9928	2711.073	2.101397	766.772	7.692856	4.115770	9.121645	9.926	9.715996	0.964393	11	10000	110000	22.14	7.01					
	dus3_31	226.58139	3340.415	2.052444	1059.415	4.992609	3.370652	6.084943	8.000	7.467316	0.597394	19	10000	190000	47.36	11.43					
	dus3_32	226.70101	3413.306	1.981819	1027.288	6.091989	3.653858	6.655619	8.668	7.956875	0.689679	13	10000	130000	29.95	8.64					
	dus3_33	226.82063	2988.279	1.746913	845.402	4.498295	3.703393	4.670171	8.781	6.411490	0.562967	11	10000	110000	25.03	7.71					
									8.773	5.419	0.472	14.55	10000	145517	33.31	8.87	33.11	2.40	t DUR	31440000	
												422	290000						OM ZETA	3.4848E+15	

	Unknowns (samples)														RAW AGES		SESSION DUR CORR		OVERALL MEAN DUR CORR	
	Name	Drift Corr. Slope	meas 238	SD %	meas 43	SD %	meas 238/43	SD %	238U Dur	RF	SD	Ns	A	rho s	t (Ma)	SD t	t (Ma)	SD t	t (Ma)	SD t
SEQ1	S06_H14	5.7428812	8064.862	3.743532	125700.473	3.821279	0.064578	2.705703	5.975	4.088349	0.244265	25	4500	555556	183.47	37.45	177.55	36.24	174.298	35.58
	S06_H13	5.7283437	5868.687	6.787141	129790.797	2.345201	0.044768	5.557884	4.152	6.352782	0.263788	21	3000	700000	328.88	74.75	318.37	72.36	312.606	71.05
	S06_H12	5.7138063	6045.529	2.806279	133972.783	2.318319	0.045281	2.989333	4.211	4.299138	0.181021	25	6000	416667	195.08	39.91	188.78	38.62	185.331	37.91
	S06_J10	5.6992688	4655.196	3.000149	124474.282	4.744731	0.038076	2.296894	3.550	3.860786	0.137047	30	5000	600000	329.73	61.53	319.20	59.57	313.416	58.49
	S06_F10	5.6847313	8293.479	3.535938	132173.330	5.295445	0.064050	2.937763	5.986	4.283538	0.256431	19	2000	950000	310.05	72.36	300.13	70.04	294.683	68.77
	S06_G8	5.6701938	5863.846	4.134097	116068.118	3.517309	0.050551	2.347923	4.737	3.914613	0.185431	31	5000	620000	256.79	47.20	248.54	45.69	244.015	44.86
	S06_F9	5.6556564	6525.675	2.969156	128880.036	3.606843	0.051237	3.920241	4.814	5.027716	0.242009	47	5000	940000	379.47	58.55	367.39	56.68	360.762	55.66
	S06_H9	5.6265814	2356.045	2.722977	115091.005	3.456910	0.020660	2.101039	1.951	3.812558	0.074382	19	4800	395833	393.80	91.58	381.28	88.67	374.412	87.07
	S06_H8	5.612044	7498.976	2.310990	119758.973	3.586887	0.063998	3.453014	6.059	4.707239	0.285212	32	3500	914286	295.16	54.00	285.70	52.27	280.517	51.32
	S06_D10	5.5248191	5673.314	3.734485	140910.793	3.169336	0.040274	2.097767	3.873	3.928151	0.152142	28	3600	777778	389.90	75.26	377.50	72.87	370.691	71.55
	S06_B9	5.5102817	5460.481	1.720734	165031.828	3.157444	0.033395	4.420271	3.220	5.542628	0.178479	10	2500	400000	243.95	78.32	236.11	75.80	231.804	74.42
	S06_A10	5.4957442	7806.131	3.982792	139956.896	2.871532	0.055628	2.179986	5.378	4.011521	0.215741	35	4200	833333	302.90	52.62	293.21	50.94	287.889	50.01
	S06_A8	5.4812067	4111.262	2.457762	133136.798	3.187953	0.031132	1.772619	3.018	3.827023	0.115493	9	2400	375000	244.03	81.88	236.19	79.25	231.882	77.80
	S06_A6	5.4666692	5340.433	1.198711	143376.561	2.610216	0.037801	2.728502	3.674	4.372486	0.160643	15	3500	428571	229.35	60.06	221.97	58.13	217.918	57.07
	S06_A5	5.4521318	5595.428	1.619115	159396.549	3.403694	0.035620	3.035270	3.471	4.589432	0.159312	15	4500	333333	189.39	49.67	183.27	48.06	179.919	47.18
	S06_B4	5.4375943	7333.896	3.444325	169590.486	4.073045	0.043602	2.667869	4.260	4.376054	0.186440	9	2400	375000	173.80	58.43	168.19	56.54	165.107	55.51
	S06_C4	5.4230568	4529.859	2.276477	140267.880	3.037099	0.032675	2.683665	3.201	4.407151	0.141089	20	4000	500000	305.26	69.57	295.49	67.34	290.128	66.12
	S06_C6	5.4085194	4448.858	3.659208	147128.642	3.443759	0.030348	2.063137	2.981	4.083191	0.121734	17	3600	472222	309.47	76.11	299.57	73.68	294.137	72.34

S06_C8	5.3939819	5250.091	2.752775	136353.322	3.021204	0.038711	1.717586	3.813	3.945567	0.150451	30	3200	937500	474.21	88.58	459.22	85.78	450.992	84.24
S06_D8	5.3067571	5206.593	3.971207	143360.086	3.844571	0.036476	2.125440	3.652	4.299475	0.157016	35	3600	972222	511.95	89.29	495.82	86.48	486.959	84.93
S06_E8	5.2922196	5772.082	2.178719	140013.632	2.900776	0.041565	1.932810	4.173	4.237148	0.176818	13	2800	464286	218.92	61.42	211.87	59.44	208.004	58.36
S06_E5	5.2776821	12615.664	3.119171	156836.888	3.248802	0.080748	2.952064	8.129	4.815530	0.391461	34	3500	971429	234.85	41.83	227.29	40.49	223.147	39.75
S06_D1	5.2631447	4501.470	2.988312	147225.881	3.938036	0.031008	2.334857	3.130	4.493395	0.140657	21	2500	840000	515.89	114.94	499.63	111.32	490.705	109.33
S06_H1	5.2486072	4988.721	3.168805	147712.950	3.067002	0.033852	1.721697	3.427	4.239716	0.145288	27	4800	562500	320.44	63.15	310.19	61.13	304.574	60.02
S06_G3	5.2340697	5023.780	2.143826	155865.578	3.749246	0.032875	4.731884	3.337	6.138505	0.204852	14	3600	388889	229.12	62.83	221.74	60.81	217.699	59.70
S06_G4	5.2195322	4662.506	4.129160	142259.093	2.287845	0.032630	2.613994	3.322	4.734003	0.157241	32	4000	800000	464.89	85.08	450.19	82.39	442.117	80.91
S06_H3	5.2049948	8253.401	3.641213	132223.734	3.354319	0.062604	2.336751	6.391	4.618810	0.295166	41	4500	911111	279.22	45.47	270.27	44.02	265.356	43.22
S06_G6	5.1904573	5014.375	2.854359	143591.355	3.778433	0.035387	2.333522	3.622	4.649892	0.168438	19	4200	452381	245.23	57.40	237.35	55.56	233.023	54.55
S06_J2	5.1759198	4277.138	1.892720	142402.467	3.757958	0.030947	3.840908	3.177	5.589278	0.177557	30	6000	500000	307.57	58.73	297.72	56.85	292.325	55.82
S04_C12	5.088695	15242.027	2.354816	154410.818	3.248732	0.099293	1.976644	10.367	4.737046	0.491108	61	3600	1694444	319.09	43.56	308.89	42.17	303.295	41.41
S04_A13A	5.0741575	8893.337	1.868399	126364.764	3.870663	0.071651	2.828839	7.503	5.187140	0.389176	63	5000	1260000	327.66	44.64	317.19	43.22	311.445	42.43
S04_A13B	5.0596201	8527.096	2.666959	140542.995	4.243985	0.061933	3.537636	6.504	5.639124	0.366752	35	3500	1000000	300.63	53.57	291.00	51.85	285.721	50.91
S04_B8	5.0450826	5050.337	2.664007	124673.198	3.047730	0.040777	2.032113	4.294	4.878974	0.209523	61	8000	762500	345.93	47.40	334.89	45.89	328.834	45.06
S04_C8	5.0305451	6676.917	3.373953	155872.955	4.425555	0.043177	3.172615	4.560	5.489980	0.250359	28	4000	700000	300.13	59.06	290.52	57.17	285.25	56.14
S04_A9	5.0160077	5616.071	4.002624	128923.944	2.611301	0.043426	2.431831	4.600	5.137826	0.236337	26	3600	722222	306.83	62.20	297.01	60.21	291.623	59.12
S04_B6	5.0014702	8373.204	2.120663	140551.464	2.420074	0.059810	1.708594	6.354	4.880732	0.310111	59	3500	1685714	510.28	70.95	494.19	68.71	485.359	67.48
S04_D6	4.9869327	5085.909	3.327921	129875.931	3.594655	0.039317	1.513569	4.189	4.860226	0.203593	15	2000	750000	348.75	91.63	337.62	88.70	331.515	87.10
S04_D5	4.9723952	31005.385	1.309458	139376.703	2.028398	0.224436	2.436432	23.982	5.263630	1.262322	86	2500	3440000	280.89	33.70	271.88	32.62	266.94	32.03
S04_D7	4.9578578	17088.813	3.983208	140664.947	4.991420	0.122584	1.665729	13.137	4.999313	0.656759	51	2000	2550000	377.25	56.09	365.24	54.31	358.65	53.33
S04_E5	4.8706329	5566.920	2.125594	143459.987	1.846493	0.038982	2.252411	4.252	5.496168	0.233718	18	2500	720000	330.28	79.94	319.73	77.38	313.94	75.98
S04_D3	4.8560955	6220.588	3.979532	141231.313	4.226208	0.044311	2.263246	4.848	5.548106	0.268984	30	3600	833333	335.16	63.95	324.46	61.91	318.584	60.79
S04_D2	4.841558	9192.171	2.677602	150909.756	4.004423	0.062029	2.568582	6.807	5.726519	0.389812	51	4500	1133333	324.91	49.15	314.52	47.58	308.825	46.72
S04_E2	4.8270205	5013.682	3.420532	140544.081	2.779955	0.035691	2.020238	3.929	5.551998	0.218114	52	6400	812500	401.20	59.93	388.45	58.03	381.452	56.98
S04_F2	4.8124831	15886.311	3.315205	164107.619	4.187193	0.097781	2.653738	10.795	5.860497	0.632669	64	3000	2133333	383.86	52.99	371.65	51.31	364.946	50.38
S04_F6	4.7979456	12771.759	1.647658	128645.590	2.565256	0.100553	2.958076	11.135	6.051872	0.673887	33	2500	1320000	233.00	42.94	225.50	41.56	221.392	40.80
S04_G6	4.7543332	4941.885	5.288100	150075.602	3.018069	0.032779	3.761428	3.663	6.619149	0.242472	20	3500	571429	304.89	71.10	295.13	68.82	289.78	67.58
S04_J10	4.7397957	8806.995	3.563702	138108.383	3.920631	0.064430	2.865575	7.222	6.204703	0.448130	52	5400	962963	261.48	39.73	253.09	38.45	248.481	37.75
S04_J6	4.6525709	21017.939	2.565793	147641.559	2.396942	0.143176	2.431246	16.351	6.341236	1.036831	56	2500	2240000	268.53	39.72	259.91	38.44	255.184	37.75
S04_J2	4.6380334	1600.083	16.677345	43350.171	16.272771	0.037433	2.826600	4.288	6.558032	0.281222	38	3500	1085714	487.82	85.36	472.42	82.66	463.961	81.18
S04_K1	4.6234959	10016.994	4.200530	145271.116	3.415635	0.068940	2.175435	7.922	6.362626	0.504076	54	4500	1200000	296.25	44.50	286.76	43.08	281.557	42.30
S04_L1	4.6089585	6871.515	2.008265	139602.445	2.786156	0.049623	1.958062	5.721	6.350723	0.363299	19	2500	760000	260.57	62.03	252.20	60.03	247.61	58.94

	S04_L4	4.594421	8315.915	4.219924	150555.957	3.705604	0.055067	1.795767	6.368	6.362756	0.405194	41	4200	976190	299.73	50.55	290.14	48.93	284.872	48.04
	S32_A9	4.5798835	5171.038	4.307150	161349.026	4.081921	0.032104	1.939422	3.724	6.465195	0.240791	69	10000	690000	360.53	49.27	349.04	47.70	342.734	46.83
	S32_C9	4.5653461	3972.770	2.601806	150199.354	3.156394	0.026648	2.084027	3.101	6.570660	0.203780	80	10000	800000	496.65	64.41	480.98	62.37	472.379	61.26
	S32_C6	4.5362711	10109.834	1.578205	157757.145	3.234858	0.065065	2.446082	7.621	6.815229	0.519382	80	4200	1904762	481.79	63.08	466.57	61.09	458.217	60.00
	S32_E10	4.4345088	17618.251	2.303251	167621.013	2.895291	0.106673	3.670874	12.781	7.757864	0.991532	40	3600	1111111	171.69	30.24	166.14	29.26	163.099	28.73
	S32_E12	4.4199714	11050.097	3.316243	147034.054	2.723628	0.075281	2.173992	9.049	7.238662	0.655061	84	6400	1312500	283.94	37.18	274.84	35.99	269.847	35.33
	S32_E14	4.4054339	13806.241	1.876176	154111.652	3.650086	0.092518	4.408372	11.158	8.251491	0.920716	120	7200	1666667	292.23	35.96	282.87	34.81	277.734	34.18
	S32_F16	4.3908964	13534.919	3.862971	140858.130	2.761330	0.095816	2.190690	11.594	7.379208	0.855562	149	6000	2483333	415.04	45.76	401.87	44.31	394.635	43.51
	S32_I13	4.3763589	8375.738	1.783248	152382.704	3.172035	0.056519	4.172573	6.862	8.251264	0.566190	73	6400	1140625	324.40	46.46	314.03	44.97	308.345	44.16
	S32_G6	4.3618215	24195.196	2.601487	139382.282	3.065749	0.174687	1.704366	21.279	7.390314	1.572580	184	4900	3755102	343.87	35.90	332.89	34.75	326.872	34.12
	S32_H2	4.347284	3971.431	2.610312	154264.889	2.645443	0.025837	1.598226	3.158	7.438069	0.234882	54	8100	666667	409.27	63.47	396.28	61.46	389.143	60.35
	S32_H1	4.3327465	9798.363	1.833801	143295.946	3.107228	0.069308	2.289061	8.499	7.686948	0.653329	123	8000	1537500	352.27	41.74	341.03	40.41	334.866	39.68
	S32_J6	4.3182091	8163.420	3.788911	154536.089	3.219111	0.052898	2.196761	6.509	7.731391	0.503208	42	3500	1200000	358.84	61.93	347.40	59.96	341.124	58.87
	S32_L1	4.3036716	3172.431	3.112692	149950.341	3.038289	0.021296	2.749614	2.629	7.976786	0.209720	33	4800	687500	503.22	96.36	487.35	93.32	478.632	91.65
SEQ2	S32_B3	5.9521675	4141.890	2.033906	123528.301	2.358955	0.033698	1.968167	3.008	2.712255	0.081586	68	7200	944444	599.64	74.51	559.779	69.56	570.551	70.90
	S32_C1	5.9649959	15552.615	1.252033	125412.398	2.798244	0.125601	2.349256	11.188	3.002175	0.335874	70	4000	1750000	305.71	37.67	284.958	35.12	290.56	35.81
	S32_M5	5.9778243	14374.696	1.700854	122517.600	3.951849	0.119714	2.320219	10.640	2.982076	0.317305	108	10000	1080000	200.02	20.15	186.334	18.77	190.026	19.14
	S32_M10	5.9906526	19690.842	2.319586	113769.773	2.581124	0.173964	1.791175	15.429	2.595543	0.400470	129	5600	2303571	292.10	26.81	272.255	24.99	277.612	25.48
	S32_O1	6.003481	4341.330	6.343384	117174.539	3.098909	0.036542	3.681142	3.234	4.135496	0.133742	38	5600	678571	406.85	68.11	379.428	63.52	386.832	64.76
	S14_K8	6.0676229	12862.005	2.246300	107804.257	2.461417	0.119867	1.629915	10.496	2.525566	0.265092	139	8100	1716049	319.19	28.25	297.542	26.33	303.386	26.85
	S14_I3	6.1445932	10244.101	5.754379	123998.695	3.328305	0.082258	3.381671	7.113	3.934180	0.279831	48	2500	1920000	518.82	77.62	484.136	72.43	493.506	73.83
	S14_G4	6.1574216	13913.723	2.691368	112356.758	3.314805	0.124779	1.859140	10.767	2.750182	0.296116	115	5600	2053571	370.86	36.06	345.802	33.62	352.568	34.28
	S14_F5	6.17025	15696.708	2.121576	124151.028	2.200863	0.126897	1.685802	10.927	2.649013	0.289461	73	3600	2027777	361.12	43.33	336.699	40.40	343.292	41.20
	S14_C4	6.1830783	10470.409	5.577310	114452.640	3.340455	0.090744	3.407287	7.798	3.982005	0.310506	27	2500	1080000	271.42	53.34	252.944	49.71	257.93	50.69
	S14_F8	6.1959067	14970.348	2.815903	114787.114	3.177594	0.131140	1.537759	11.246	2.585733	0.290785	108	5000	2160000	373.41	37.21	348.179	34.69	354.99	35.37
	S14_A5	6.2087351	13103.370	2.392067	110256.949	2.308651	0.119258	1.802161	10.206	2.765273	0.282216	78	4200	1857142	354.30	41.30	330.328	38.50	336.799	39.26
	S14_B5	6.2215635	15777.253	4.764928	115435.850	3.210581	0.136194	2.569221	11.631	3.328745	0.387165	70	3600	1944444	326.21	40.47	304.098	37.73	310.068	38.47
	S14_D6	6.2343919	8581.263	6.325860	117715.280	3.533252	0.072208	3.975462	6.154	4.513054	0.277729	62	4200	1476190	463.08	62.41	431.993	58.22	440.389	59.36
	S14_B9	6.2472202	13824.656	4.283533	118698.132	2.529713	0.116035	3.087119	9.869	3.765679	0.371623	45	2500	1800000	355.10	54.60	331.079	50.90	337.564	51.90
	S14_B10	6.2600486	12751.744	3.127970	111415.678	3.305207	0.115108	1.913360	9.770	2.898378	0.283165	65	4500	1444444	289.33	36.85	269.662	34.35	274.97	35.02
	S14_H9	6.3370189	19103.663	3.808575	138486.106	2.940685	0.138234	2.760742	11.590	3.599802	0.417221	74	2500	2960000	491.91	59.86	458.956	55.85	467.856	56.94
	S14_H10	6.3498473	13151.159	3.630423	109430.010	2.669405	0.120039	2.145207	10.044	3.169844	0.318386	76	3600	2111111	407.52	48.50	380.056	45.23	387.472	46.11

S14_L12	6.375504	15520.165	2.749817	113960.835	3.543969	0.137621	2.836662	11.469	3.703887	0.424800	132	7200	1833333	312.25	29.54	291.066	27.53	296.785	28.07
S14_N14	6.3883324	16078.037	3.102483	111731.970	3.233856	0.145186	2.576173	12.075	3.525017	0.425652	123	6400	1921875	310.94	30.10	289.834	28.06	295.53	28.61
S09_J3	6.4011608	9577.196	1.475851	109913.124	2.912600	0.088681	2.889562	7.361	3.775994	0.277946	38	3500	1085714	288.66	48.08	269.036	44.81	274.331	45.69
S09_I5A	6.4268176	11386.468	2.434450	123499.730	5.573694	0.095037	5.371033	7.857	5.916335	0.464842	39	2500	1560000	385.63	65.83	359.6	61.39	366.629	62.59
S09_I3	6.4524743	21949.619	1.767561	126525.957	3.484565	0.176003	4.324091	14.493	5.010889	0.726215	38	2400	1583333	215.04	36.51	200.343	34.02	204.308	34.69
S09_H3	6.5294446	3982.475	2.930874	110438.592	3.278573	0.036226	1.406208	2.948	3.035366	0.089478	18	3600	500000	330.85	78.62	308.425	73.30	314.477	74.74
S09_H7	6.542273	7165.882	2.623670	108354.313	2.184137	0.066268	1.865240	5.382	3.295522	0.177361	29	3500	828571	301.00	56.77	280.562	52.91	286.08	53.95
S09_I7	6.5551014	21809.976	7.204945	120383.117	3.149278	0.179037	4.848095	14.512	5.570715	0.808409	33	2000	1650000	223.65	40.88	208.374	38.09	212.495	38.84
S09_H11	6.5679297	5819.607	2.843911	110746.254	2.464451	0.052640	1.853849	4.258	3.333950	0.141973	36	4000	900000	409.71	69.64	382.103	64.95	389.558	66.21
S09_G9	6.5935865	15935.600	3.273985	104891.571	3.361743	0.152568	1.712789	12.294	3.304190	0.406223	51	2400	2125000	336.99	48.48	314.161	45.20	320.323	46.09
S09_G6	6.6064149	12160.221	3.843351	114333.347	3.027297	0.106220	2.136637	8.543	3.564424	0.304501	41	2500	1640000	373.22	59.79	348.007	55.75	354.814	56.84
S09_F7	6.6192433	7951.345	2.893791	117314.373	2.992081	0.068040	1.864844	5.462	3.431537	0.187414	22	3000	733333	263.30	56.86	245.366	52.99	250.205	54.03
S09_E7	6.6320716	6292.852	3.541541	128134.509	3.616457	0.049890	5.947143	3.997	6.620137	0.264597	24	3000	800000	388.66	83.40	362.43	77.77	369.512	79.29
S09_F11	6.6449	14890.067	3.270946	152181.037	5.374501	0.099189	5.985482	7.931	6.666752	0.528747	38	2800	1357142	333.70	58.53	311.092	54.56	317.195	55.63
S09_D10	6.7218703	29976.222	3.828247	109511.292	2.888015	0.273800	2.314319	21.642	3.871292	0.837831	82	2800	2928571	265.30	31.05	247.24	28.93	252.115	29.50
S09_C8	6.7346987	27363.860	1.010862	101993.960	2.927494	0.272867	2.559807	21.527	4.044553	0.870685	30	2400	1250000	115.18	21.54	107.255	20.06	109.394	20.46
S09_C7	6.747527	5075.645	2.486466	112866.272	3.160396	0.045379	1.988212	3.573	3.733032	0.133391	19	3000	633333	345.33	80.27	321.956	74.83	328.267	76.30
S09_B4	6.7603554	7245.621	2.876487	100759.426	2.847217	0.072185	1.760620	5.673	3.641539	0.206594	20	2500	800000	276.23	62.58	257.439	58.32	262.511	59.47
S09_A2	6.7731838	10683.243	1.288411	110948.315	2.835116	0.097571	2.607238	7.654	4.139919	0.316868	12	2000	600000	155.02	45.21	144.381	42.11	147.251	42.94
S05_K11	6.7860122	6158.364	4.584732	78971.031	2.286585	0.077598	3.335079	6.076	4.652516	0.282671	60	4000	1500000	476.12	65.34	444.189	60.95	452.813	62.14
S05_J6	6.7988406	7723.547	9.755844	130790.014	8.047489	0.058526	3.472458	4.574	4.771238	0.218226	43	4000	1075000	454.05	72.55	423.552	67.68	431.788	68.99
S05_G10A	6.8244973	2634.465	3.312729	101369.538	2.627038	0.026138	3.882905	2.035	5.114275	0.104074	42	7000	600000	564.66	91.79	527.034	85.67	537.201	87.33
S05_G10B	6.8373257	3100.868	3.416775	88201.361	3.578542	0.035326	1.643676	2.745	3.737515	0.102601	17	2500	680000	477.65	117.21	445.617	109.35	454.269	111.48
S05_G9	6.914296	6543.098	2.235804	79904.924	2.661026	0.082649	2.389303	6.351	4.259063	0.270497	39	3000	1300000	397.19	65.81	370.404	61.37	377.637	62.57
S05_F7	6.9271244	6167.115	5.069499	86286.292	4.349115	0.071451	2.442486	5.480	4.312278	0.236331	64	5600	1142857	404.43	53.48	377.163	49.87	384.525	50.85
S05_G7	6.9399527	5832.716	5.311517	87581.998	5.553962	0.066919	1.694336	5.123	3.962496	0.203011	38	3500	1085714	410.78	68.60	383.101	63.97	390.575	65.22
S05_G4	6.9527811	5334.445	5.261783	92876.476	4.078527	0.057075	2.385000	4.362	4.326758	0.188715	31	3500	885714	394.15	72.82	367.56	67.90	374.74	69.23
S05_E7	6.9656095	10186.741	2.845620	97824.167	3.763741	0.105316	3.539220	8.033	5.075638	0.407739	22	2500	880000	215.61	47.25	200.875	44.02	204.85	44.89
S05_E8	6.9784379	5947.536	3.255115	83719.700	4.316279	0.071957	1.937095	5.479	4.146463	0.227168	50	5000	1000000	355.35	52.37	331.314	48.83	337.804	49.78
S05_F10	6.9912663	6135.992	2.526714	83521.243	2.602596	0.073943	2.290637	5.619	4.346722	0.244264	25	2500	1000000	346.68	70.95	323.212	66.15	329.547	67.45
S05_C10	7.016923	5330.579	5.184984	90387.266	3.687414	0.058703	2.442489	4.445	4.475384	0.198931	55	4200	1309523	564.22	80.16	526.621	74.82	536.78	76.26
S05_C9	7.0297514	4914.100	5.598138	76100.124	3.383328	0.064274	3.489503	4.858	5.142963	0.249843	12	2000	600000	242.58	71.13	226.037	66.28	230.501	67.59
S05_C7	7.1195501	6387.382	3.655167	87710.126	3.180977	0.072902	1.952021	5.441	4.426034	0.240801	39	2500	1560000	549.78	91.34	513.099	85.24	523.008	86.89

	S05_B8	7.1323784	9800.441	2.632923	89687.524	3.539796	0.110514	2.168486	8.233	4.549907	0.374580	58	3500	1657142	390.79	54.31	364.42	50.64	371.54	51.63
	S05_B9	7.1452068	4664.066	2.615174	80762.588	2.508775	0.058164	2.468986	4.325	4.724012	0.204318	21	2500	840000	377.45	84.27	351.958	78.58	358.842	80.12
	S05_A6	7.1580352	8555.011	2.049230	83885.523	3.177590	0.103397	2.556683	7.675	4.793666	0.367908	22	2500	880000	225.50	49.28	210.103	45.91	214.258	46.82
	S05_C5	7.1708636	21202.380	4.655526	83662.959	3.383636	0.252702	2.461291	18.724	4.766957	0.892556	29	1200	2416666	253.29	48.56	236.029	45.25	240.687	46.14
	S05_B4	7.183692	6257.925	2.829539	86953.888	2.181094	0.072170	2.291327	5.338	4.705372	0.251167	36	4800	750000	275.26	47.67	256.532	44.43	261.586	45.30
	S05_A3	7.1965203	7096.085	4.629796	83255.131	2.804433	0.084593	2.300873	6.246	4.733907	0.295658	51	3600	1416666	438.72	64.85	409.222	60.49	417.189	61.67
	S05_B2	7.2093487	3071.407	4.215444	89515.736	3.234505	0.034215	2.268275	2.522	4.742098	0.119578	15	2500	600000	459.47	120.62	428.617	112.52	436.949	114.71
	S05_A1	7.2221771	5975.970	4.751273	82935.079	2.316004	0.071672	3.293475	5.273	5.330762	0.281077	41	3200	1281250	468.88	77.38	437.419	72.18	445.916	73.59
SEQ3	S56_A4	104.25506	5214.272	2.806248	2526.606	3.724634	2.088860	3.052785	10.646	4.167804	0.443687	90	2500	3600000	643.62	72.95	509.322	57.73	612.493	69.43
	S56_A5	104.48501	1378.996	3.398062	1954.257	4.629863	0.727487	3.830422	3.699	4.767419	0.176365	48	4800	1000000	519.53	78.97	403.264	61.30	494.176	75.12
	S56_B2	104.71496	5686.635	3.492429	2068.900	4.358263	2.835922	4.782092	14.389	5.561986	0.800337	59	2500	2360000	320.18	45.33	247.67	35.06	304.327	43.08
	S56_C4	104.94491	5466.338	3.736885	1724.065	4.806629	3.288627	4.620781	16.650	5.425498	0.903338	66	3200	2062500	243.29	32.73	187.936	25.28	231.173	31.10
	S56_D2	105.17485	1596.344	2.857993	1851.607	3.379844	0.878964	3.816651	4.440	4.761753	0.211438	75	6000	1250000	540.16	67.47	419.432	52.39	513.846	64.18
	S56_D4	105.4048	2486.611	4.310160	2260.800	3.332514	1.105253	3.511710	5.571	4.524208	0.252058	45	3600	1250000	434.11	67.63	336.466	52.42	412.796	64.31
	S56_E4	105.63475	4846.322	4.699517	1927.215	5.364025	2.596431	4.405191	13.060	5.251353	0.685802	48	2500	1920000	287.74	44.19	222.45	34.17	273.46	42.00
	S56_F1	105.8647	4332.160	2.866897	2038.683	3.349553	2.158728	3.217570	10.834	4.308607	0.466811	48	2500	1920000	345.28	52.01	267.201	40.25	328.214	49.44
	S56_E6	106.09465	5189.394	1.732170	2472.958	3.496558	2.158448	3.701954	10.809	4.686336	0.506569	58	3500	1657142	299.76	41.79	231.791	32.32	284.896	39.72
	S56_E7	106.3246	3097.733	2.845051	2394.069	3.476630	1.329769	4.227180	6.645	5.116426	0.339990	46	4000	1150000	337.39	52.66	261.064	40.74	320.711	50.05
	S56_G6	107.7043	7525.126	5.012655	2636.112	3.852984	2.887265	4.177423	14.243	5.116715	0.728790	79	3000	2633333	359.81	44.47	278.517	34.42	342.047	42.28
	S56_I1	107.93425	1014.680	7.171259	1969.398	10.819555	0.548205	4.403851	2.699	5.311503	0.143337	40	6000	666666	476.40	79.46	369.517	61.63	453.085	75.57
	S56_I2	108.1642	1599.680	2.971570	1766.773	3.301243	0.919967	3.317913	4.519	4.463176	0.201693	43	4000	1075000	459.36	72.99	356.19	56.60	436.845	69.41
	S56_J7	108.39415	1901.286	2.975165	2472.088	4.964743	0.802244	4.306398	3.932	5.249248	0.206422	34	3500	971428	476.39	85.44	369.504	66.27	453.07	81.26
	S56_G10	108.85405	2283.112	3.167765	2006.390	4.359202	1.173785	4.086406	5.729	5.091074	0.291683	30	3500	857142	292.69	55.48	226.298	42.89	278.171	52.72
	S56_H10	108.6241	2616.719	4.007532	2690.874	4.666161	0.990208	3.189183	4.843	4.391290	0.212691	60	3000	2000000	777.62	106.04	616.684	84.09	740.384	101.0
	S56_B12	109.31395	2639.094	6.865946	2349.497	5.530897	1.139815	5.087539	5.540	5.944159	0.329311	69	3500	1971428	675.56	90.70	525.783	70.59	642.969	86.33
	S56_B8	109.5439	5976.991	4.318260	2381.445	4.309182	2.546480	3.401382	12.351	4.597950	0.567902	56	3500	1600000	254.20	35.92	196.404	27.76	241.553	34.14
	S56_A9	109.77385	4067.300	4.322363	2155.373	4.708443	1.936426	4.494802	9.373	5.468207	0.512512	82	3000	2733333	558.77	68.86	434.015	53.48	531.578	65.51
	S28_K8	111.15355	5310.842	2.653472	2188.705	3.805507	2.492584	3.828559	11.915	5.020523	0.598181	73	3500	2085714	341.18	43.45	264.01	33.62	324.313	41.30
	S28_I12	111.61345	4612.340	2.204505	2176.036	3.200655	2.160149	3.167925	10.283	4.571701	0.470113	34	2500	1360000	259.42	46.04	200.455	35.58	246.517	43.75

S28_H11	111.8434	4997.388	2.483697	2215.796	4.039592	2.330549	4.154229	11.071	5.318537	0.588840	22	2000	1100000	195.85	43.04	151.168	33.22	186.066	40.89
S28_I10	112.07335	5042.328	3.096017	2030.019	4.563766	2.566498	3.987869	12.167	5.205843	0.633413	45	3500	1285714	208.10	32.86	160.657	25.37	197.713	31.22
S28_J7	112.3033	4145.399	3.916226	2007.639	4.191021	2.092947	3.328286	9.902	4.737890	0.469146	33	2500	1320000	261.44	47.17	202.023	36.45	248.438	44.82
S28_K5	112.53325	7365.790	2.381097	1896.001	4.873107	4.081307	4.936722	19.270	5.993130	1.154860	65	2500	2600000	264.55	36.44	204.44	28.16	251.4	34.63
S28_K4	112.7632	6060.551	2.617659	2044.985	5.669416	3.072299	3.318005	14.476	4.768189	0.690251	35	2500	1400000	190.72	33.50	147.191	25.85	181.184	31.82
S28_I5	112.99315	3200.332	2.760273	1930.883	5.522931	1.729750	4.099448	8.134	5.358711	0.435862	49	3600	1361111	326.52	49.82	252.605	38.54	310.364	47.35
S28_I2	113.2231	6034.794	6.383616	1937.633	5.620988	3.151366	4.268195	14.788	5.505938	0.814240	98	5000	1960000	259.96	29.91	200.874	23.11	247.03	28.42
S28_F8	114.60279	906.797	2.766668	2143.772	3.715364	0.431575	3.295970	2.001	4.915470	0.098352	19	8000	237500	233.30	54.74	180.192	42.28	221.677	52.01
S28_G7	114.83274	5081.934	2.329888	1991.764	4.746334	2.650822	4.118200	12.265	5.519981	0.677033	33	2500	1320000	211.88	38.69	163.589	29.87	201.31	36.76
S28_F6	115.06269	4874.009	2.566051	1942.838	3.401332	2.565700	3.713864	11.848	5.245847	0.621505	66	3500	1885714	310.95	41.61	240.488	32.18	295.541	39.54
S28_F5	115.29264	2378.517	3.537410	1953.705	5.491399	1.252108	3.604822	5.770	5.190345	0.299498	43	6000	716666	243.91	39.29	188.421	30.35	231.767	37.34
S28_G4	115.52259	4963.871	4.390052	1929.509	5.668240	2.660107	3.698224	12.235	5.276727	0.645586	41	2500	1640000	262.86	43.33	203.127	33.48	249.791	41.18
S28_F2	115.75254	725.304	3.050441	1919.732	4.798073	0.392370	4.758519	1.801	6.085700	0.109606	12	4500	266666	289.74	85.48	224.002	66.09	275.36	81.24
S28_A1	116.67234	4101.042	2.412970	1954.301	4.013189	2.163775	4.004433	9.854	5.599985	0.551809	46	3000	153333	304.16	47.97	235.213	37.10	289.084	45.59
S28_C10	118.05204	3639.035	2.624488	2017.849	2.711786	1.825528	3.305782	8.216	5.266838	0.432735	22	2500	880000	210.88	46.31	162.812	35.76	200.358	44.00
S28_C7	118.28199	4604.122	2.504077	2115.780	4.695521	2.253924	3.884886	10.125	5.671104	0.574177	52	3500	1485714	287.21	43.03	222.039	33.27	272.957	40.90
S28_C5	118.51194	1402.941	3.580039	1701.202	4.232266	0.839553	4.184258	3.764	5.902331	0.222160	41	5000	820000	421.92	70.44	332.693	55.54	401.19	66.98
S28_C4	118.74189	4905.065	3.659004	1914.259	5.286074	2.662535	4.172853	11.914	5.916526	0.704880	68	3600	1888888	309.77	41.80	239.572	32.33	294.419	39.73
S28_B5	118.97184	5944.400	1.480673	1973.230	2.849736	3.068264	3.270010	13.703	5.343339	0.732181	56	3500	1600000	229.57	33.04	177.297	25.52	218.127	31.39
S28_A5	119.20179	6562.329	3.657090	2087.277	4.404037	3.226151	3.817066	14.380	5.718095	0.822263	49	2500	1960000	267.19	41.11	206.489	31.77	253.91	39.07
S28_A7	119.43174	8001.114	1.855007	2118.905	3.691627	3.882909	3.709204	17.274	5.670601	0.979544	55	2500	2200000	250.00	36.57	193.143	28.25	237.555	34.75
S28_D5	119.66169	1341.666	2.597464	1914.877	4.175443	0.726871	4.390882	3.227	6.160421	0.198825	18	4000	450000	273.19	66.56	211.151	51.44	259.622	63.25
S28_D6	119.89164	1200.854	3.011958	1824.369	4.968998	0.687368	4.701028	3.046	6.406756	0.195162	18	5600	321428	207.81	50.76	160.43	39.19	197.434	48.22
S28_E7	120.12159	5741.023	2.404938	1971.516	3.948881	2.969890	3.311280	13.136	5.494527	0.721783	35	2500	1400000	209.85	37.30	162.015	28.80	199.38	35.44
S72_B4	121.50129	7832.064	2.131199	2118.905	3.067436	3.777313	3.852693	16.518	5.982358	0.988170	44	1600	2750000	324.89	52.69	251.335	40.76	308.811	50.09
S72_B1	121.73124	8590.463	5.970479	1929.110	5.709688	4.498272	3.520418	19.634	5.799430	1.138640	84	2500	3360000	333.74	41.24	258.217	31.91	317.228	39.20
S72_D1	121.96119	2448.766	2.918808	2190.791	3.841730	1.145679	3.701734	4.991	5.936308	0.296289	20	2000	1000000	389.03	90.00	301.291	69.70	369.867	85.57
S72_C4	122.19114	9040.524	2.070575	2060.562	3.774592	4.548613	4.573037	19.779	6.538245	1.293177	132	4000	3300000	325.58	35.44	251.871	27.42	309.467	33.69

	S72_C5	122.42109	5635.305	2.351861	1922.630	4.703324	3.133260	6.591962	13.599	8.098835	1.101337	44	2000	2200000	315.93	54.07	244.366	41.82	300.285	51.39
	S72_E6	122.65104	6949.713	2.482356	1953.255	3.873539	3.655319	3.765809	15.835	6.051592	0.958255	85	3000	2833333	348.54	43.29	269.738	33.50	331.315	41.15
	S72_D8	122.88099	11549.344	1.871615	1921.308	5.629969	6.159855	5.595636	26.634	7.352344	1.958254	123	2500	4920000	359.51	41.83	278.283	32.38	341.761	39.76
	S72_A10	123.11094	6909.149	3.135386	2138.972	3.577288	3.262853	2.893581	14.082	5.605895	0.789411	36	2500	1440000	201.49	35.43	155.535	27.35	191.427	33.66
	S72_B11	123.34089	9581.543	3.812762	2085.475	5.003292	4.731123	4.185670	20.380	6.393943	1.303117	75	2000	3750000	358.14	47.27	277.216	36.59	340.456	44.94
	S72_J1	124.95053	5638.611	6.569488	1987.900	7.002153	2.974655	5.687857	12.649	7.611476	0.962775	53	2000	2650000	406.25	63.80	314.716	49.42	386.258	60.66
	S72_J2	125.18048	2599.625	2.340113	1851.156	2.994425	1.418636	2.854931	6.021	5.835928	0.351400	32	2800	1142857	369.11	68.71	285.767	53.20	350.905	65.32
	S72_I2	125.41043	4473.474	4.718972	1821.991	5.410242	2.531171	4.773252	10.724	7.001264	0.750795	46	2500	1840000	334.59	54.61	258.879	42.25	318.038	51.91
	S72_H3	125.64038	5013.390	5.605562	1561.712	5.306392	3.317843	5.712195	14.031	7.693570	1.079473	56	2500	2240000	311.87	48.09	241.205	37.19	296.418	45.71
	S72_H5	125.87033	6935.185	4.774067	1605.090	4.606873	4.447591	4.891284	18.774	7.128556	1.338321	51	2400	2125000	222.66	34.99	171.937	27.02	211.552	33.24
	S72_I8	126.10028	16438.787	2.407830	1734.856	4.890870	9.896473	4.520415	41.699	6.903427	2.878634	107	2500	4280000	202.23	24.02	156.108	18.54	192.131	22.82
	S72_H9	126.33023	1984.231	3.848764	1817.819	3.349458	1.101568	3.893088	4.633	6.535476	0.302788	22	2500	880000	369.38	82.37	285.974	63.77	351.158	78.31
	S72_J9	126.56018	14873.313	4.669538	2066.397	5.088690	7.314108	3.316003	30.706	6.235944	1.914802	63	2000	3150000	202.12	28.41	156.026	21.93	192.029	26.99
	S72_K7	126.79013	7544.302	6.227662	1989.135	6.070108	3.852174	3.917587	16.143	6.601140	1.065606	63	2000	3150000	379.19	53.93	293.615	41.76	360.492	51.27
	S72_K9	127.02008	8162.553	4.447344	2001.183	6.012841	4.276496	5.052492	17.888	7.354812	1.315663	46	1600	2875000	313.91	51.72	242.792	40.00	298.359	49.16
SEQ4	S67_B1	212.70548	9269.038	2.779898	1438.613	4.398320	6.654355	4.234378	16.622	4.269294	0.709644	62	2500	2480000	291.91	39.11	308.472	41.33	277.429	37.17
	S67_C2	212.94472	7640.071	3.297257	1541.794	3.398974	5.045922	3.788858	12.590	3.834170	0.482728	49	2500	1960000	304.29	45.01	321.536	47.56	289.208	42.78
	S67_C5	213.06434	3486.627	2.426656	1375.316	5.559104	2.705720	5.350114	6.747	5.384924	0.363336	33	3500	942857	273.79	49.89	289.344	52.72	260.187	47.41
	S67_D6B	213.30358	10430.992	3.779488	1325.061	4.820326	8.046041	3.334551	20.042	3.399620	0.681352	67	2500	2680000	262.23	33.25	277.144	35.14	249.193	31.60
	S67_A11	213.54282	10529.086	2.256525	1175.926	5.571031	9.536670	5.236506	23.728	5.285288	1.254116	118	3500	3371428	278.29	29.54	294.091	31.22	264.466	28.07
	S67_D9	214.26054	8916.947	3.467846	1304.562	5.131517	7.154998	4.705140	17.743	4.789530	0.849802	74	3000	2466666	272.42	34.25	287.894	36.20	258.881	32.55
	S67_F7	214.38016	12277.061	2.526363	1376.107	4.312123	9.252327	4.370700	22.931	4.467810	1.024515	74	2000	3700000	315.12	39.24	332.962	41.47	299.511	37.30
	S67_F5	214.49978	11951.817	5.267708	1477.160	5.289758	8.337579	4.591737	20.652	4.690627	0.968727	94	2500	3760000	354.47	40.16	374.475	42.43	336.962	38.18
	S67_E3	214.6194	12391.133	3.140327	1422.197	6.091043	9.182026	4.036344	22.731	4.155981	0.944714	71	1600	4437500	379.34	47.70	400.705	50.39	360.637	45.35
	S67_G1	214.97826	6633.711	1.953574	1218.800	4.089704	5.651679	4.444651	13.968	4.575675	0.639139	66	2500	2640000	367.60	48.27	388.327	51.00	349.464	45.89
	S67_G2	215.09788	3525.844	3.490217	1244.429	5.340883	3.004859	5.587928	7.422	5.699046	0.423007	29	2500	1160000	305.45	59.33	322.757	62.69	290.309	56.39
	S67_H2	215.2175	3538.211	5.065875	1197.779	5.401611	3.051385	4.924802	7.533	5.057934	0.381022	47	4000	1175000	304.86	47.07	322.14	49.73	289.753	44.73
	S67_I5	216.05484	7464.855	4.793359	1426.820	4.504882	5.392580	4.837080	13.261	5.031876	0.667298	66	2500	2640000	386.62	51.41	408.381	54.31	367.567	48.88

S67_K5	216.29408	10550.199	1.943543	1322.342	4.127636	8.221453	3.660062	20.196	3.938297	0.795371	98	2500	3920000	377.23	40.90	398.486	43.20	358.634	38.88
S67_K7	216.4137	9410.734	3.714248	1300.875	4.678195	7.461881	4.459746	18.320	4.701378	0.861283	84	2500	3360000	357.02	42.42	377.166	44.81	339.39	40.32
S67_I10	216.53332	7718.048	2.533304	1279.226	5.690901	6.391358	5.168056	15.683	5.387424	0.844903	75	2400	3125000	386.97	49.31	408.755	52.08	367.905	46.88
S67_M10	216.65294	14095.436	2.311145	1239.287	1.875456	11.382864	1.947991	27.915	2.492895	0.695902	154	3600	4277777	299.64	25.27	316.625	26.71	284.78	24.02
S67_L4	216.77256	4195.231	2.702646	1020.166	8.530637	4.682369	7.161117	11.477	7.335406	0.841866	75	3600	2083333	353.45	48.35	373.406	51.08	335.998	45.96
S67_L2	216.89218	10489.101	3.129167	1105.671	4.714386	9.921573	4.969313	24.305	5.227789	1.270609	51	1600	3187500	257.29	38.46	271.922	40.64	244.488	36.54
S67_L1	217.0118	6856.345	3.371639	1131.922	5.748599	6.468050	5.663658	15.836	5.901207	0.934519	46	2500	1840000	228.46	36.28	241.486	38.35	217.071	34.47
S67_M2	217.13142	4127.506	2.078443	1088.582	4.349627	3.949335	4.494323	9.664	4.802089	0.464076	37	2500	1480000	299.45	51.29	316.432	54.20	284.606	48.74
S53_D2	217.96876	4543.737	1.783986	1315.311	4.965241	3.646842	4.980464	8.890	5.341289	0.474817	43	2500	1720000	376.07	60.77	397.263	64.19	357.53	57.77
S53_C2	218.08838	12621.530	4.551826	1067.749	4.838829	12.140772	4.364911	29.578	4.786381	1.415723	92	2500	3680000	244.33	28.03	258.243	29.63	232.165	26.63
S53_C3	218.208	7183.367	2.025172	1206.302	4.301865	6.215465	4.702160	15.134	5.109037	0.773213	79	2500	3160000	404.92	50.03	427.682	52.85	384.997	47.57
S53_A4	218.32762	14900.523	4.472730	1112.171	6.420226	14.345196	6.063220	34.910	6.394673	2.232408	150	3000	5000000	280.47	29.09	296.396	30.74	266.544	27.64
S53_A5	218.44724	20288.774	2.557286	1385.780	5.257492	14.925476	2.996613	36.303	3.639842	1.321361	109	1600	6812500	365.06	37.41	385.649	39.52	347.047	35.56
S53_B7	218.68648	9586.946	3.130336	1210.022	5.892066	8.350350	5.219277	20.288	5.638755	1.143993	77	2500	3080000	296.91	37.75	313.747	39.89	282.185	35.88
S53_A8	218.8061	7886.350	4.237215	1120.431	4.332448	7.160634	3.683112	17.388	4.273921	0.743149	98	2500	3920000	436.13	47.84	460.585	50.52	414.72	45.49
S53_D11	218.92572	15778.709	3.169289	1206.300	4.566863	13.587724	4.567727	32.977	5.070884	1.672210	155	3600	4305555	256.16	24.33	270.739	25.72	243.422	23.12
S53_D10	219.64344	5706.804	1.936671	1144.171	5.309042	5.384538	6.179061	13.025	6.630947	0.863700	51	2500	2040000	306.09	47.42	323.432	50.11	290.917	45.07
S53_D8	219.76306	16173.096	3.986444	1352.441	6.582589	12.772047	5.121895	30.879	5.673335	1.751869	81	1600	5062500	320.06	39.93	338.175	42.19	304.213	37.95
S53_E8	219.88268	14194.646	1.943451	1237.056	6.166959	12.581815	6.454532	30.403	6.912335	2.101524	89	2500	3560000	230.21	29.13	243.332	30.79	218.733	27.68
S53_F7	220.0023	9208.639	3.194701	1067.842	4.814806	8.980791	4.646210	21.689	5.279708	1.145129	86	2500	3440000	309.88	37.21	327.43	39.31	294.522	35.36
S53_F4	220.12192	3987.999	3.692812	1267.656	5.247203	3.240959	4.457146	7.823	5.130795	0.401377	48	2400	2000000	492.41	75.43	519.892	79.64	468.333	71.74
S53_G7	220.24154	20864.671	1.663585	1230.451	5.076582	17.889383	5.251903	43.157	5.849308	2.524399	111	2500	4440000	202.69	22.60	214.275	23.89	192.571	21.47
S53_F10	220.36116	6793.965	4.920400	1238.181	7.247003	5.799890	4.465405	13.984	5.171746	0.723235	63	2500	2520000	350.94	47.80	370.758	50.49	333.607	45.43
S53_H9	220.48078	15729.440	3.055538	1198.554	6.505934	14.220567	5.904716	34.269	6.469169	2.216930	68	1600	4250000	243.56	33.48	257.434	35.38	231.435	31.81
S53_I11	220.6004	9954.011	4.557805	1086.502	5.314064	9.558179	5.206979	23.021	5.854625	1.347799	128	2500	5120000	430.45	45.64	454.592	48.20	409.305	43.39
S53_J8	220.72002	9236.943	2.402825	1104.171	6.319127	9.151457	6.311242	22.030	6.868583	1.513119	130	3600	3611111	320.01	35.65	338.124	37.67	304.167	33.88
S57_A4	221.43774	2281.746	3.325734	1060.790	5.103761	2.270367	5.601219	5.448	6.313006	0.343905	34	3500	971428	347.38	63.48	367.002	67.07	330.218	60.35
S57_B5	221.55736	3117.998	2.628335	952.615	5.563457	3.455269	5.194202	8.286	5.971318	0.494793	37	2500	1480000	347.93	60.86	367.577	64.29	330.737	57.85

S57_E4	221.91622	1167.778	2.619324	762.237	5.699689	1.628115	5.639261	3.898	6.409385	0.249844	37	4000	925000	458.26	80.86	483.912	85.39	435.802	76.90
S57_F4	222.03584	3528.377	1.950303	861.484	6.140637	4.443248	5.948972	10.632	6.698810	0.712250	47	3000	1566666	288.37	46.29	304.731	48.91	274.057	43.99
S57_G3	222.15546	2922.549	3.169534	793.232	6.256447	3.912234	5.250426	9.357	6.103906	0.571127	60	5000	1200000	251.71	35.95	266.038	37.99	239.187	34.16
S57_I1	222.27508	4410.094	2.097587	938.275	5.619242	4.996031	5.719989	11.942	6.528240	0.779629	36	2400	1500000	246.62	44.14	260.657	46.66	234.339	41.95
S57_J6	222.3947	1590.928	2.951507	994.829	6.080554	1.728817	6.377382	4.130	7.126124	0.294331	28	4000	700000	330.59	66.77	349.283	70.55	314.233	63.47
S57_J12	222.51432	3425.010	2.377392	1075.418	4.926024	3.392528	5.978968	8.101	6.787618	0.549845	29	2500	1160000	280.42	55.44	296.343	58.59	266.496	52.69
S57_I10	223.23204	4705.195	2.036739	1068.790	5.225064	4.648919	5.157762	11.065	6.184415	0.684308	53	4200	1261904	224.31	33.79	237.106	35.72	213.127	32.11
S57_I11	223.35166	1941.010	2.586689	1050.447	4.764290	1.940224	5.287170	4.616	6.310769	0.291274	39	3500	1114285	465.95	80.20	492.015	84.68	443.126	76.27
S57_H8	223.5909	2639.237	2.909283	912.532	6.101838	3.136306	6.035314	7.453	6.982615	0.520403	47	3600	1305555	341.41	55.21	360.701	58.33	324.533	52.48
S57_G7	223.71052	1519.671	3.715253	716.686	6.150343	2.293048	6.606487	5.446	7.497376	0.408313	23	3000	766666	275.77	61.11	291.44	64.58	262.076	58.07
S57_F8	223.83014	1116.090	4.511280	797.942	6.768338	1.579949	8.746536	3.750	9.449970	0.354415	53	8000	662500	344.20	57.39	363.645	60.63	327.189	54.55
S57_F9	223.94976	1253.933	2.258421	856.277	4.412841	1.512658	4.272487	3.589	5.593854	0.200751	29	3600	805555	434.30	84.23	458.656	88.95	412.977	80.09
S57_G11	224.06938	5274.645	5.976510	778.148	5.208256	7.186085	7.446703	17.040	8.290321	1.412663	98	3600	2722222	312.07	40.78	329.748	43.09	296.613	38.76
S57_E8	224.30861	8576.675	1.794967	981.285	4.891394	9.121949	4.082453	21.607	5.515999	1.191854	118	4000	2950000	267.63	28.72	282.84	30.35	254.326	27.29
S57_B7	225.26557	1491.807	2.057554	759.270	4.166509	2.060306	5.279602	4.860	6.606512	0.321045	30	3600	833333	334.40	64.93	353.305	68.60	317.86	61.72
S57_C8	225.38519	1510.710	2.128206	870.861	5.540404	1.867157	6.267479	4.402	7.437280	0.327361	18	2500	720000	319.35	78.93	337.43	83.40	303.541	75.02
S57_A9	225.50481	1517.018	2.810326	864.231	4.368029	1.826927	5.292828	4.304	6.656409	0.286525	56	7000	800000	361.65	53.99	382.045	57.04	343.794	51.33
S57_D7	225.62443	711.813	3.245894	854.784	6.411895	0.899564	6.179528	2.118	7.398925	0.156737	20	4800	416666	382.12	90.00	403.644	95.07	363.29	85.57
S57_C11	225.86367	1490.500	2.210228	846.900	3.690139	1.818989	4.461057	4.279	6.082080	0.260251	44	6300	698412	318.67	51.80	336.713	54.74	302.894	49.24
S57_B12	225.98329	3647.160	2.307395	815.650	5.551264	4.826193	6.535842	11.347	7.750951	0.879510	50	3500	1428571	247.18	39.86	261.256	42.13	234.879	37.88
S57_A11	226.10291	2740.031	3.324971	748.771	4.371006	3.783705	5.162868	8.891	6.654803	0.591703	34	3200	1062500	234.84	43.20	248.229	45.66	223.144	41.05

APPENDIX D: HEFTY TIME–TEMPERATURE MODELS

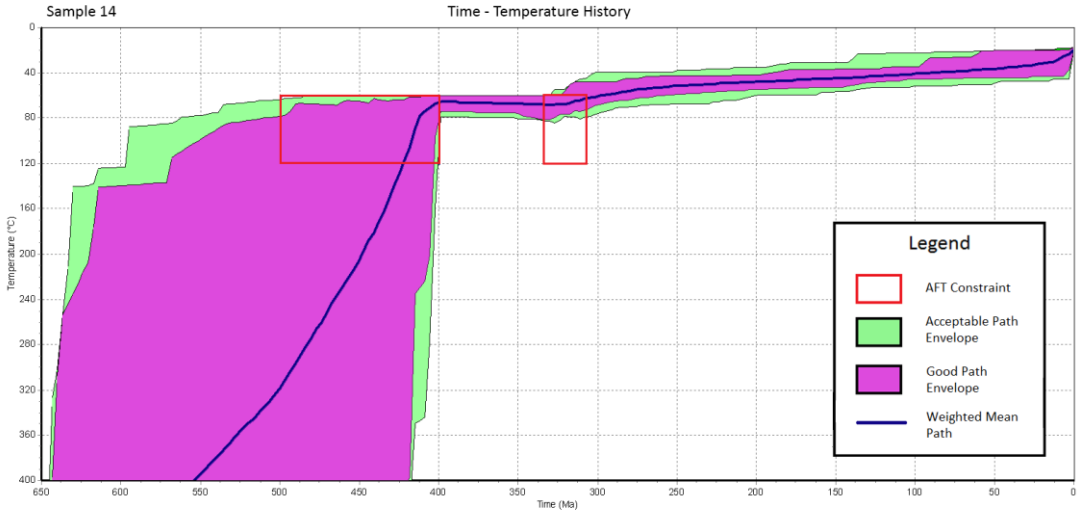

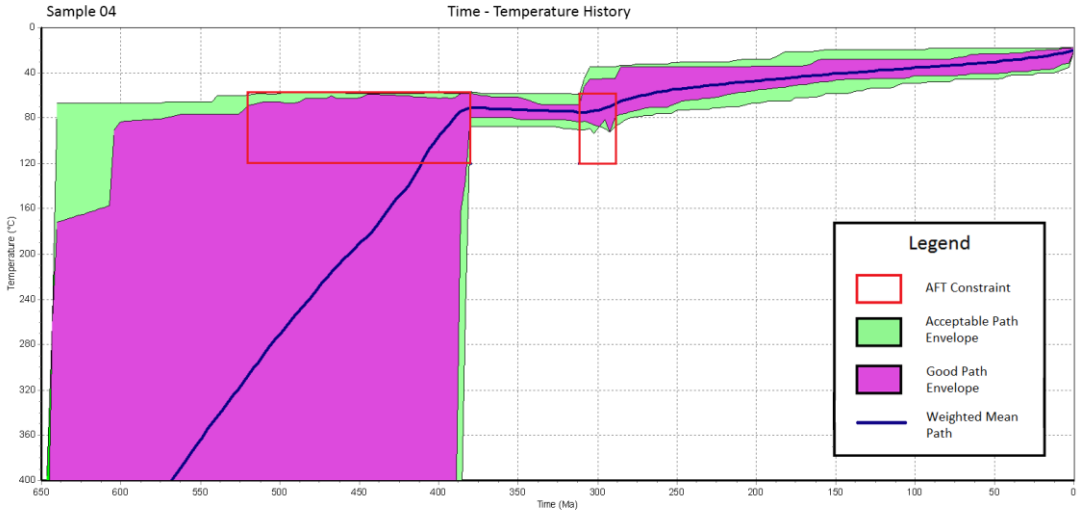

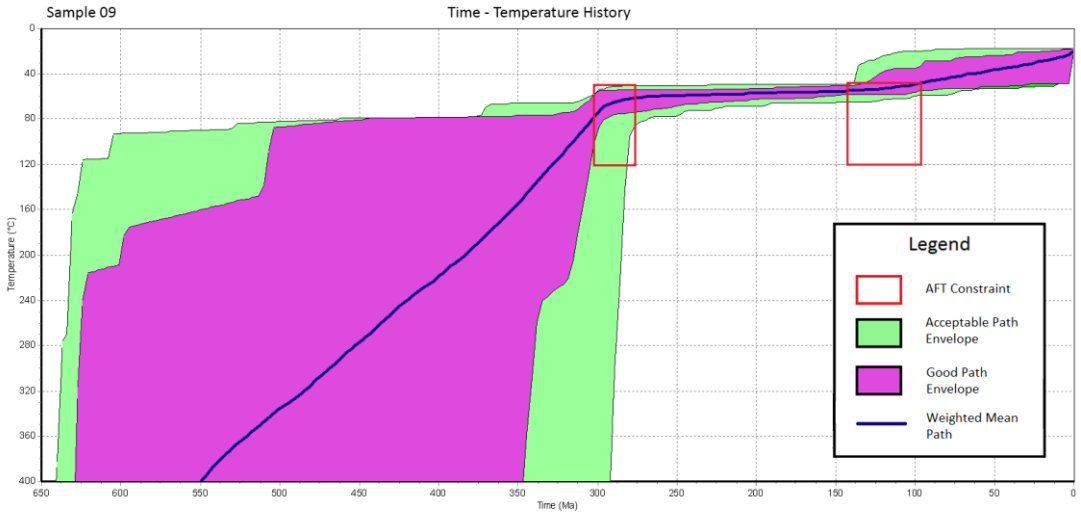

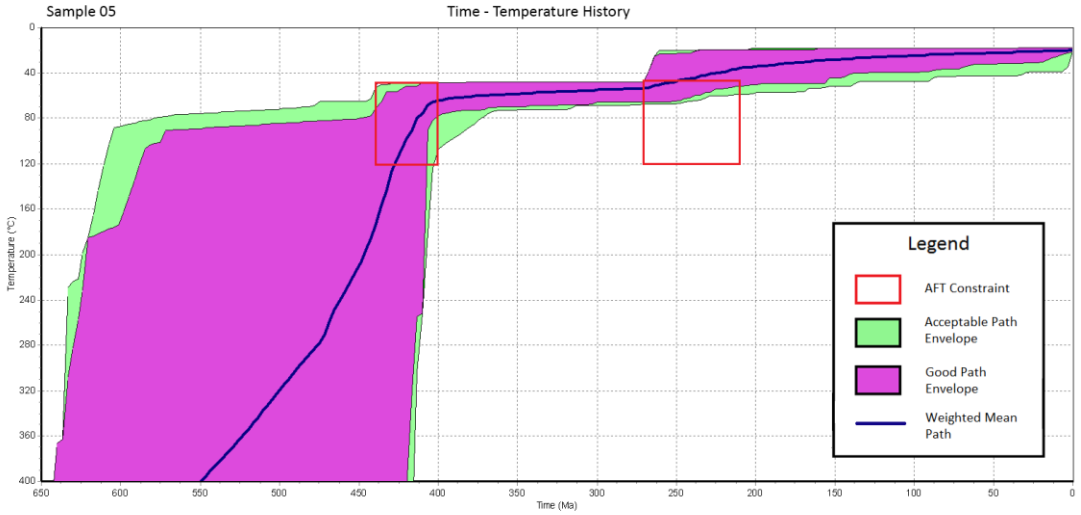
Sample 05
Time - Temperature History
Temperature (°C)
Time (Ma)
Legend
AFT Constraint
Acceptable Path Envelope
Good Path Envelope
Weighted Mean Path

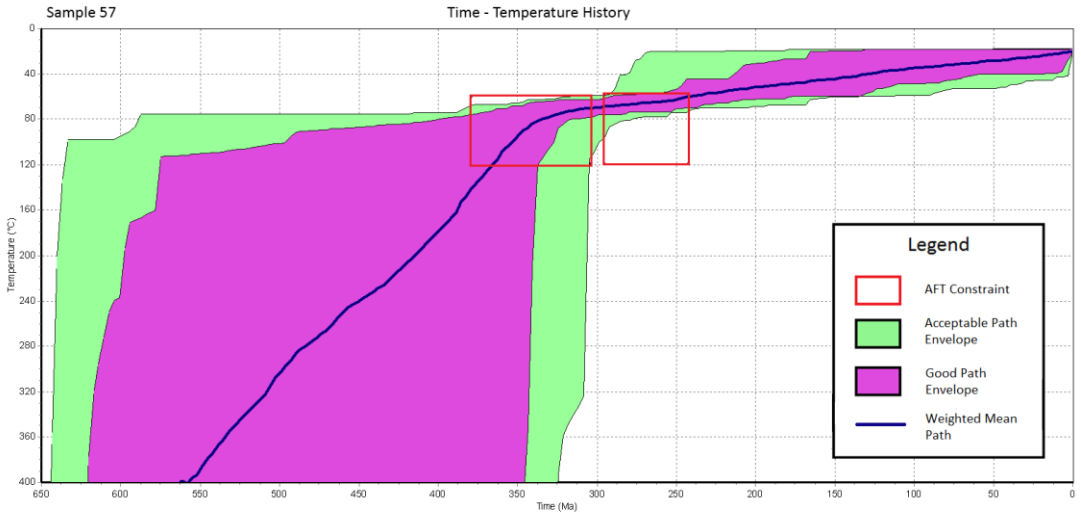
Sample 57
Time - Temperature History
Temperature (°C)
Time (Ma)
Legend
AFT Constraint
Acceptable Path Envelope
Good Path Envelope
Weighted Mean Path

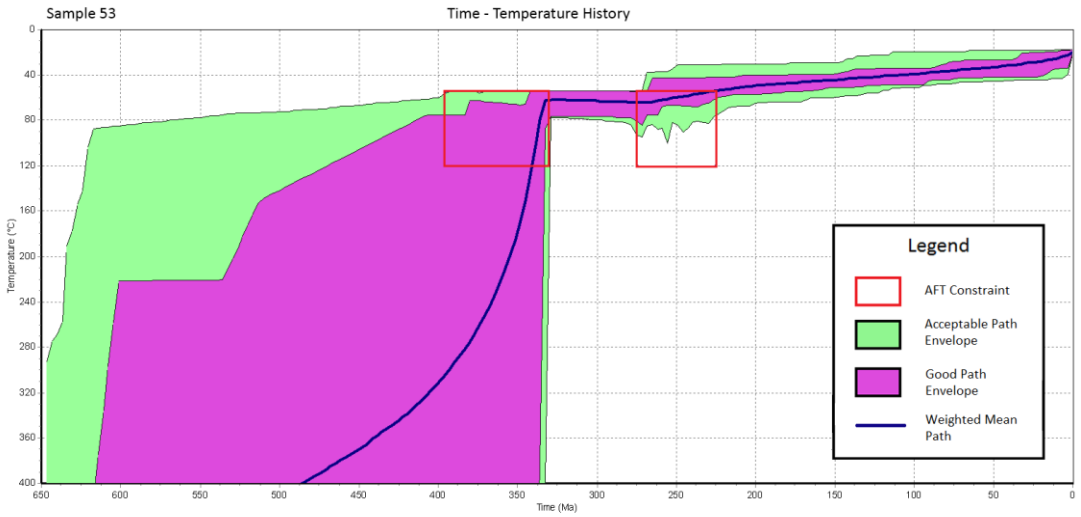
Sample 53
Time - Temperature History
Temperature (°C)
Time (Ma)
Legend
AFT Constraint
Acceptable Path Envelope
Good Path Envelope
Weighted Mean Path

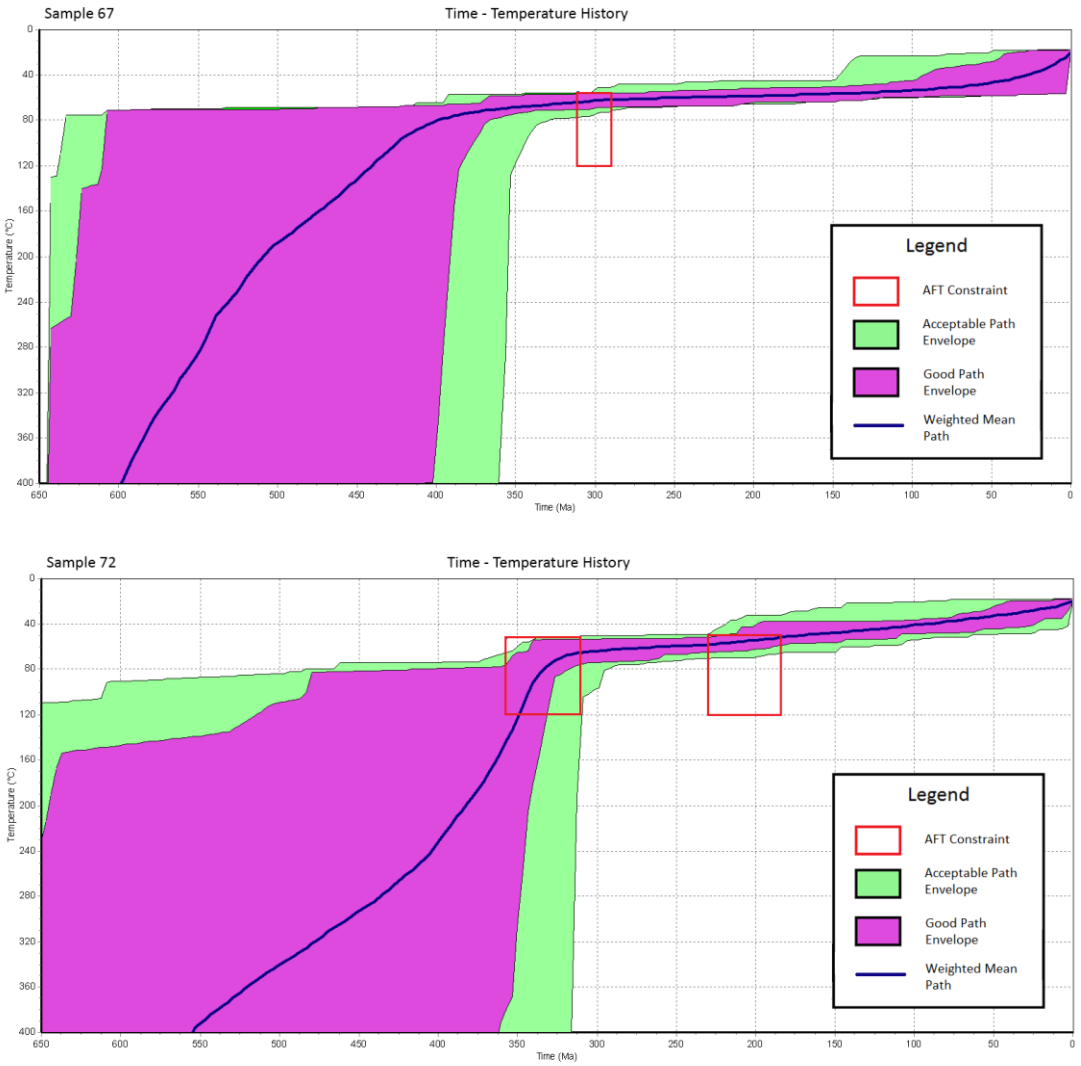

Figure 6: Time-Temperature models for samples 14, 04, 09, 05, 57, 53, 72 and 67, constrained by AFT age and length data only. Models were constructed using the modelling software *HeFTy* (Ketcham 2005). Low–T AFT constraints are shown as red boxes representing the age ranges of AFT peaks within the AFT PAZ zone (120–60°C). Acceptable cooling path envelopes are shown in green, statistically good fit path envelopes are shown in purple. For all samples the default merit value for good paths of 0.5 and merit value for acceptable paths of 0.05 were used.

Figure 6 above shows *HeFTy* time-temperature models for samples 14, 04, 09, 05, 57, 53, 72 and 67, for which only AFT ages and length data was available. These models are not well constrained and therefore were only used for reference purposes to confirm the general cooling rates and trends in each study region.

Sample 14 shows a simple cooling history, with the sample being brought to AFT closure temperatures (~120–60^{o}C) between ~500–400 Ma (Neoproterozoic–Cambrian). The sample then remained within this temperature range until the Carboniferous where it then slowly cooled to near surface conditions until present day.

Samples 04 and 05 exhibit very similar modelled cooling histories, with both samples being brought to upper crustal temperatures (~120–60°C) by the Devonian (~400 Ma). The rocks then remained within this temperature range until a second pulse of cooling occurred, for sample 04 during the late Carboniferous–early Permian and for sample 05 during the Permian–Triassic. Samples then remained near surface temperatures until the present day. Sample 09 lies between samples 04 and 05, and alternatively shows more prolonged cooling from pre-Petermann age through to reaching upper crustal temperatures around the Permian. AFT constraints show sample 09 remained at this temperature until a second cooling event around the early Cretaceous, a preserving the youngest event out of the four samples in this middle region.

In the mid-north of the study region, samples 57 and 53 show similar modelled time-temperature histories, with these samples being brought to temperatures between ~120–60°C by the early Carboniferous. Both samples remained at this temperature range

throughout the remainder of the Paleozoic before slowly cooling to near surface conditions over the Mesozoic–Cenozoic. It was not possible to calculate a *HeFTy* model for sample 28 due to the lack of confined fission track lengths observable under the optical microscope.

In the top northeast corner of the study region, only AFT constraints and length data was available for modeling both samples 72 and 67, and similarities can be seen between the two cooling histories. Both samples were brought up to temperatures between ~120–60°C at some stage during the Devonian, and from thereon continued a protracted cooling path through the upper crust until the present day. Although the single AFT age peak for sample 67 constrains the path at AFT closure temperatures at 300 Ma, the combination of this along with the distribution of length data likely sees the sample reaching these temperatures earlier ~400 Ma.